The chloroplast calcium sensor protein CAS is part of the STN7/STN8 kinase phosphorylation network and is required for photoacclimation

Dissertation

zur

Erlangung des Doktorgrades (Dr. rer. nat.)

der

Mathematisch-Naturwissenschaftlichen Fakultät

der

Rheinischen Friedrich-Wilhelms-Universität Bonn

vorgelegt von

Edoardo Andrea Cutolo

aus

Genua, Italien

Bonn, 2018

Angefertigt mit Genehmigung der Mathematisch-Naturwissenschaftlichen Fakultät der Rheinischen Friedrich-Wilhelms-Universität Bonn

1. Gutachter: Prof. Dr. Ute Vothknecht

2. Gutachter: Prof. Dr. Dorothea Bartels

Tag der Promotion: 21/03/2019

Erscheinungsjahr: 2020

Table of contents

1 Abbreviations

α-CT-CAS	Anti C-terminal CAS Domain Serum
α -NT-CAS	Anti N-terminal CAS Domain Serum
α -pThr	Anti Phosphorylated Threonine Antibody
CAS	Calcium Sensing Receptor
CAS-C	Recombinant fragment of the C-terminus of CAS
CAS-N	Recombinant fragment of the N-terminus of CAS
CBB	Calvin Benson Bassham Cycle
CCA1	CIRCADIAN CLOCK ASSOCIATED 1 (Transcription Factor)
cDNA	Complementary Deoxyribonucleic Acid
CDPK	Calcium-Dependent Protein Kinase
CEF/CET	Cyclic Electron Flow/Transfer
EOD	End of Day
EON	End of Night
ETC	Electron Transfer Chain
FHAD	Fork Head Associated Domain
FNR	Ferrodoxin $NADP^+$ reductase
GFP	Green Fluorescent Protein
GL	Growth light
HL	High light
LD	Light/Dark (diel) Growing Conditions
LEF/LET	Linear Electron Flow/Transfer
LHCII	Light Harvesting Complex proteins of photosystem II
Lhcb1 and Lhcb2	Light Harvesting Chlorophyll *a*/*b* Binding protein 1 and 2
LL	Light/Light, Constant Light Growing Conditions
mRNA	Messenger Ribonucleic acid
MSA	Multiple Sequence Alignment
NADPH	Nicotinamide Adenine Dinucleotide Phosphate
NPQ	Non-Photochemical Quenching
PAR	Photosynthetically Active radiation
PCR	Polymerase Chain Reaction
PGR5	Proton Gradient Regulator 5

PhANGs	Photosynthesis-Associated Nuclear Genes
PPI	Protein-Protein Interaction
PSI	Photosystem I
PSII	Photosystem II
pS/T	Phosphorylated Serine/Threonine
RNA	Ribonucleic Acid
ROS	Reactive Oxygen Species
RuBisCO	Ribulose-1, 5-bisphosphate carboxylase/oxygenase
RT-qPCR	Real Time Quantitative Polymerase Chain Reaction
saGFP	Self Assembling Green Fluorescent Protein
SDS PAGE	Sodium Dodecyl Sulfate Polyacrylamide Gel Electrophoresis
STC	State Transition Complex
STN7	State Transition Kinase 7
STN8	State Transition Kinase 8
TAP38	Thylakoid-Associated Phosphatase 38
TF	Transcription Factor
TP	Transit Peptide
TMD	Trans Membrane Domain
TOC1	TIMING OF CAB EXPRESSION 1 (Transcription Factor)
YFP	Yellow Fluorescent Protein

2 Figures and tables

3 Summary

In the present work, the phosphorylation profile of the chloroplast-localized Calcium Sensing Receptor (CAS) from *A. thaliana* was investigated and it could be shown that CAS is a target of multiple protein kinases acting differentially on several residues. Phosphoproteomics followed up by biochemical kinase assays strongly indicated that CAS is part of a phosphorylation network involving the important state transistion kinases STN7 and STN8 as well as, at least, one other calcium-regulated protein kinase. The role of light and calcium behind the activation of CAS phosphorylation was investigated *in vitro* in more detail and revealed that, at least under normal growth light conditions, STN7 might be the major kinase acting on CAS.

The analysis was extended at the level of individual residues by studying the phylogenetic conservation of experimentally described phosphoresidues of the *A. thaliana* CAS isoform and by conducting *in vitro* assays using recombinant CAS fragments carrying mutations at selected positions. These analyses confirmed the relevance of the previously described phosphorylation site Thr-380, but also showed that other residues, in particular Thr-376, are possible targets.

A spectrometric analysis of *cas* mutant plants revealed that CAS is very likely involved in the processes of photoacclimation to high light, as evidenced by a persistent strong excitation of PSI under this condition. The analysis of the phosphorylation status of several known thylakoid phosphoproteins in the *cas* mutant further suggested a potential defect in the dephosphorylation of the important light harvesting protein LHCII under high irradiance, suggesting a possible role for CAS in mediating the activity of the TAP38 phosphatase.

In addition to the post-translational modification of CAS, a potential involvement of CAS in the circadian network of the chloroplast was explored. RT-PCR analyses revealed that the transcription of the CAS follows a regular diurnal rhythm, with the highest levels of its transcript levels found at the end of the night and lowest levels at the end of the day. Interestingly, the levels of the CAS protein appear to follow an opposite, 12 hours shifted rhythm, suggesting a physiological requirement for higher abundance of CAS during the day.

In light of these results, a possible working model is discussed that integrates the evidences on the phosphorylation profiles and the diurnal regulation with a suggested involvement of CAS in photoacclimation responses.

3.1 Zusammenfassung

Reversible Phosphorylierung ist eine wichtige post-transationale Modifikation, welche an der Regulierung zahlreicher zellulärer Prozesse beteiligt ist. In der vorliegenden Arbeit wurde die Phosphorylierung des chloroplastidären Calcium Sensing Receptor Proteins (CAS) aus A. thaliana untersucht. CAS kommt in allen photosynthetischen Eukaryoten vor und spielt eine wichtige Rolle in der zellulären Antwort auf Umweltreize. Durch Phosphoproteomic-Analyse gefolgt von biochemischen Kinase-Assays konnte gezeigt werden, dass CAS durch mehreren Proteinkinasen und an verschiedene Aminosäurepositionen phosphoryliert wird. Die Ergebnisse legen nahe, dass CAS Teil eines Phosphorylierungsnetzwerks ist, an dem zwei wichtige, an der Adaptation der Photosysteme beteiligte Kinasen, die State-Transition Kinase 7 (STN7) und 8 (STN8), sowie mindestens eine weitere durch Calcium regulierte Proteinkinase beteiligt sind. Weitergehende Untersuchungen zur Rolle von Licht und Calcium in der Aktivierung der CAS-Phosphorylierung lassen vermuten, dass zumindest unter normalen Wachstumslicht-bedingungen STN7 die Hauptkinase ist, die CAS phosphoryliert.

Die Relevanz der verschiedenen, durch Phospho-Proteom-Analyse identifizierten Phosphorylierungstellen in Arabidopsis wurde anschließend durch die Verwendung rekombinanter, mutierter CAS-Fragmente in in vitro Kinase-Assays näher untersucht. Eine phylogenetische Analyse zahlreicher CAS Sequenzen photosynthetischer Organismen, zeigte zudem die evolutionäre Konservierung der Phosphorylierungstellen auf. Diese Analysen bestätigten die Relevanz der zuvor beschriebenen Phosphorylierungsstelle Thr-380, zeigten jedoch auch, dass andere Aminosäuren, insbesondere Thr-376 und Thr-378, ein wichtiges, evolutionär konserviertes Ziel der Phosphorylierung von CAS darstellen.

Eine spektrometrische Analyse von cas-Mutanten zeigte, dass CAS wahrscheinlich am Prozess der Photo-Akklimatisierung unter Starklichtbedingungen beteiligt ist, was durch eine anhaltende starke Anregung von Photosystem I unter dieser Bedingung belegt wird. Die Analyse des Posphorylierungsstatus mehrerer bekannter Phosphoproteine der Thylakoide in der cas-Mutante deutete weiterhin auf einen potenziellen Defekt bei der Dephosphorylierung des wichtigen Lichtsammelproteins LHCII unter Starklichtbedingungen. Dieses Ergebnis lässt auf eine mögliche Rolle von CAS bei der Vermittlung der Aktivität der TAP38-Phosphatase, eines Gegenspielers der STN7 Kinase, schließen.

Neben der posttranslationalen Modifikation von CAS wurde eine mögliche Beteiligung von CAS im „circadian“ Netzwerk der Chloroplasten untersucht. RT-PCR-Analysen zeigten, dass die Transkription des CAS einem regelmäßigen Tagesrhythmus folgt, wobei der höchste Transkriptionslevel am Ende der Nacht und der niedrigste am Ende des Tages gefunden wurde. Interessanterweise scheint der Level des gebildeten CAS-Proteins einem um 12 Stunden versetzten Rhythmus zu folgen, was auf eine physiologische Anforderung für größere Mengen an CAS während des Tages schließen lässt.

Basierend auf den Ergebnissen dieser Arbeiten wird ein mögliches Arbeitsmodell diskutiert, das die Phosphorylierungsprofile und die circadiane Regulierung mit einer Beteiligung von CAS in den Photo-Akklimatisierungsreaktionen verbindet.

4 Introduction

4.1 Photosynthesis: the light-dependent primary reactions

In all photosynthetic organisms, solar radiation is used to produce chemical energy to sustain metabolism during growth and development. In higher plants and algae, photosynthesis takes place in a specialized organelle, the chloroplast, where all the components of the photosynthetic machinery can be found on a membrane network known as the thylakoids (Figure 1). Primary photochemistry reactions are initiated by the harvesting of light energy by two functionally linked, pigment-containing protein complexes known as Photosystem II and I (PSII and PSI) (Witmarsh and Govindjee, 2002, Busch and Hippler, 2011). PSII and PSI capture light energy via their antenna systems, consisting of a diverse set of chlorophyll-binding proteins known as the Light harvesting Complexes (LHCs) and then funnel it towards their respective reaction centers via resonance transfer mechanisms.

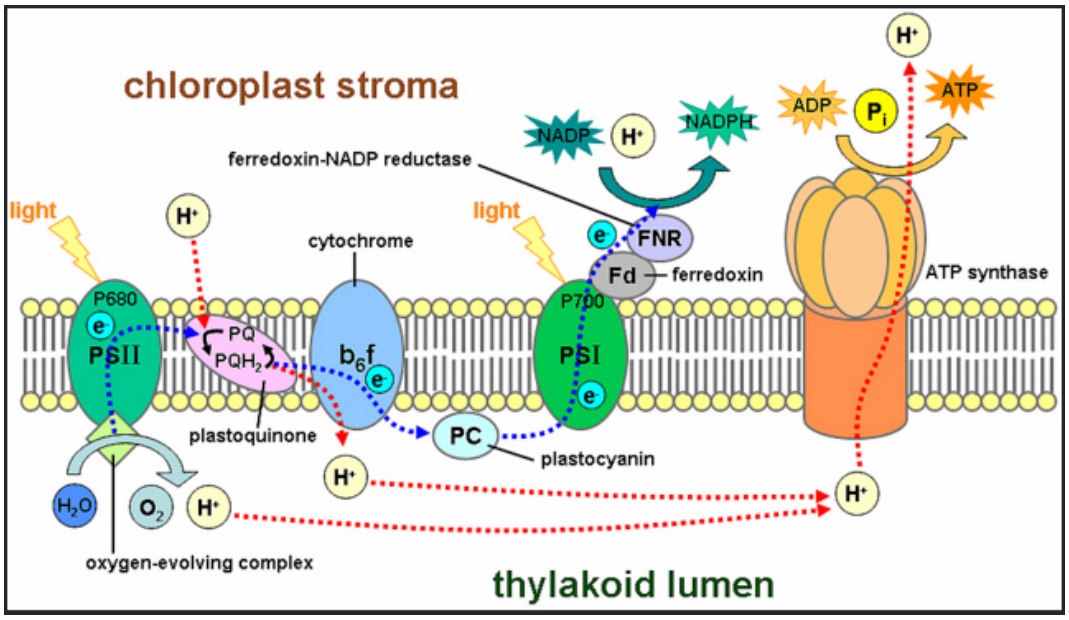

Figure 1: The photosynthetic apparatus

PSII and PSI then perform the essential steps of photochemistry, which truly represent the most important chemical reactions on earth, enabling the existence of complex ecosystems. At PSII, light-derived energy activates the process of water splitting, resulting in the removal of electrons and protons (H^+) from H_2O molecules and leading to oxygen evolution – hence the definition oxygenic photosynthesis. Light harvesting at the level of PSI promotes the oxidation of intersystem components and further flow of electrons. By operating in parallel, PSII and PSI initiate a linear electron flow (LEF) that involves a series of redox exchange reactions and results in the stepwise transfer of electrons between the two major complexes embedded in the thylakoid membrane, the plastoquinone pool and the cytochrome b_6f. This transfer of electrons, coupled to the creation of a proton gradient across the thylakoid membrane, ultimately fuels the production of reducing equivalents in the form of adenosine triphosphate (ATP) and nicotinamide adenine dinucleotide phosphate (NADPH), via the ATP synthase and the enzyme ferrodoxin $NADP^+$ reductase, respectively. The high-energy organic compound NADPH is then used as electron donors in the following reactions of photosynthesis - collectively referred to as the Calvin Benson Bassham Cycle cycle (CBB) – to promote the enzyme-catalyzed fixation of atmospheric CO_2 and the synthesis of energy-storing carbohydrate macromolecules.

4.2 The chloroplast: structural organization and functions

The chloroplast is not just the site where photosynthesis occurs, but it hosts many important metabolic processes such as the partial or whole synthesis of pigments, fatty acids and plant hormones. Moreover, it also acts as sensor of various environmental cues. Just like the mitochondrion, the other major organelle of the eukaryotic cell, the chloroplast is a semiautonomous organelle, meaning that it is able to synthetize a fraction of its own proteins but yet it largely depends on the products of nuclear genes. The chloroplasts is in fact described as the product of an endosymbiotic event that occurred about 1.6 – 1.5 billion years ago, in which a heterotrophic eukaryotic host engulfed an autotrophic, photosynthetic prokaryotic bacterium (Keeling, 2010, Zimorski et al., 2014, Schimper, 1883, Sagan, 1967).

Over the course of evolution a significant proportion of the bacterial ancestral genome was transferred to the nucleus, leaving the chloroplast genome with a current set of about 80 – 100 protein coding genes that are mainly involved in the process of photosynthesis and transcription and translation (Sugiura, 1995).

The size of the chloroplast proteome – i.e. the number of chloroplast localized proteins – is estimated between 2000 and 4000 proteins, while the currently annotated proteome contains about 1565 proteins (Huang et al., 2013). Most of the proteins that compose its proteome, including those belonging to the photosynthetic apparatus, are nuclear encoded and thus synthetized in the cytoplasm and must be post-translationally imported as precursor proteins into the organelle (Strittmatter et al., 2010). A defining feature of most known nuclear-encoded chloroplast-localized proteins is the presence of an N-terminal amino acid extension referred to as transit peptide (TP) that is required to guide the precursor protein towards the organelle and to promote its transport via the chloroplast import machinery (Bruce, 2000). Despite the larger control exerted by the nucleus over chloroplast functions, the organelle is nonetheless able to influence nuclear gene expression according to its metabolic and developmental status by a series of processes known as retrograde signaling (Leister, 2012). Retrograde signals are sent from the organelle in the form of metabolic intermediates or relatively long lived reactive oxygen species (ROS) and are able to activate intracellular signaling pathways that ultimately lead to specific transcriptional responses in the nucleus (Chan et al., 2016). Importantly, the chloroplast is able to send to the nucleus specific information concerning the functionality of the photosynthetic apparatus, thereby achieving acclimation in response changes in the light environment (Gollan et al., 2015, Tikkanen et al., 2012a).

The chloroplast itself is surrounded by a double membrane system and includes an aqueous compartment - the stroma - in which a network of interconnected flattened membranes - the thylakoids - physically separates the stromal environment from a second continuous inner aqueous phase known as the thylakoid lumen. Two major regions can be defined within the thylakoid membrane system: the grana and the stroma lamellae.

While the grana are composed of several layers of stacked piles of compact thylakoid membranes – known as *cisternae* – the stromal lamellae are mostly single layer elongated membrane sacks that interconnect several grana (Austin and Staehelin, 2011).

This special structural organization allows a spatial distribution and segregation of the main components of the photosynthetic apparatus within specific regions of the thylakoid system - a feature known as lateral heterogeneity (Pribil et al., 2014). In fact, while the PSII complexes are found almost exclusively in the grana stacks and on their margins, PSI and the ATP synthase are enriched in the stroma lamellae. A defining feature of the thylakoids is their plasticity and ability to undergo substantial structural rearrangements in response to environmental cues, especially to the fluctuations of the light environment (Anderson et al., 2012, Kirchhoff, 2013).

4.3 Fluctuations of the light environment and their impact on photosynthesis

Photosynthetic operating efficiency can be severely limited under both biotic and abiotic stress conditions. Often, multiple stressors such as temperature extremes, water scarcity and strong irradiation occur simultaneously, thus exacerbating their negative impact on photosynthesis and imposing dramatic constraints on the physiology of the organism.

Of all the challenging situations that photosynthetic organism can possibly face, the sudden and frequent fluctuations in light quality and quantity are probably the most frequent (Kaiser et al., 2018).

Primary photochemical reactions can be inhibited by high irradiation. In particular, PSII is extremely sensitive to high light conditions and some components of the PSII centers can undergo irreversible damage following sustained stress. This situation is counteracted by a continuous activity of removal of damaged PSII core components, their *de novo* synthesis and newly insertion – a process known as the PSII repair cycle (Theis and Schroda, 2016). Moreover, due to the differences in the spectral properties of the specific chlorophyll species that are found in PSII and PSI reaction centers, the two photosystems are poised to slightly different wavelengths of optimal maximum absorption, i.e. 680 nm (red-shifted, R) and 700 nm (far red-shifted, FR) for PSII and PSI, respectively.

The composition of light spectrum can in fact change dramatically during the day both on a regular, predictable basis and unexpectedly. The incident photosynthetic active radiation (PAR) can be selectively enriched in the far-red component of the spectrum at dawn and dusk, or inside dense canopies, where the shading effect of above standing plants can filter the red-shifted wavelengths producing an enrichment of far-red wavelengths. In addition, the chlorophyll fluorescence that is reflected by neighboring plants can also create a light environment that is selectively enriched in the far-red spectrum. In normal midday conditions the ratio between the incident red and far red light (R/FR ratio, 660nm/730nm) is usually 1.2, but at twilight and under dense forest canopies it can reach values of 0.96 and 0.13, respectively (Smith, 1982). Depending on the prevailing condition, these differences in the light quality can lead to the preferential excitation of the two photosystems, altering the net fluxes of electrons and leading to over-reduction and over-oxidation of intersystem components. This situation may ultimately result into severe imbalances in the ability of the photosynthetic machinery to couple light harvesting with its conversion into chemical energy.

4.4 Photosynthetic acclimation strategies to fluctuating light

The evolution of photosynthesis has proceeded hand in hand with the acquisition of a series of protective mechanisms that allow organisms to optimize their photochemical performance under stress (Goss and Lepetit, 2015). Photosynthetic organisms exploit multi-layered acclimation strategies to cope with variations in the light environment thus ensuring proper functionality of the photosynthetic apparatus under limiting light, while minimizing the potential damage to its components under high light irradiance (Tikkanen et al., 2012b, Rochaix, 2014, Tikkanen and Aro, 2014, Pinnola and Bassi, 2018). Temporary imbalances in the relative excitation of the two photosystems activate compensatory mechanisms that relieve the excitation pressure on the photosynthetic apparatus and prevent the inhibition of photochemical reactions. These rapid acclimation responses are usually activated by the sensing of the redox status of intersystem components by specific sensor proteins, which are activated by over-reduction or over-oxidation of intersystem components or via pH-dependent mechanisms initiated by the massive buildup of proton concentration in the lumen compartment.

In general, the process of dissipation of excitation energy is achieved through the release of excess energy in the form of heat via a series of mechanisms collectively known under the term of Non-Photochemical Quenching (NPQ). Indeed, NPQ consists of several converging and differentially regulated pathways operating in the scale of seconds to hours. Of these, the fast, reversible, energy-dependent (pH-dependent) component qE is the best studied and is considered the main contributor against photoinactivation and photodamage by promoting the thermal dissipation of excess excitation energy (Muller et al., 2001). In plants, this process is mediated by the PsbS protein (Roach and Krieger-Liszkay, 2012) and by its homolog LHCSR3 in the green alga *Chlamydomonas reinhardtii* (later referred to as *C. reinhardtii*) (Bonente et al., 2011).

Under prolonged light stress, additional long-term acclimation strategies can be put in place by photosynthetic organisms, which include the rearrangement of the thylakoid architecture and of the supramolecular organization and stoichiometry of photosynthetic complexes. Additional control of photosynthesis is achieved through regulatory mechanisms that operate in a light-independent mode and rely on feedback signaling from the metabolic status of the cell and its interaction with circadian rhythms (Atkins and Dodd, 2014, Dodd et al., 2015) via the expression of the so called photosynthesis-associated nuclear genes (PhANGs).

4.5 State Transitions and phosphorylation-mediated photoacclimation

One of the best studied short-term regulatory acclimation mechanism that higher plants utilize to ensure optimal photosynthetic performance under fluctuating light conditions is the so-called phenomenon of “state transitions” (Minagawa, 2011). This process is used to balance the relative excitation of the two photosystems by relocating a mobile portion of the Light Harvesting Complex proteins of PSII (LHCII) between PSII and PSI. By doing so, the cross section of the antenna system of PSII and PSI can be dynamically adjusted according to the prevailing light environment in order to optimize their photochemical activity.

State transitions operate on a time scale of minutes and are believed to restore the photosynthetic redox poise of the electron transfer chain (Clausen et al., 2014).

This process is mediated by the reversible phosphorylation (Cohen, 2000) of residues of the Light Harvesting Chlorophyll *a/b* Binding protein 1 and 2 (Lhcb1 and Lhcb2) (Bennett, 1977) and Lhcb4.2 (Tikkanen et al., 2006) by the thylakoid-localized protein State Transition Kinase 7 (STN7) (Bellafiore et al., 2005, Rochaix et al., 2012).
Phosphorylation of mobile LHCII is activated under low light irradiance that preferentially drives PSII photochemistry (state 2). In this situation, the preferential excitation of PSII leads to the over-reduction of the plastoquinone pool, resulting in an imbalance of the redox state of the photosynthetic ETC. The binding of the reduced plastoquinone to a specific site of the cytochrome b_6f in turn activates the STN7 kinase, which phosphorylates the LHCII (Kruse, 2001). This process is reversed upon light to dark transition and by light conditions that preferentially drive photochemistry at PSI (state 1), such as a FR enriched light environment. Active dephosphorylation of LHCII is required for returning to state 1 - a process that is accomplished by the thylakoid-associated protein phosphatase TAP38 (Pribil et al., 2010).

Upon high light conditions the activity of STN7 on LHCII is abolished and only minor phosphorylation of LHCII is detected (Mekala et al., 2015). Instead, under these circumstances a close paralog of STN7, the protein State Transition Kinase 8 (STN8) is active and phosphorylates several components of the PSII core, namely the D1, D2 and CP43 proteins (Vainonen et al., 2005). PSII reaction centers are in fact extremely susceptible to photoinhibition under high light stress and they regularly undergo irreversible damage. For this reason, the role of STN8 has been connected with the fine tuning of the repair cycle of damaged PSII reaction centers (Baena-Gonzalez et al., 1998), where it participates in the process of controlled removal of damaged PSII core proteins and induces macroscopic rearrangements in the architecture of thylakoid membranes (Fristedt et al., 2009).

The availability of *stn7*, *stn8* and *stn7/stn8* double mutants of the model plant *Arabidopsis thaliana* (later referred to as *A. thaliana*) has been instrumental in the understanding of the biological roles of these two proteins kinases. It enabled the establishment of precise kinase-substrate relationships, which, nevertheless, highlighted a significant overlap in their substrate specificity (Bonardi et al., 2005). A preferential localization was also described for the two kinases, with STN7 being mostly enriched in the stroma lamellae, whereas STN8 being found primarily in the grana region of thylakoids (Wunder et al., 2013).

4.6 Phosphorylation networks in the chloroplast: the current picture

Such as in the cytoplasm and other cellular compartments, reversible phosphorylation of chloroplast proteins has been described as a regulatory mechanism not only required to mediate short-term acclimation to the changing light environment but to regulate virtually all physiological processes of the organelle.

In fact, it is estimated that the size of the chloroplast phosphoproteome – the collection of proteins that undergo reversible cycles of phosphorylation – consists of over 420 entities and comprises proteins with functions that go beyond photosynthetic light reactions and includes metabolic enzymes of the CBB cycle and also components of the transcriptionally active chromosome – the protein synthesis machinery of the chloroplast (Baginsky, 2016).

Despite a relatively abundant plastid phosphoproteome, the number of characterized chloroplast-localized kinases and phosphatases is relatively small. To date, only 15 protein kinases, including STN7 and STN8, and 10 phosphatases have been experimentally unambiguously confirmed to reside in the plastid (Schliebner et al., 2008, Bayer et al., 2012).

The phosphorylation of chloroplast proteins does not only have an impact on the regulation of plastidial physiological processes but might activate intracellular signaling pathways that ultimately lead to the regulation of the expression of nuclear photosynthetic genes resulting in long-term acclimation responses (Bonardi et al., 2005, Tikkanen et al., 2006).

The current understanding of chloroplast phosphorylation networks (Schonberg and Baginsky, 2012, Baginsky and Gruissem, 2009) has been mainly derived from large-scale proteomics-based studies (Reiland et al., 2009), including mutants of known chloroplast protein kinases (Schonberg et al., 2017, Reiland et al., 2011), but is still far away from a comprehensive picture. Indeed, the majority of the described chloroplast phosphoproteins, in particular those involved in subtle regulatory processes, have not been yet characterized in terms of their client kinase, nor the regulation behind their transient modification(s).

4.7 The Calcium Sensing Receptor: a poorly characterized chloroplast phosphoprotein

One of the less functionally characterized chloroplast phosphoprotein is the Calcium Sensing Receptor (CAS). CAS is a nuclear encoded protein of 387 amino acids and 40 kDa (mature size: 354 amino acids and 35 kDa) (Weinl et al., 2008), whose plastid localization is also strongly supported by several *in silico* prediction tools by possessing a classical N-terminal transit peptide sequence (Figure 2). *In silico* prediction tools define two main protein domains of CAS interrupted by a predicted transmembrane domain (TMD): an N-terminal domain (NTD) with proposed Ca^{2+} binding activity and a C-terminal domain (CTD), which is described as the target of phosphorylation. This latter domain is predicted to containing two potential functional sub-domains: a Rhodanese Homology Domain, lacking any functional characterization and a region of amino acids with potential protein-protein interaction ability.

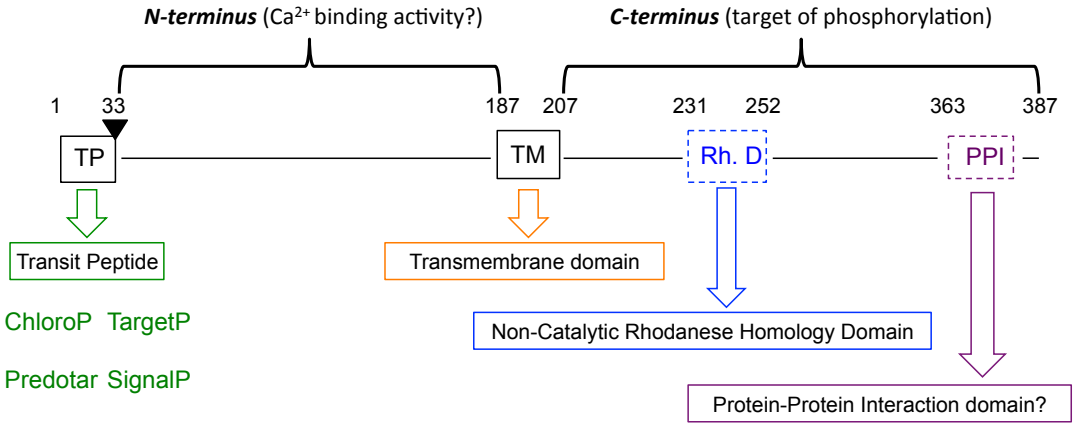

Figure 2: Schematic representation of the predicted structure of the CAS protein

CAS orthologs are found in green algae and higher plants but not in cyanobacteria. So far, no precise molecular activity has been yet assigned to CAS. At least in *A. thaliana*, this protein has been described to be involved in a number of physiological processes, ranging from the regulation of stomatal closure (Nomura et al., 2008, Weinl et al., 2008) and the activation of retrograde signals (Guo et al., 2016) to the modulation of immunity-related gene expression (Nomura et al., 2012).

The name CAS itself originated from the initial description of the ability of its NTD to bind Ca^{2+} *in vitro* (Han et al., 2003), a notion further supported by experimental evidence for its involvement in mediating both chloroplastic and cytosolic transient oscillations of free Ca^{2+} in response to external stimuli (Nomura et al., 2012, Nomura et al., 2008, Weinl et al., 2008). Nevertheless, no mechanistic insight regarding the function of CAS in shaping intracellular Ca^{2+} oscillations has been provided. Intriguingly, the proposed role of CAS in mediating stomatal closure appears to require both cytosolic Ca^{2+} transients together with the production of hydrogen peroxide (H_2O_2) at the level of thylakoid membranes, highlighting a possible CAS-mediated crosstalk between these two independent signaling pathways (Wang et al., 2016). In *C. reinhardtii* CAS was shown to be required in the acclimation response to high light stress by promoting the process of thermal energy dissipation NPQ (Petroutsos et al., 2011). In the same model organism, CAS was described to physically interact with some components of the PSII-independent electron route known as cyclic electron flow (CEF) (Terashima et al., 2012). The CEF represent an alternative electron transfer pathway exclusively active around PSI that contributes to the generation of the proton gradient across the thylakoid membrane and ATP synthesis without the accumulation of $NADPH_2$. It is thus believed to serve as a photoprotective mechanism with a central role in the fine-tuning of photosynthesis (Yamori and Shikanai, 2016).

When CAS was described as a phosphoprotein in *A. thaliana,* it was assigned as a substrate of the STN8 kinase and its modification on a specific threonine residue (Thr-380) was suggested to occur in response to increasing light intensity (Vainonen et al., 2008).

Later, CAS was identified, among several other candidates, as a target of Ca^{2+}-regulated phosphorylation in the chloroplast (Stael et al., 2012a). All these evidences already pointed to a differential regulation of the activity of CAS via phosphorylation, possibly mediated by different protein kinases responding to different stimuli and targeting different residues.

A number of potential *in vivo* phosphorylated residues of CAS have experimentally described in large-scale phosphoproteomics studies and they can be found in publicly available databases such as *PhosPhAt 4.0* (Arsova and Schulze, 2012). Nevertheless, the identity of these residues as true *in vivo* targets of kinases has not been confirmed via complementary experimental approaches. In general, the biological significance of the phosphorylation event(s) of CAS still remains largely elusive as well as the regulation behind it. Also, the involvement of CAS in the regulation of photosynthetic processes has not been explored in detail, nor has the role of its phosphorylation been functionally investigated in this context.

5 Aim of the work

Aim of this work was to investigate the differential phosphorylation of the chloroplast-localized protein Calcium Sensing Receptor (CAS) and to explore the regulation behind its post-translational reversible modification, with a special attention to the roles of Ca^{2+} and light.

A major focus of the work was the elucidation of the protein kinases involved in the phosphorylation of CAS and, in particular, the study of the involvement of the two main thylakoid-localized protein kinases State Transition Kinase 7 and 8 (STN7, STN8).

The analysis of the phosphorylation profile of CAS was directed at the level of individual residues and took advantage of a bioinformatics analysis of the evolutionary conservation of a number of predicted phosphorylation sites of the *A. thaliana* protein isoform and their subsequent characterization *in vitro* via biochemical approaches.

Guided by the analysis of cellular, biochemical and physiological parameters, this work undertook a functional and structural characterization of the CAS protein and of its phosphorylation profile and tried to fill some of the current gaps in the understanding of the role of phosphorylation-mediated dynamic photosynthetic acclimation.

6 Materials and Methods

6.1 Plant methods

6.1.1 Plant material and growth conditions

The *A. thaliana* ecotype Columbia 0 (Col-0) was used as wild type in this work for all biochemical and physiological experiments. Previously described mutant lines used in this work were *cas-1* (SALK_070416), *stn7* (SALK_073254), *stn8* (SALK_060869), *stn7*/*stn8* double mutant (kind gift of Prof. Eva Mari Aro, University of Turku, Finland) and *cca1* (kind gift of Prof. George Coupland, Max Planck Institute for Plant Breeding Research, Cologne, Germany). Plants were grown on soil (Floradur, Floragard, Oldenburg, Germany) under controlled conditions in a growth chamber under a 16h/8h day/night regime under 100 µmol photons $m^{-2}s^{-1}$ illumination (growth light, GL). Tobacco plants (*Nicotiana benthamiana*) were used for Agrobacterium-mediated infiltration and transient expression of constructs for microscopy-based localization and topology analyses.

6.1.2 Chloroplast isolation, fractionation and isolation of total leaf protein extracts

Intact chloroplasts were purified from 4-week-old *A. thaliana* plants as previously described (Seigneurin-Berny et al., 2008) starting from leaf material that was harvested at the end of the dark period or after 4 hours of acclimation to GL. Intact chloroplast pellets were frozen in N_2 (l) and stored at 193 K (-80°C) for further use.

Thylakoid membrane and stromal protein fractions were obtained as previously described (Rocha et al., 2014) by disrupting intact chloroplasts in lysis buffer (20 mM Tricine (pH 7.6), 10% (v/v) glycerol and 1 mM DTT) supplemented with protease inhibitors (complete™, EDTA-free; Roche, Mannheim, Germany) and, depending on the type of experiment, with phosphatase inhibitors (Phospho-Stop; Roche, Mannheim, Germany). After incubation on ice for 15 min, the membrane and the soluble stromal fractions were separated by centrifugation at 20000 g for 10 minutes and the pellet corresponding to the thylakoid-enriched fraction was washed several times with lysis buffer in order to remove stromal contamination or loosely attached proteins. All procedures were carried out at 4°C.

Total leaf protein extracts were prepared starting from 100 mg of fresh tissue according to the method described in (Martinez-Garcia et al., 1999). Protein concentration of protein extracts was determined by using the Coomassie Bradford protein assay kit (Life Technologies,

Darmstadt, Germany) according to manufacturer's instructions. Chlorophyll concentration was determined as previously described (Porra et al., 1989) after extraction with 80% acetone.

6.1.3 Agrobacterium-mediated transient transformation of tobacco, protoplast preparation and fluorescence microscopy

Agrobacterium-mediated transient transformation of tobacco leaf cells was performed as previously described (Voinnet et al., 2003). Briefly, *Agrobacterium tumefaciens* strain LBA1334 was transformed with the constructs of interest via electroporation. Transformed *Agrobacteria* were grown overnight in LB medium supplemented with 50 mg/ml kanamycin in 5 ml culture volume. Cells were harvested by centrifugation and resuspended in agromix solution containing 10 mM MES pH 6.0, 10 mM $MgCl_2$ and 200 µM acetosyringone until a final OD 600 of 1.0 was reached. After a 2 hours incubation at 30°C, the cell suspensions were used to infiltrate or co-infiltrate leaves of 3 - 4 weeks old tobacco plants. Infiltrated leaves with transiently expressed and co-expressed proteins of interest were harvested after 48 hours and used for protoplast isolation as described previously (Koop et al., 1996).
The subcellular localization of protein was analysed using a Leica TCS SP5 confocal laser scanning microscope (Leica Microsystems, Germany) and image processing was performed using the Leica Application Suite for Advanced Fluorescence (LAS AF) software.

6.1.4 Analysis of growth and photosynthetic performance under drought

The analysis of growth and photosynthetic performance of the *A. thaliana* wild type, *cas*, *stn7* and *stn8* mutants under normal and drought stress conditions was performed in collaboration with Dr. Klara Panzarova at PSI (Photon System Instruments, Brno, Czech Republic) using the PlantScreen™ (PSI, Czech Republic) phenotying system and applying previously described screening protocols (Awlia et al., 2016). Seeds of the four *A. thaliana* lines were sown and stratified for 2 days at 4°C in the dark and seedlings were grown in a climate controlled growth chamber (FS_WI, PSI, Czech Republic) under cool-white LED and far-red LED lighting with the following environmental parameters: 16 h light/8 h dark regime; standard white LED illumination (~ 120 µE) with 25% (5.5 µE) far-red; 22°C/19°C, respectively and 60 % humidity.

The watering regime for the control plants was set at 60 % of the soil water-holding capacity at 100% according to a previously described protocol (Awlia et al., 2016).

Ten healthy seedlings (seven days old) of similar size for each genotype were subsequently transplanted into 150 ml pots with soil watered 3 hours prior to the transplantation up to 60% of the full water holding capacity. All pots were automatically weighed and watered every third day inside the PlantScreen™ Compact System (PSI, Czech Republic) to reach and maintain the reference weight corresponding to the desired soil-water content.

When seedling reached 16 days of age, all pots (total 80) were randomly placed in trays (5 × 4 pots per tray), registered in the PlantScreen™ server and equally distributed into one of the two watering regimes: 60% and 0%.

The drought stress application protocol started on day 18 and continued until water-stressed plants reached wilting (day 30). Control and water-stressed plants were automatically phenotyped for RGB and kinetic chlorophyll fluorescence traits using the PlantScreen™ system. To do so, trays were transported within the PlantScreen™ unit on conveyor belts between the light-isolated imaging cabinets, weighing and watering station and the dark/light acclimation chamber. A single round of measurement consisted first of an initial 15 minutes dark-adaptation period inside the acclimation chamber followed by chlorophyll fluorescence and RGB imaging, weighing and watering. To assess plant growth and morphological traits, RGB images (resolution 2560 × 1920 pixels) of 5 × 4 plants per tray were captured using the GigE uEye UI-5580SE- C/M 5 Mpx Camera (IDS, Germany) from the top view.

To extract features from the RGB images the PlantScreen™ system performs a separation of the background from the plant shoot tissue allowing the pixel number per plant and rosette area to be counted. Pixel count, color and fluorescence intensity were subsequently evaluated from the captured images using the PlantScreen™ Data Analyzer Software (PSI, Czech Republic). To assess the effect of water stress on the photosynthetic performance, chlorophyll fluorescence data were acquired using an enhanced version of the FluorCam FC-800MF pulse amplitude modulated (PAM) chlorophyll fluorometer (PSI, Czech Republic).

This chlorophyll imaging station is mounted on a robotic arm with an LED light panel and a high-speed charge-coupled device camera (pixel resolution of 720 × 560, frame rate 50 fps and 12-bit depth) positioned in the middle of the light panel. The LED panel is equipped with 3 × 64 orange-red (618 nm) and 64 cool-white LEDs (6500 K).

For the examination of the impact of the drought stress in the four *A. thaliana* genotypes, the rate of photosynthesis was quantified at different photon irradiances using a light curve protocol (Henley, 1993), which is known to provide detailed information on chlorophyll fluorescence under different stress conditions. To do so, after the 15 minutes dark-adaptation period, when PSII reaction centers open, the trays were automatically transported to the chlorophyll fluorescence imaging cabinet. A 5 seconds flash of a weak measuring light was applied to measure the minimum level of fluorescence in the dark-adapted state (F_o), followed by a saturation pulse of 800 milliseconds (with irradiance of 1200 μmol m^{-2} s^{-1}) used to determine the maximum fluorescence in the dark-adapted state (F_m).

Plants were relaxed in the dark for 17 seconds and then subjected to 70 seconds of cool-white actinic lights to drive photosynthesis and measure the peak rise in fluorescence (F_p).

Next, 5 minutes intervals of cool-white actinic light at 35, 125, 250, and 1194 μmol m^{-2} s^{-1}, corresponding to the L1, L2, L3, and L4 steps, respectively, were applied. Four saturation pulses were applied during each step of the actinic light treatment to acquire the maximal fluorescence in the light-adapted state (F_m'), with the chlorophyll fluorescence signal being measured just before the application of the saturation. The chlorophyll fluorescence parameters were extracted and processed using the PlantScreen™ Data Analyzer Software and the values for commonly used parameters were obtained using known formulas (Rungrat et al., 2016, Baker, 2008). The F_v/F_m parameter, known as the maximum quantum efficiency of PSII, was calculated using the formula: $(F_m - F_o)/F_m$. The operating efficiency of the primary photochemistry in PSII (ΦPSII, here referred to as QY) was measured for each time point corresponding to application of the saturating light flash during the curves of increasing light intensity using the formula: $F_q'/F_m' = (F_m' - F')/F_m'$, where F_q' is the difference between F_m' and F'. Measures of F_q'/F_m' in light-adapted plants indicate photosynthetic efficiency, or what proportion of the absorbed light is being utilized for photochemistry.

NPQ was calculated from the ratio of change in F_m and F_m' during the illumination as shown in the equation: $NPQ = (F_m - F_m')/F_m'$.

6.1.5 Analysis of chlorophyll fluorescence emission spectra at 77K

The analysis of chlorophyll emission spectra at 77K was performed in collaboration with Dr. Larosa Veronique (University of Liege, Belgium). Chlorophyll fluorescence emission spectra were recorded at 77K (-196°C) from frozen isolated thylakoids. Thylakoid membranes were extracted as previously described (Tikkanen et al., 2006) from leaves of 3 weeks old plants after the following light treatments: end of night (dark, D), 2 hour of growth light (100 μmol $m^{-2} s^{-1}$, GL) and 2 hours of high light (1000 μmol $m^{-2} s^{-1}$, HL; after 2 hours of acclimation in GL). Briefly, leaves were flash frozen in liquid nitrogen and grinded into powder in a homogenization buffer containing 50 mM Hepes/KOH, pH 7.5, 330 mM sorbitol, 2 mM EDTA, 1 mM $MgCl_2$, 5 mM ascorbate, 0.05% (w/v) BSA and 10 mM of the phosphatase inhibitor NaF. All steps were performed at 4°C and under dim green light illumination.

The material was subsequently filtered through Miracloth and pelleted by centrifugation at 2500 g for 4 minutes at 4°C followed by a second wash step in homogenization buffer.

For measurements, thylakoids were diluted to a concentration of 1 μg/ml chlorophyll. Chlorophyll fluorescence emission was measured from frozen thylakoids by exciting the samples at 480 nm and recording the emission spectrum between 650 and 800 nm using an Ocean Optics QE Pro Spectrometer. Three biological and technical replicates for each genotype and treatment were measured.

6.2 Nucleic acid methods and molecular cloning

6.2.1 Generation of CAS expression constructs

The CAS-C construct for expression in *E. coli*, corresponding to a fragment including amino acid positions 216 to 387 of the CAS protein, was cloned into the pTWIN1 vector (New England Biolabs, Frankfurt, Germany) by Stael and coworkers and provided as a kind gift (Stael et al., 2012a). All non-phosphorylatable/phospho-mutant CAS-C variants (CAS-C_{T350V}, CAS-C_{S373A}, CAS-C_{T376V}, CAS-C_{S378A}, CAS-C_{T380V}) were obtained by performing QuickChange site directed mutagenesis (Zheng et al., 2004) on the original CAS-C construct using partially overlapping primers that contained mismatches for selected serine and threonine residues, allowing their conversion into alanine and valine, respectively.
PCR reaction products were treated with *Dpn*I enzyme in order to digest the template vector DNA and subsequently transformed in *E. coli* DH5α cells for plasmid amplification.
The CAS-N fragment (without the N-terminal transit sequence) was cloned into the pTWIN1 following the manufacturer's instructions. To this end, the sequence corresponding to amino acid positions 34 to 147 of CAS was amplified by PCR from *A. thaliana* cDNA using primers containing the restriction sites for *Nco*I and *Pst*I. The amplified PCR product was thus cloned in-frame with an N-terminal intein tag.

The CAS-YFP construct, used for localization analysis *in planta*, was obtained by fusing the full-length CAS coding sequence (AT5G23060, amino acids 1-387) N-terminally to the yellow fluorescent protein (YFP) under the control of the 35S-promotor. Cloning was performed using *Apa*I and *Not*I restriction sites into the plant expression vector pBIN19 (Datla et al., 1992). A truncated variant of this construct (ΔTP-CAS-YFP), lacking the first 33 amino acids corresponding to the predicted transit peptide (TP), was generated in an identical fashion.

For the use of the self-assembly green fluorescent protein (saGFP) system (Cabantous et al., 2005), the full-length coding sequences of CAS was cloned into the pBIN19-saGFP$_{1–10}$ and pBIN19-saGFP$_{11}$ vectors using *Apa*I and *Not*I restriction sites, thereby creating the fusion constructs saCAS-GFP$_{1-10}$ and saCAS-GFP$_{11}$, respectively. A similar cloning strategy was employed in order to create a stromal marker that could be used as the interacting partner for reconstituting the full-length GFP.

In this case, the full-length coding sequence of the Ribulose-1, 5-bisphosphate carboxylase/oxygenase small chain 1A (RBCS-1A; AT1G67090.1) was used to create the saRUBISCO-GFP$_{1-10}$ and saRUBISCO-GFP$_{11}$ constructs.

6.2.2 RNA isolation, cDNA synthesis and RT-qPCR conditions

RT-qPCR analyses were performed in collaboration with Dr. Valentino Giarola (IMBIO, University of Bonn, Germany). Total RNA was extracted from 100 mg of 3 weeks old previously frozen *A. thaliana* leaf samples using the innuPREP Plant RNA Kit (analytic jena, Jena, Germany) according to manufacturer's instructions. The concentration and purity of the RNA samples were determined by measuring the OD 260, 280, 230 using a Biospec-nano spectrophotometer (Shimadzu Biotech, Japan). The RNA integrity was additionally assessed on a 2.0% (w/v) agarose gel (data not shown). To remove any genomic DNA contamination, 4 µg of total extracted RNA were treated with the enzyme *DNase I* (Thermo Fisher Scientific, St Leon-Rot, Germany). *DNase I*-treated RNA (2 μg) was subsequently reverse transcribed using the RevertAid Reverse Transcriptase (Thermo Fisher Scientific, St Leon-Rot, Germany) following manufacturer's instructions, while the remaining 2 µg of RNA served as negative control for the reverse transcription reaction. cDNA samples were diluted 15 times with diethylpyrocarbonate-treated (DEPC) water and 5 µl were utilized as a template for 20 µl PCR reactions.

Specific primers for the CAS gene to be used in the RT-qPCR analysis were designed to amplify a 102 bp fragment in the 3′ region of the CAS transcript using the Primer3 software (version 0.4.0) (Untergasser et al., 2012, Koressaar and Remm, 2007). The resulting target sequences were checked in order to exclude the potential risk of secondary structures using the M-fold web server (http://mfold.rit.albany.edu/?q=mfold/DNA-Folding-Form) using corrections for ionic conditions of 50 mM Na^{2+} and 25 mM Mg^{2+} (Zuker, 2003).

The reference gene used for the normalization of relative transcript abundance was PDF2 (regulatory subunit of protein phosphatase 2A, PP2A, AT1G13320). PDF2 primers were retrieved from a published list of stably expressed superior reference genes (Czechowski et al., 2005).

The evening-peaking cycling gene TOC1 gene (Timing of CAB expression 1, AT5G61380) was used as an internal control for diurnally regulated gene expression. Primers specific for TOC1 transcript were retrieved from published studies (Wenden et al., 2011).

PCR amplification efficiencies were estimated using standard curves with cDNA dilutions spanning four sequential dilutions (1:5) (Supplementary Figure 4), while the primer specificities were confirmed by analysing the profile of the melting-curve after the amplification of the subsequent RT-qPCR analysis (Supplementary Figure 5).

RT-qPCR analysis was performed as previously described (Giarola et al., 2015) in a 96-well plate (FrameStar® 96, 4titude, Surrey UK, 4ti-0960/C), using Mastercycler® ep realplex2 (Eppendorf AG, Hamburg, Germany) and the Luminaris Color HiGreen qPCR Master Mix (Thermo Fisher Scientific, St Leon-Rot, Germany). PCR reactions were performed in a final volume of 20 µl. Each reaction contained 5 µl of diluted cDNAs, Luminaris Color HiGreen qPCR Master Mix (2×) and 0.35 µM of each primer.

The following conditions were used for the PCR: 95°C for 10 min, followed by 40 cycles of 95°C for 15 seconds, 60°C for 30 seconds and 72°C for 30 seconds followed by 95°C for 15 seconds. The melting curves were analysed at 60°C–95°C after 40 cycles in sequential steps by increasing the temperature in 0.5°C steps for 20 minutes. Controls for reverse transcription were included in the PCR reactions to reveal any DNA contamination.

Each PCR analysis was performed with three biological replicates and two technical replicates and the mean values were used for the analysis. The quantification cycle (Cq) for each amplification curve was determined using the CalQplexTM algorithm embedded in the realplex 2.2 software (Eppendorf AG, Hamburg, Germany). Cq and efficiency values were imported in qbasePLUS software V.1.3.5 (Biogazelle NV, Zwijnaarde, BE) to calculate relative abundance. PDF2 was used to normalize expression data of target genes CAS and TOC1. Relative abundance values were calculated by using the mean value of the sum of all biological and technical replicate samples.

6.3 Protein methods

6.3.1 Expression and purification of recombinant CAS fragments

Recombinant CAS-C and CAS-N fragments, including all non-phosphorylatable CAS-C variants, were expressed in *E. coli* strain ER2566 cells and purified under native conditions using the IMPACT™-TWIN system (New England Biolabs, Frankfurt, Germany) following manufacturer's instructions. Protein concentration of purified recombinant proteins was determined using the Coomassie Bradford protein assay kit (Life Technologies, Darmstadt, Germany) according to manufacturer's instructions.

6.3.2 SDS PAGE analysis and BN-PAGE gel electrophoresis

For SDS-polyacrylamide gel electrophoresis (SDS-PAGE) analysis, samples were mixed with a standard 4X SDS solubilization buffer (40% Glycerol, 240 mM Tris/HCl pH 6.8, 8% SDS, 0.04% bromophenol blue, 5% beta-mercaptoethanol), heated for 5 minutes at 96°C and loaded on 12.5% SDS-PAGE gels according to Laemmli (Laemmli, 1970). Gels were subsequently stained with Coomassie Brilliant Blue R250 and dried, if required by the specific experimental protocol.

The analysis of thylakoid membrane mega-complexes was performed as previously described (Jarvi et al., 2011) by loading the equivalent of 8 μg of chlorophyll per sample of thylakoid membranes isolated from plants after specific light treatments (see chapter 6.1.5 for a description of sample preparation procedure) on blue native PAGE gels. To visualize the PSI-LHCII "state transition complex" (STC), thylakoid membrane samples were treated with 1% digitonin, which is sufficient to promote the solubilisation of the less packed grana margins and stroma lamellae domains of thylakoid membrane.

6.3.3 Production of antibodies

Custom polyclonal primary antibodies were generated against different domains of the CAS protein. To this end, the above described (see chapter 6.2.1) CAS-C and CAS-N recombinant fragments were purified and used as immunizing antigens in immunosuppressed rabbits in order to produce the α-CAS-CT and α-CAS-NT antisera, respectively (Davids Biotechnologies, Regensburg, Germany).

6.3.4 Immunoblot analysis

Western blotting was performed by first separating the proteins on SDS PAGE followed by their transfer on a polyvinylidene (PVDF) membrane using a semidry blotting system. In most experiments thylakoid and total leaf protein extracts corresponding to 0.5 - 2µg chlorophyll were loaded (unless stated otherwise). For immune-detection of specific proteins, membranes were incubated after the transfer with primary antibodies overnight at 4°C in blocking buffer containing Tris-Buffered Saline solution (Sigma Aldrich, Saint Louis, MO, USA) supplemented with 0.01% (v/v) Tween® 20 (Sigma Aldrich, Saint Louis, MO, USA) (TBS-T) and 5 % (w/v) skim milk powder (SERVA, Heidelberg, Germany). After repeated washing with blocking buffer, membranes were further incubated with an anti-rabbit antibody coupled to horseradish peroxidase (HRP) (Sigma Aldrich, Saint Louis, MO, USA) and an enhanced chemiluminescence kit (SERVALight EOS, SERVA, Heidelberg, Germany) was employed to detect the signals using a Chemidoc Imaging System (BioRad).

The phosphorylation status of thylakoid proteins in response to different light treatments (dark, D; growth light, 100 µmol photons $m^{-2}s^{-1}$ GL; high light 1000 µmol photons $m^{-2}s^{-1}$, HL) was investigated using a commercially available threonine antibody (α–pThr) that reacts with phosphorylated threonine (Cell Signaling Technology, Danvers, Massachussets, USA) according to the manufacturer's instructions and the protocol previously described (Mekala et al., 2015). To this end, thylakoid membranes were isolated as described below (see chapter 6.1.5 for a description of sample preparation procedure) and a total amount of proteins equivalent of 0.5 µg of chlorophyll was separated on SDS-PAGE. In contrast to the Western Blot experiments described above, membranes were blocked and incubated in blocking buffer containing 5% (w/v) bovine serum albumin (BSA) instead of milk powder and 0.01% (v/v) Tween® 20.

6.3.5 Protease protection assay

For the immunodetection-based topology analysis of the CAS CTD and NTD, a protease (thermolysin) treatment of isolated thylakoids was performed as previously described (Torabi et al., 2014). To this end, isolated thylakoid membranes were first dissolved in HS buffer (0.1 M sucrose, 10 mM HEPES-NaOH, pH 8.0) at a final concentration of 0.5 mg chlorophyll/ml.

Depending on the type of sample, the detergent digitonin was included to a concentration of 1% (v/v) before the addition of the protease in a total volume of 100 µl reaction. Untreated and detergent-treated thylakoid samples were incubated with thermolysin (Sigma Aldrich, Saint Louis, MO, USA) in a concentration of 100 µg/ml and $CaCl_2$ 1mM. All steps were performed at 4°C. The digestion reaction was stopped by adding EDTA at a final concentration of 20 mM and 4× SDS-sample buffer followed by boiling at 96°C.

Digestion products were separated on SDS-PAGE and analysed by western blotting using α-CAS-CT and α-CAS-NT antibodies.

An antiserum for the OE23 oxygen evolving complex subunit 23 protein (kind gift from Prof. Jürgen Soll, LMU Munich, Germany) was used as a control for the degradation of luminal exposed protein domains.

6.3.6 In vitro phosphorylation assays

In vitro phosphorylation of recombinant CAS-C fragments were conducted as previously described (Stael et al., 2012a, Rocha et al., 2014) using ~100–200 ng of CAS-C substrates and catalytic amounts (equivalent to ~2 µg of chlorophyll) of *A. thaliana* thylakoid membranes. All assays were carried out for 10 minutes (unless stated otherwise) at room temperature (22°C) in a total volume of 25 µl kinase buffer containing 20 mM Tricine pH 7.6, 10 mM $MgCl_2$, 10% (v/v) glycerol, 1 mM DTT, 5 µM ATP and 70 – 180 kBq of [γ32-P] ATP (PerkinElmer, Waltham, MA, USA). Depending on the experiment, assays were conducted at ambient light, reproducing the growth light conditions in which the membranes had been isolated, or in dark and supplemented with 50 µM $CaCl_2$ or 2 mM EGTA.

Reactions were stopped by the addition of 4× SDS solubilization buffer and boiling at 96°C for 3 minutes. Reaction products were separated via SDS-PAGE, and the gel was stained overnight in Coomassie Brilliant Blue R250 solution and dried on filter paper. Phosphorylation signals were revealed by exposing dried gels to X-ray films (Carestream® Kodak® X-Omat LS film, Rochester, NY, USA) followed by film processing and development (AGFA G153 developer, Fix AG fixer, Mortsel, Belgium). Equal loading of thylakoid proteins and recombinant substrates for each assay are shown in Supplementary Figures 9 -14.

6.4 Proteomics methods

6.4.1 Preparation of surface-exposed peptides from thylakoid membranes

Intact chloroplasts from WT and *stn8* mutant plants were isolated as described after 4 hours of growth light (GL) exposure. Preparation of surface-exposed peptides from thylakoid membranes was performed as described (Rokka et al., 2011). Briefly, three independent chloroplast pellet preparation for each genotype were resuspended in 60 ml of the preparation buffer, and centrifuged for 5 minutes at 3000 g. Pellets were resuspended in 50 ml of lysis buffer (10 mM sodium phosphate, pH 7.8, 5 mM $MgCl_2$ and 10 mM NaF), and homogenized five times in a potter grinder followed by centrifugugation for 5 minutes at 7500 g.

Pellets of thylakoid membranes were washed twice with the wash buffer (100 mM sorbitol, 50 mM sodium phosphate, pH 7.8, 5 mM $MgCl_2$, and 10 mM NaF) and three times with 25 mM NH_4HCO_3 (pH 8.0) and 10 mM NaF. Thylakoids were centrifuged for 5 minutes at 6000 g after each resuspension. These washing steps were performed since they are known to promote the destacking of thylakoids, thereby increasing the accessibility of trypsin to the surface-exposed regions of thylakoid membrane proteins and NH_4HCO_3 is fully compatible with direct analyses by mass spectrometry. Finally, thylakoid pellets were resuspended to 3 mg of chlorophyll/ml in 25 mM NH_4HCO_3 to a final volume about 3 ml.

Thylakoid suspensions were incubated with sequencing-grade modified trypsin (Sigma Aldrich), (8 µg trypsin/mg chlorophyll) at 22°C for 3 h. Samples were flash frozen in liquid nitrogen, thawed, and the digestion products were centrifuged for 20 minutes at 14000 g. Subsequently, peptides were lyophilized to dryness in a vacuum concentrator. Enrichment of released phosphopeptides was performed using 5 mg of TiO2 (Glygen Corp.) as described previously (Bodenmiller et al., 2007, Chen et al., 2010) and dried in a vacuum concentrator.

6.4.2 LC-MS/MS phosphoproteomics analysis of phosphopepetides

LC-MS/MS analysis of phoshopeptides was performed in collaboration with Valentin Roustan at the department of Molecular Systems Biology (MOSYS) at the University of Vienna, Austria. Lyophilized samples were dissolved in 11 µl of 2% (v/v) acetone and 0.1% (v/v) formic acid and 5 µl of the mixture was separated on an EASY-Spray PepMap RSLC 75 µm × 50 cm column (Thermo Fisher Scientific Inc., Waltham, USA).

Peptides were eluted using a 160 minutes linear gradient from 2 to 40 % of mobile phase B (mobile phase A: 0.1 % (v/v) formic acid in water; mobile phase B: 0.1 % (v/v) formic acid in 90 % (v/v) aceton with 300 nl/min flow rate generated with an UltiMate 3000 RSLCnano system. Peptides were measured with an LTQ-Orbitrap Elite (Thermo) using the following mass analyser settings: ion transfer capillary temperature 275°C, full scan range 350-1800 m/z, FTMS resolution 120000. Each FTMS full scan was followed by up to ten data dependent (Bolouri Moghaddam and Van den Ende) CID tandem mass spectra (MS/MS spectra) in the linear triple quadrupole (LTQ) mass analyser. Dynamic exclusion was enabled using list size 500 m/z values with exclusion width ±10 ppm for 60 seconds.

Charge state screening was enabled and unassigned and +1 charged ions were excluded from MS/MS acquisitions. For injection control, automatic gain control for full scan acquisition in the Orbitrap was set to 5 x 105 ion population, the maximum injection time (max IT) was set to 200ms. Orbitrap online calibration using internal lock mass calibration on m/z 371.10123 from polydimethylcyclosiloxane was used. Multistage activation was enabled with neural losses of 24.49, 32.66, 48.999, 97.97, 195.94, and 293.91 Daltons for the 10 most intense precursor ions. Prediction of ion injection time was enabled and the trap was set to gather 5 x 103 ions for up to 50 milliseconds.

6.4.3 Data analysis and statistics

MaxQuant 1.5 (http://www.maxquant.org) and the Andromeda search algorithm were used against the TAIR-10 database to perform peptide identification, phosphorylation site mapping and phosphopeptide quantification (Cox and Mann, 2008, Cox et al., 2011).

Three missed cleavages were allowed. Methionine oxidation and protein N-terminal acetylation were endorsed as dynamic modifications. Additionally, phosphorylation of serine, threonine and tyrosine residues was permitted to occur as dynamic modifications.

Mass tolerance was set to 5 p.p.m. for parental ions and 0.5 Da for the MS/MS fragment.

For both peptide and protein levels, false discovery rate was set to 1%. Quantification was done at the peptide level. Perseus 1.5 software was used for further filtering and data processing (Tyanova et al., 2016). Phosphopeptides were accounted for quantification if they could have been quantified in at least 70% of the biological samples.

Additionally, only phosphopeptides that passed the class I criteria (phosphosite probability >75% and score difference >5) were included in the final dataset (Olsen et al., 2006).

Moreover, phosphopeptide abundance was normalized to the median of each sample, log2 transformed. MS/MS spectra of the identified CAS phosphopeptides are shown in Supplementary Figures 6-8.

6.5 Bioinformatics analyses

6.5.1 Analysis of evolutionary conservation of phospho-residues

Orthologs of CAS in various organisms were identified by blastp or tblastn searches in NCBI or from website dedicated to specific organisms or phylogenetic groups. Alignments were performed with Clustal X 2.0 (Thompson et al., 1997) using up to 80 of the C-proximal amino acids. Some hand-alignment was performed to give what was considered the best fit.

7 Results

7.1 Analysis of CAS localization and topology

The CAS protein possesses a N-terminal transit sequence of about 33 AAs that is required to guide its import and ultimate localization in the chloroplast. Moreover, according to several prediction tools, CAS is divided into two domains of roughly similar size by a single TMD characterized by a high hybrophobicity, which would define its localization on the thylakoid membrane or could serve as an anchoring or docking module. Considering the proposed function of CAS as a calcium sensor protein and its potential phosphorylation-regulated interaction with other proteins, knowledge about the exact topology of the protein is essential. While the orientation of the N-terminus of CAS into the stroma was determined by Western Blot analyses (Nomura et al., 2008), no consensus has yet been reached regarding its complete topological arrangement on the thylakoid membrane, and in particular, the orientation of the C-terminal domain. Therefore, different experimental methods were employed to clarify these issues.

7.1.1 Microscopy-based methods

7.1.1.1 Analysis of CAS localization via YFP fusion

In a first approach, the full-length CAS sequence was transiently expressed in tobacco mesophyll cells as a fusion to the yellow fluorescent protein (CAS-YFP).

Confocal microscopic analysis of mesophyll protoplasts isolated from transfected leaves showed a clear overlap of the YFP signal with the chlorophyll fluorescence (Figure 3, left panel), confirming the localization of CAS in plastids.

By contrast, a cytosolic localization was observed when the predicted transit peptide (AAs 1-33) was omitted in the construct (Figure 3 ΔTP-CAS-YFP).

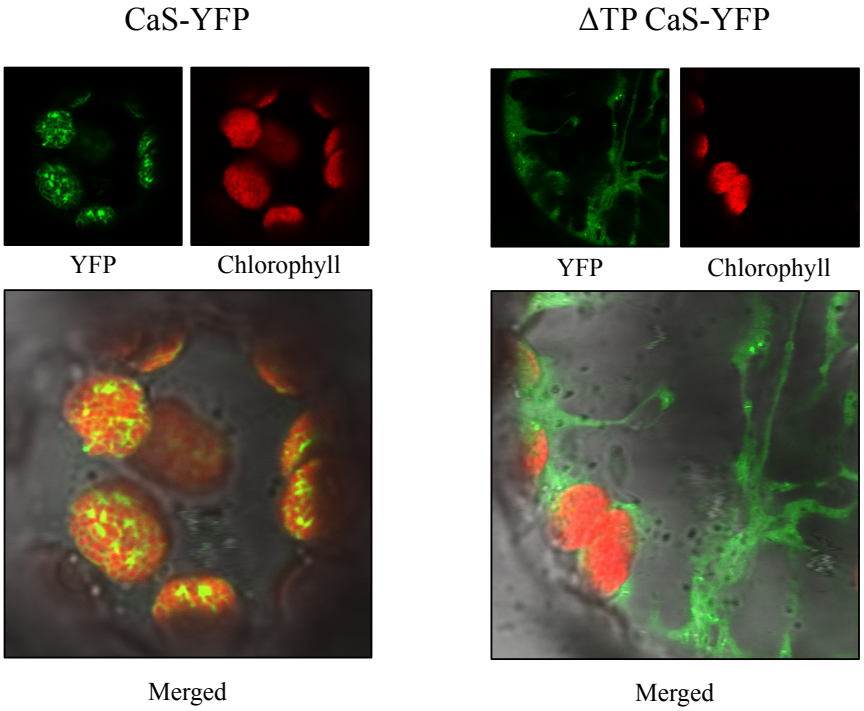

Figure 3: Localization of different CAS-YFP fusion constructs in transiently transformed tobacco protoplasts. While the full-length CAS-YFP fusion (CAS-YFP, left panel) shows a clear overlap with the chlorophyll fluorescence, a cytoplasmic pattern is observed for the YFP signal in the absence of the predicted TP (ΔTP-CaS-YFP, right panel).

7.1.1.2 Analysis of the CAS C-terminus orientation with the sa-GFP system

In order to elucidate the topology of CAS, a microscopy approach was employed based on the use of a tool known as the "*self-assembling GFP system"* (saGFP), which had been previously successfully used to study the topology of plant membrane proteins (Cabantous et al., 2005; Machettira et al., 2011). To do so, a vector containing the full-length sequence of CAS N-terminally fused to the 11th beta sheet of the GFP protein (CAS-saGFP$_{11}$) was created and was used in combination with a similarly created stromal marker vector that contains the nuclear encoded small subunit of RuBisCO (ssRub-saGFP$_{1-10}$).

Assembly of the full-length GFP and a corresponding fluorescence signal can only occur if the C-terminus of CAS is exposed to the stromal environment. Co-transfection of both vectors via *Agrobacterium*-mediated transformation into tobacco leaves resulted in a clear GFP fluorescence signal that overlapped with the chlorophyll fluorescence (Figure 4).

The same result was achieved when the reciprocal fusion constructs (CAS-saGFP$_{1-10}$ + ssRub-saGFP$_{11}$) were co-transfected (data not shown). Since RuBisCO is a soluble protein exclusively found in the stroma, these results strongly support an extrusion of the C-terminal domain of CAS into this compartment.

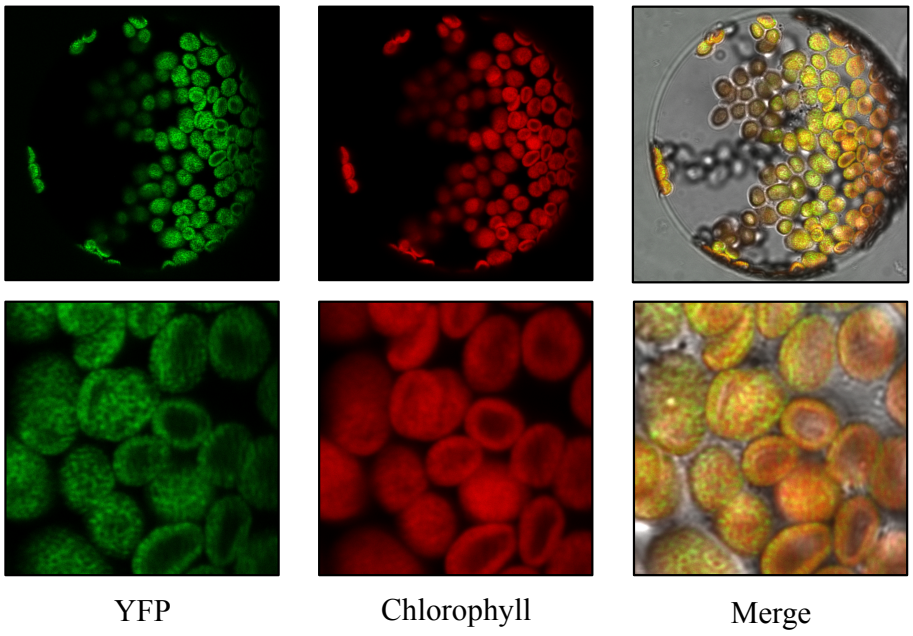

Figure 4: saGFP-based analysis of the orientation of the C-terminus of CAS.

The orientation of the C-terminus of CAS was investigated using the saGFP system via confocal microscopy. Co-transfection of tobacco protoplasts with CAS-saGFP11 and ssRub-saGFP1-10 (stromal marker) confirmed the localization of this domain in the chloroplast stroma.

7.1.2 Immunodetection-based methods

7.1.2.1 Analysis of CAS localization in fractionated chloroplasts

The enrichment of the CAS protein in the thylakoid membranes was confirmed via immunodetection. This analysis was conducted by fractionating whole isolated chloroplasts into a soluble (stromal) and membrane (thylakoid) fractions followed by probing these two different fractions via immunoblotting using a polyclonal antibody specifically recognizing the CAS CTD (α-CT-CAS). The antibody recognized a protein of the appropriate mature size of CAS (35 kDa) exclusively in the thylakoid fraction, while no signal was detected in the stroma (Figure 5). Control blots were performed using antibodies specific for the ATPase (α-ATPase) and Transketolase (α-TKL) proteins to ensure purity of thylakoid and stromal fractions, respectively.

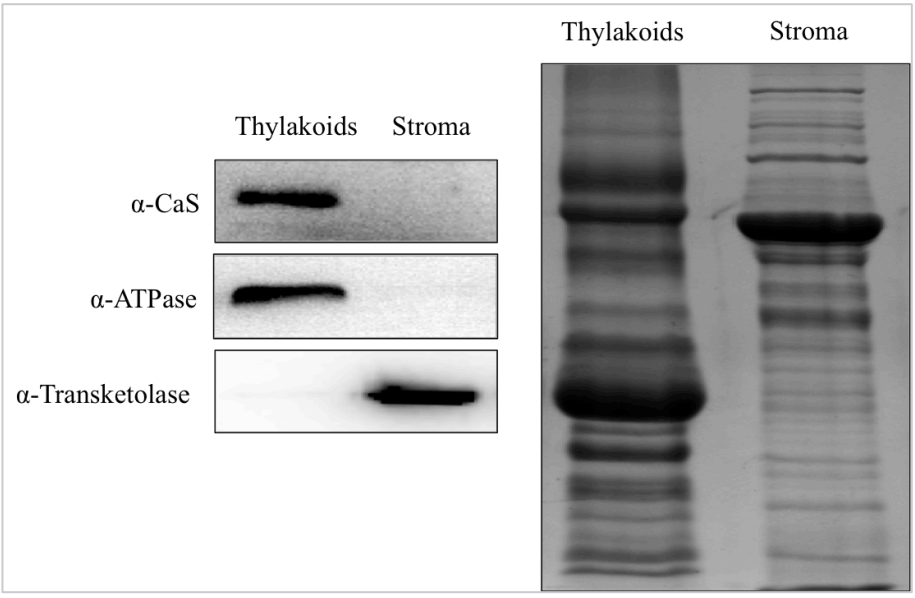

Figure 5: Membrane localization of CAS elucidated via immunodetection.

The exclusive membrane localization of CAS in the chloroplast was investigated via immunodetection using a CAS specific antibody by probing soluble (stromal) and thylakoid (membrane) protein fractions. Control antibody reactions for stromal (α-TKL) and thylakoid (α-ATPase) proteins were included to verify the purity of the two fractions.

7.1.2.2 Analysis of CAS N-terminus orientation via protease protection assay

In order to clarify the orientation of the N-terminus of CAS, an immunodetection-based approach was chosen instead of the saFGP system. In fact, it is expected that any fusion of a GFP fragment either in front or in between the TP and the N-terminal region of the CAS protein would compromise its native import process and potentially lead to an artificial mislocalization.

For this reason, another experimental setup based on a previously described protocol was employed (Torabi et al., 2014), which relies on the treatment of isolated thylakoids with a proteinase (thermolysin) and their subsequent immunological probing with antibodies that are specific for the protein of interest. To this end, a second antibody that selectively recognized the N-terminus of CAS (α-NT-CAS) was raised against a recombinant fragment corresponding to its N-terminal domain (NTD). Both CAS antibodies (α-CT-CAS and α-NT-CAS) were checked with regards to potential cross-reactivity and proved to exclusively recognize the recombinant protein domain against which they were raised (Supplementary Figure 1). Both antibodies also recognized a protein of the same size (35 kDa) both in total leaf and whole chloroplast protein extracts, while no band was detected in the *cas* mutant background, confirming their specificity (Supplementary Figures 2-3).

The feasibility of the system was initially tested by probing proteinase-treated thylakoids with a control antibody specifically recognizing the lumen-exposed protein Oxygen Evolving Complex Subunit 23 (OE23, α-OEP23). As expected, degradation of OEP23 could only be achieved when a detergent (digitonin) was added to the thylakoid membranes in combination with the proteinase.

When the thylakoids were probed with the antibody against the CTD, no reaction occurred in the thermolysin treated sample, indicating a complete degradation of the CTD after the proteinase treatment, thus corroborating the microscopy results. When the thylakoids were probed with the α-NT-CAS serum, a similar picture was obtained, indicating that also the NTD of CAS is exposed to the stroma (Figure 6).

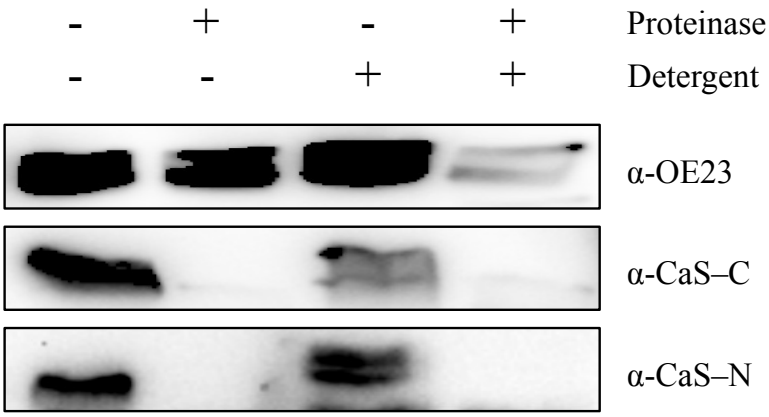

Figure 6: Elucidation of the orientation of both CAS termini via immunodetection.

The orientation of both CAS termini was further investigated via immunodetection via a protease protection assay. Degradation of both termini could be achieved after a protease treatment of isolated thylakoids suggesting their extrusion inside the stromal environment. Degradation of the lumen-exposed protein OE23 could only be achieved when a detergent is included in the assay.

These results provide for the first time unambiguous evidence concerning the overall topology of CAS and confirm a previously suggested configuration (Nomura et al., 2008) whereby both termini of the protein are exposed to the stromal environment (Figure 7).

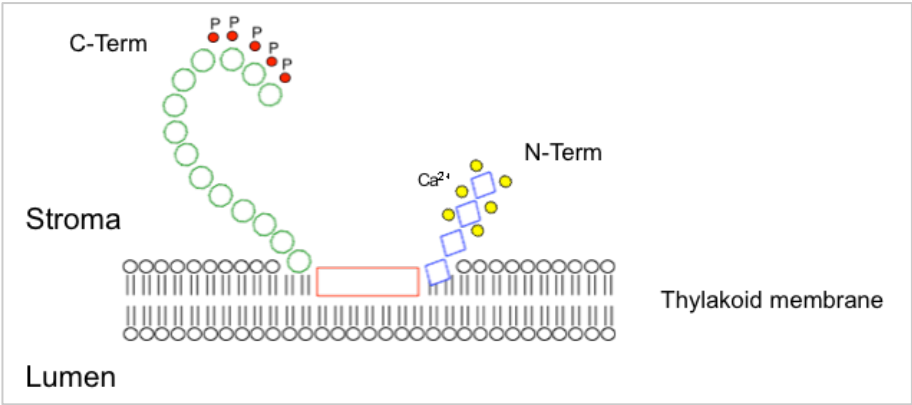

Figure 7: Proposed topological arrangement of CAS on the thylakoid membrane.

7.2 Analysis of CAS phosphorylation

CAS was first described as a phosphoprotein by Vainonen and co-workers (Vainonen et al., 2008). They provided experimental evidence of its modification at the level of the Thr-380 residue via phosphoproteomics and assigned CAS as a target of the State Transition Kinase 8 protein (STN8). They also proposed that its phosphorylation is enhanced under increasing light intensity, as evidenced via immunoblots on SDS-PAGE-separated total thylakoid proteins using an anti phosphorylated threonine (a-pThy) antibody. Subsequently, another study described CAS as a target of Ca^{2+}-regulated phosphorylation by using whole chloroplast protein extracts and a recombinant fragment corresponding to the C-terminal of CAS. (Stael et al., 2012a). However, neither the protein kinase(s) responsible for this modification nor the identity of the phosphorylated residue(s) was elucidated in this work.
A number of CAS phosphopeptides can be retrieved from databases containing phosphoproteomics data from studies conducted on *A. thaliana,* but also on several other species, making it possible to compare the evolutionary conservation status of candidate phosphoresidues.

7.2.1 In silico analysis of CAS phosphorylation

7.2.1.1 Experimentally described pS/T residues of CAS

To investigate the *in vivo* phosphorylation profile of CAS, the publicly available databases containing experimentally described phosphoresidues were searched, in particular the online Arabidopsis Protein Phosphorylation Site Database (PhosPhat 4.0) (Heazlewood et al., 2008). This database contains regularly updated information about the identity and properties of annotated phosphorylated residues - mostly deriving from large-scale mass spectrometry experiments - as well as the details about the experimental procedures and analytical methods from which they originated. This *in silico* analysis revealed the existence of several experimentally described phosphoserines and phosphothreonines (pS/Ts) within the CAS sequence (highlighted in yellow in Figure 8).

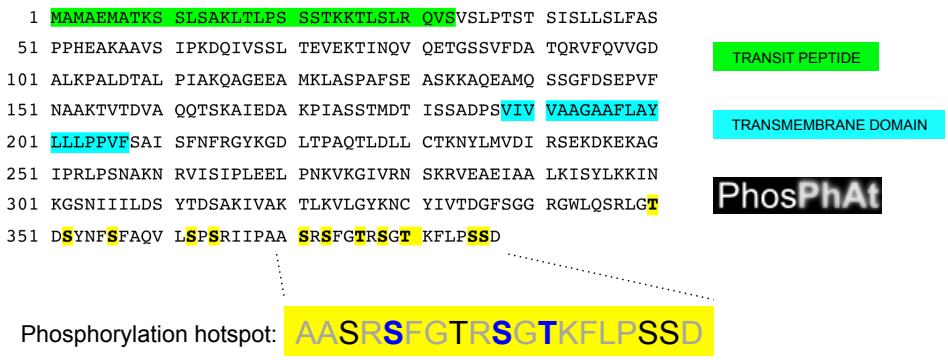

Figure 8: Amino acid sequence *of A. thaliana* CAS isoform and candidate pS/Ts.

Quite interestingly, all these residues map at the very end of the CTD. Moreover, within an amino acid stretch of roughly 20 residues (positions 368 – 387), at least 7 potential phosphorylation sites are found, creating a kind of "*phosphorylation hotspot*". Intriguingly, this latter region overlaps with a portion of CAS that previous works have suggested to display protein-protein interaction ability based on *in silico* predictions (Vainonen et al., 2008). Overall, these observations suggest that the phosphorylation of CAS could have a functional significance by promoting its transient association with other protein(s).

A closer inspection of the analytical information provided by the PhosPhat 4.0 database and within the original publications revealed that 3 out of the 12 described phospho-residues (namely Thr-376, Ser-378 and Thr-380) can be considered non-ambiguous and possessing high prediction scores, including the Thr-380 residue identified by Vainonen and coworkers (Vainonen et al., 2008).

7.2.1.2 Phylogenetic conservation of pS/T residues

It is reasonable to assume that the conservation of pS/Ts across CAS orthologs from species belonging to different phylogenetic groups could provide valuable information concerning their functional relevance and this knowledge could be used to further pinpoint relevant pS/Ts via biochemical approaches.

An in *silico* search with the Basic Local Alignment Search Tool (protein BLAST) of the NCBI website (Altschul et al., 1990) using the amino acid sequence of the *A. thaliana* CAS isoform as query and a search of species-specific databases allowed the retrieval of many CAS orthologs belonging to different photosynthetic organisms (total number of species: 102), ranging from the unicellular green algae to angiosperms, virtually covering the whole evolutionary range of the *viridiplantae* clade (see list of retrieved CAS orthologs in Table 1 in the Appendix). Of note, no CAS isoform could be found among cyanobacteria, red algae or glaucophyta, all of which contain phycobilisomes and do not possess LHCII complexes, suggesting that the presence of CAS could correlate with specific functions associated with these elements.

Next, the conservation status of the described *A. thaliana* pS/Ts was analyzed by creating a multiple sequence alignment (MSA) using all the sequences of the retrieved CAS isoforms.

Since this work is primarily concerned with the analysis of the phosphorylation profile of CAS, the comparative analysis was restricted to the C-terminal region of CAS (AA 344 to 387 for AtCAS), where all the described pS/Ts are found.

The focus of the comparative phylogenetic analysis was thus placed on the following 12 experimentally described *A. thaliana* pS/Ts: Thr-350, Ser-352, Ser-356, Ser-362, Ser-364, Ser-371, Ser-373, Tht-376, Ser-378, Thr-380, Ser-385 and Ser-386.

For clarity purposes, the MSA included only the following species for which reliable phoshoproteomics datasets were available: *Medicago truncatula* (dicots), *Gossypium hirsutum* (dicots), *Zea mays* (monocots), *Brachypodium distachyon* (monocots), *Oryza sativa* (monocots) and *Chlamydomonas reinhardtii* (green algae) (all identified phosphopeptides, including their bibliographic references, are listed in table 2). In the MSA were also included the following organisms representing specific phylogenetic groups: the fern *Pteris vittata* and the bryophytes *Physcomitrella patens* and *Marchantia polymorpha*. The lycophyte *Selaginella moellendorffii* was included since it represents a critical node in the evolutionary development of green plants and belongs to an early diverging lineage of vascular plant. Finally, for those phylogenetic groups containing multiple CAS orthologs - such as the dicots (71 species), monocots (27 species), gymnosperms (4 species) and the green algae (6 species) – consensus sequences were created using the MergeAlign online tool (Collingridge and Kelly, 2012) and these were included in the MSA to provide a general view of the conservation status of individual residues within phylogenetic groups. The output of the MSA showing the evolutionary conservation of 12 *A. thaliana* CAS pS/Ts is presented in figure 9.

At least 3 residues (Thr-350, Ser-364 and Thr-376) show either complete or nearly complete conservation across the evolutionary gradient. Other residues show less conservation but in several cases are substituted by another potentially phosphorylatable amino acid, i.e. threonine or serine. This suggests a selective pressure for specific positions, either a structural function or as regulatory sites via phosphorylation. Nevertheless, only until the serine residue at position 371 of the *A. thaliana* CAS isoform all ortholog sequences display a good degree of similarity while from there onwards the overall conservation is very low. For this reason, a critical interpretation of the conservation status of the remaining residues was required in several cases.

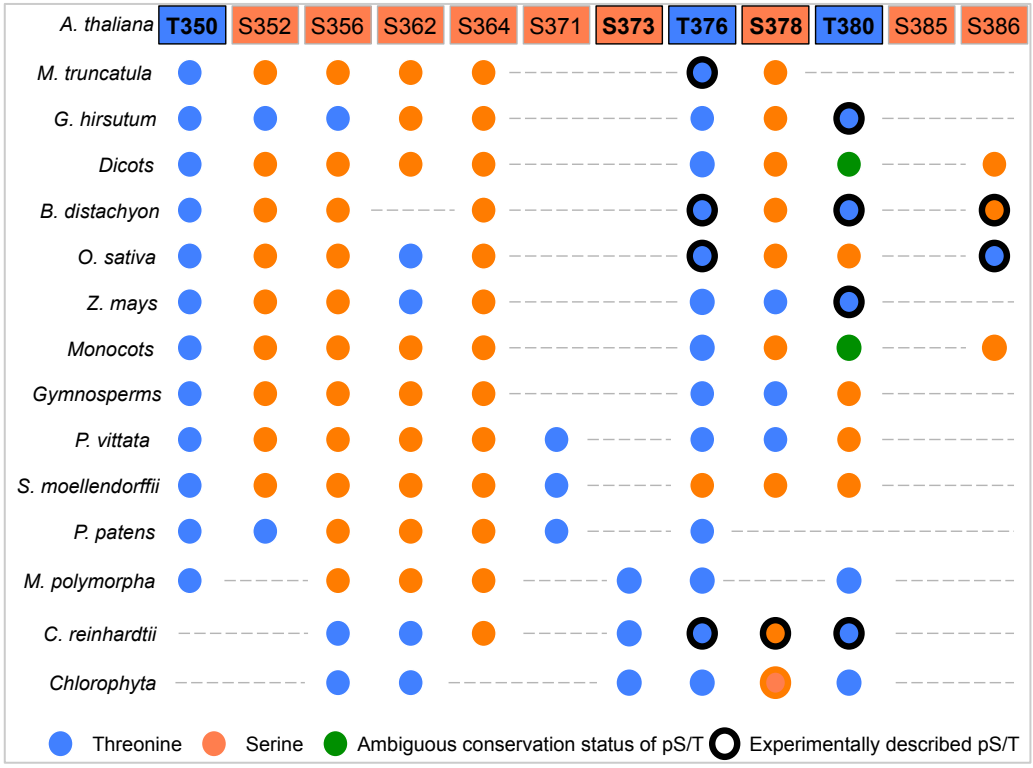

Figure 9: Evolutionary conservation of *A. thaliana* candidate pS/Ts.

A phylogenetic analysis of experimentally described pS/Ts of the *A. thaliana* CAS isoform was conducted to investigate their conservation status in different evolutionary groups. A high level of conservation is observed for residues Thr-350, Ser-364 and Thr-376. Other positions are less conserved or substituted by other potentially phosphorylatable residue. For some organisms, experimental evidence was found for phosphorylated residues matching the corresponding positions in the *A. thaliana* CAS isoform (circled in bold).

This comparative analysis highlighted that the 3 described *A. thaliana* pS/Ts showing higher prediction scores (Thr-376, Ser-378 and Thr-380) were also found phosphorylated in other organisms on amino acid residues that are matching the corresponding *A. thaliana* position in the MSA (Thr-376: *M. truncatula, B. distachyon, O sativa, C. reinhardtii*; Ser-378: *C. reinhardtii*; Thr-380: *G. hirsutum, B. distachyon, Z. mays, C. reinhardtii).*

In the two monocot species *B. distachyon* and *O sativa,* their serine residues corresponding to the *A. thaliana* position Ser-386 were found phosphorylated in independent studies.

Overall, these results suggested that residues Thr-376, Ser-378 and Thr-380 of *A. thaliana* CAS deserved further attention.

In addition to the above-mentioned analysis, an MSA including all the 102 retrieved CAS orhtolog sequences was created and this alignment was submitted to the online sequence logo generator tool WebLogo (Crooks et al., 2004). By doing so, the entire MSA was collapsed into a single consensus sequence, which offered a graphical representation of the pattern of conservation and sequence similarity across the CTD region of CAS. In the generated picture, the overall height of the symbols within the stack reflects relative frequency, and thus the level of sequence conservation for every amino acid position. Two of the amino acids showing the highest level of conservation in the Weblogo were the positions corresponding to the residues Thr-350 and Thr-376 of the *A. thaliana* isoform (Figure 10).

Figure 10: Evolutionary conservation of residues Thr-350 and Thr-376.

The WebLogo images created using the MSA of all the retrieved CAS ortholog sequences highlighted a high level of evolutionary conservation for two *A. thaliana* positions: Thr-350 (left) and Thr-376 (right). The amino acid regions surrounding the two sites are also very conserved and in the case of Thr-350 resemble a described minimal phosphorylation motif of the STN7 kinase (Schonberg et al., 2017).

Importantly, the region surrounding position Thr-350 matches a recently described minimal consensus motif of phosphorylation for the protein kinase STN7 (Schonberg et al., 2017), by possessing a glycin (G) at position -1 to the threonine target of phosphorylation and an aspartate (D) at position +1.

In the next sections the experimental approaches used to characterize the phosphorylation profile of CAS will be described, including included a phosphoproteomics approach to define the kinase involved and the use of a recombinant CAS fragment and of several phosphomutant variants by means of *in vitro* kinase assays.

7.2.3 LC-MS/MS analysis of the in vivo phosphoresidues of CAS

The *in silico* analysis provided very useful information for a further characterization of candidate residues. It suggested the existence of multiple phosphorylation sites on CAS and the potential involvement of additional protein kinase(s) aside from STN8.

To test this hypothesis, a phosphoproteomics approach was employed in order to compare the *in vivo* phosphorylation status of CAS in wild type *A. thaliana* plants and in the *stn8* mutant line lacking the STN8 kinase. This latter was in fact suggested as the main kinase active on CAS (Vainonen et al., 2008). Phosphopeptides were obtained from wild type and *stn8* plants acclimated to growth light in order to promote light-activated phosphorylation events.

As shown in figure 11, in the *stn8* mutant CAS phosphopeptides could be detected from three independently sample preparations, albeit with significantly lower abundance compared to the wild type samples. In particular, residual phosphorylation could be observed for the three previously described, high confidence, phosphorylation sites: Thr-376, Ser-378 and Thr-380.

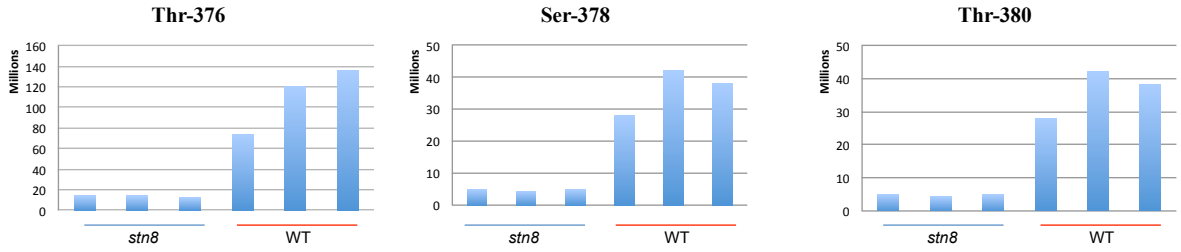

Figure 11: Residual phosphorylation of CAS in the absence of the STN8 kinase.

CAS phosphopeptides are detected in the stn8 mutant background, albeit with lower abundance than in the wild type. This suggests the involvement of more than one kinase in the phosphorylation of CAS. Three biological replicates for the genotypes are shown for the three different phosphorylated residues (Thr-376, Ser-378 and Thr-380).

7.2.4 In vitro analysis of CAS phosphoresidues

After having clarified the involvement of multiple kinases in the phosphorylation of CAS via bioinformatics and proteomics approaches, the gathered information was used to further investigate *in vitro* the relevance of selected residues, to dissect the contribution of candidate protein kinases and to explore the regulation behind their activity.

7.2.4.1 Phosphorylation of recombinant CAS by thylakoid membranes

An *in vitro* kinase assay approach was employed using catalytically active isolated thylakoid membranes and a recombinant substrate corresponding to the 122 C-terminal AA of CAS.
As shown in figure 12, ≈ 200 ng of the recombinant CAS substrate could be phosphorylated *in vitro* by thylakoid membranes and the intensity of the detected signal correlated linearly with the amount of catalytically active kinases provided in the assay.
Unless stated otherwise, all experiments were conducted at ambient light using thylakoids originating from growth light (GL) acclimated plants and in the presence of 1 μM $CaCl_2$, to promote the full activation of all the potentially involved kinases.

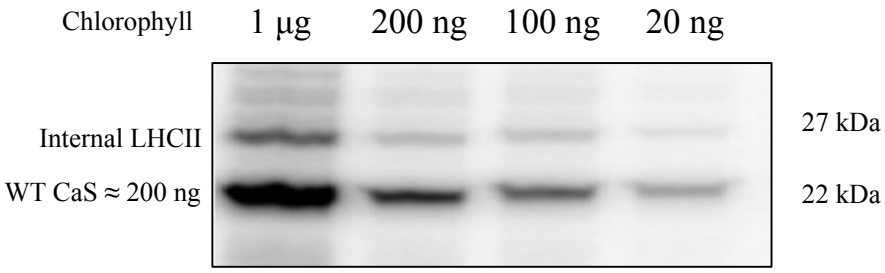

Figure 12: CAS *in vitro* phosphorylation by catalytically active thylakoids.

A recombinant CAS fragment of 122 amino acids corresponding to its C-terminus is phosphorylated *in vitro* by catalytically active thylakoid membranes. The intensity of the detected phosphorylation signal of the substrate correlates with the amount of thylakoid proteins that are provided in the assay.

7.2.4.2 In vitro phosphorylation of CAS recombinant phospho-mutant substrates

The phosphorylation profile of a series of recombinant CAS fragments carrying individually substituted candidate phosphorylation residues was next investigated *in vitro*. In total, five phospho-mutants were generated following the information gathered from the *in silico* analysis. By doing that, it was possible to confirm the relevance of three residues: Thr-376, Ser-378 and Thr-380. Thr-350 also emerged as an additional phosphosite (Figure 13).

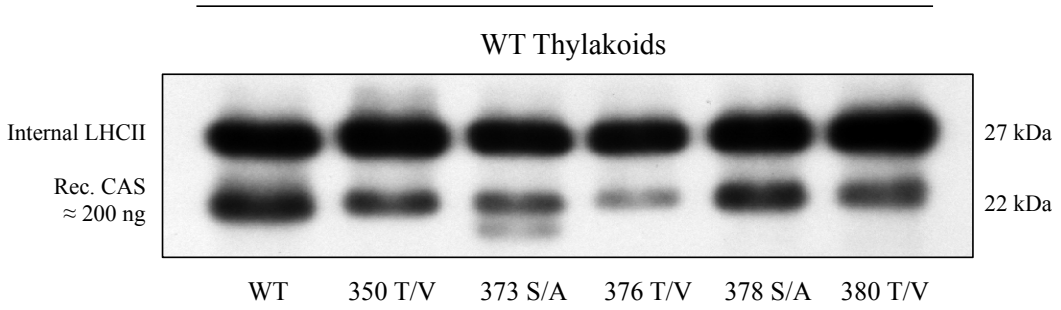

Figure 13: Several residues of CAS are required to reach full phosphorylation *in vitro*.

When specific threonine or serine residues of the recombinant CAS fragment are mutated to non-phosphorylatable valines and alanines, respectively, the detected phosphorylation signal is significantly reduced. All mutations affected the phosphorylation if compared with the wild type substrate but strongest reduction could be observed when positions Thr-376, Thr-380 and Thr-350 were mutated.

This experiment could show that several residues are required in order to obtain a full phosphorylation of CAS *in vitro*. Among these, thr-376 appears to be most relevant one, followed by Thr-380, Thr-350 and, possibly, Ser-378 as well. These results are in agreement with the information contained in the PhosPhat 4.0 database, but also with other results generated in this work, which also indicated that Ser-378 and Thr-380 are the most relevant phosphoresidues of CAS. Furthermore, these data are also consistent with the results of the bioinformatics analysis, which suggested a strong phylogenetic conservation for Thr-350 and Thr-376, this latter being found phosphorylated in several CAS orthologs.

Despite a strong reduction in phosphorylation observed in the absence of Ser-373, this residue was not considered relevant since in all preparations and assays this phospho-mutant substrate showed of a lower band indicating its instability or partial degradation.

7.2.4.3 In vitro CAS phosphorylation by STN mutant thylakoids

The involvement of candidate thylakoid-localized kinases in the phosphorylation of CAS was subsequently tested *in vitro* using membranes derived from single mutant *A. thaliana* lines lacking the two major thylakoid-localized protein kinases STN7 and STN8 (*stn7* and *stn8*) and from the double mutant *stn7*/*stn8*. As seen in figure 14, the wild type CAS substrate (this recombinant fragment was used in all the following described assays) could be phosphorylated equally by the single mutant thylakoids as by the wild type, while a significant reduction in phosphorylation was observed only with the *stn7*/*stn8* double mutant. The 27 kDa strongly phosphorylated band corresponds to the internal LHCII proteins provided in the assay together with the thylakoid membranes. As expected, no phosphorylation of this band could be detected when *stn7* or *stn7*/*stn8* lines were used, due to the absence of the LHCII kinase.

These results indicated that CAS can be targeted by both STNs but also highlighted the presence of residual phosphorylation that could be ascribed to the activity of additional thylakoid localized kinase(s).

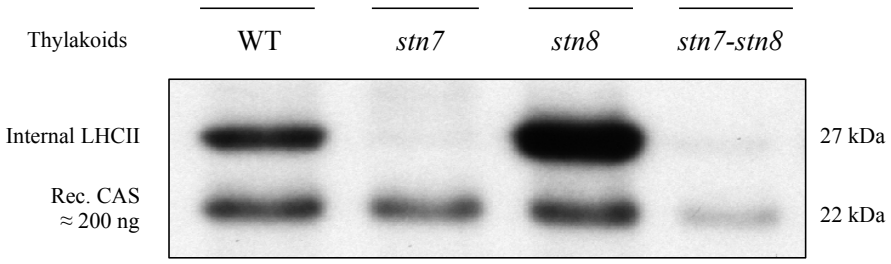

Figure 14: *In vitro* phosphorylation of recombinant CAS by STN7 and STN8.

The CAS recombinant substrate is equally phosphorylated *in vitro* in the absence of the STN8 and STN7 kinases. A strong reduction in the phosphorylation is observed when both kinases are absent in the stn7/stn8 mutant. Residual phosphorylation is still observed in this latter case.

7.2.4.4 Light-activated phosphorylation of CAS

The first work that investigated the *in vivo* phosphorylation status of CAS (Vainonen et al., 2008) suggested a light regulation behind this event involving the activity of the STN8 kinase and, in particular, in response to increasing light intensity. Accordingly, the present work explored the role of light in the phosphorylation of CAS by means of *in vitro* kinase assays. However, due to technical limitations of the experimental set up, only the impact of growth light (GL) and dark (D) conditions could be assessed. Initially, the impact of GL exposure (4 hours of 100 μmol m^{-2} s^{-1} white fluorescent light) or dark (end of the 8 hours dark phase without any light exposure) was compared using thylakoid membranes derived from wild type plants and the *stn7*/*stn8* double mutant. As seen in figure 15, a clear difference in the phosphorylation intensity of the substrate could be observed between these two conditions in the presence of wild type thylakoids, while no difference emerged in the case of the *stn7*/*stn8* mutant. The stronger phosphorylation signal caused by the GL exposure was equally reflected at the level of the artificial substrate and of the LHCII, indicating a physiological light activation of the kinase(s).

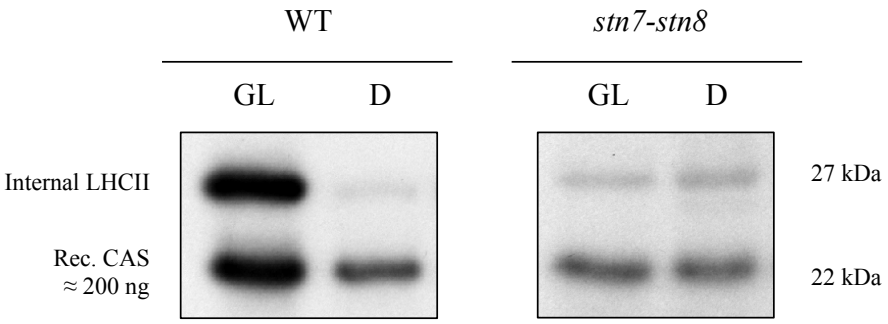

Figure 15: Light-activated *in vitro* phosphorylation of CAS by wild type thylakoids.

A light-activated *in vitro* phosphorylation of CAS is observed when light- and dark-harvested wild type thylakoid membranes are compared. No difference is visible in the case of the stn7/stn8 double mutant, suggesting that one of the two STNs is likely involved in this event.

7.2.4.5 Role of the STN kinases in the light-activated phosphorylation of CAS

The involvement of the two STNs in this light-regulated event was subsequently investigated by comparing the two light treatments using thylakoid membranes originating from the single STN mutant lines (Figure 16). By doing so, the previously observed light-dependent difference in the CAS phosphorylation intensity could only be reproduced in the case of the *stn8* single mutant, where the residual activity of STN7 is predominating. In the case of the *stn7* mutant, where STN8 is acting as the main membrane kinase, no difference could be seen between the two treatments. It is worth noting that the phosphorylation of both the substrate and the internal LHCII is stronger in the GL reaction with the *stn8* thylakoids compared to the wild type in the same condition. This observation possibly reflects a higher activity or upregulation of STN7 in this mutant background as a compensatory mechanism to further promote the dissociation of the antennas from PSII in order to relieve part of the excitation pressure from an already repair/recycle-impaired photosystem. However, this condition was not tested in this work via immunoblotting with STN7-specific antibodies, but a similar condition can be observed in other studies (Bonardi et al., 2005, Wunder et al., 2013).

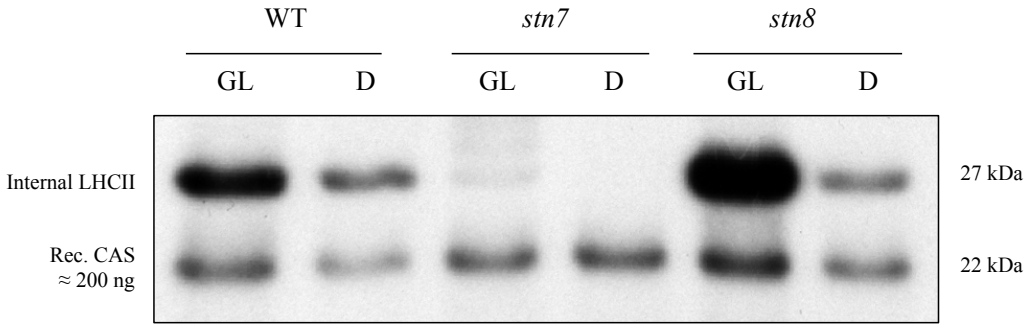

Figure 16: STN7-dependent light-regulated *in vitro* phosphorylation of CAS.

When growth light- and dark-harvested wild type thylakoid membranes from different genotypes are compared, the light-dependent activation of the *in vitro* phosphorylation of CAS becomes evident in the stn8 mutant, suggesting a role for the STN7 kinase in this event.

7.2.4.6 Ca^{2+}-regulated phosphorylation of CAS by a thylakoid-localized kinase

The following experiment further investigated the already described Ca^{2+}-dependent *in vitro* phosphorylation of CAS (Stael et al., 2012a). Since in the previous assay we could detect a residual substrate phosphorylation in the case of *stn7*/*stn8* mutant, it was decided to check whether this *Ca^{2+}*-dependency could be ascribed to a thylakoid-localized kinase.

In their previous work, Stael et al. used total chloroplast protein extracts and could not pinpoint the identity of the involved kinase. They only investigated the impact of the presence or absence of Ca^{2+} by comparing these two conditions using wild type extracts.

In this work it could also be shown a strong Ca^{2+} requirement for the phosphorylation of CAS, which was strongly predominant in the case of the double mutant (figure 17).

These observations suggest that the Ca^{2+}-dependent phosphorylation of CAS does not relate to any of the two STN kinases, but rather to another still non-characterized thylakoid protein kinase.

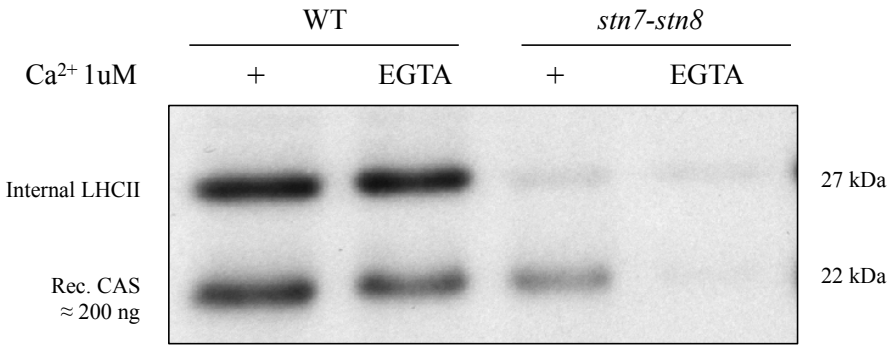

Figure 17: Ca^{2+}-dependent phosphorylation of CAS by a thylakoid-localized kinase.

When the Ca^{2+} is completely removed from the reaction by chelation with EGTA, a strong reduction of the residual phosphorylation of the CAS recombinant substrate can be observed in the case of the *stn7*/*stn8* double mutant. Ca^{2+} regulation does not involve any of the STNs.

The Ca^{2+}-dependency for the *in vitro* phosphorylation of CAS was further investigated by using the soluble stromal protein fraction obtained from the fractionation of whole chloroplasts. As seen in figure 18, an even stronger difference in the phosphorylation intensity of the recombinant CAS substrate could be observed.

This observation suggests that the Ca^{2+}-dependent kinase involved in this event is likely a loosely membrane-attached protein that is released by the washing steps performed during the fractionation procedure.

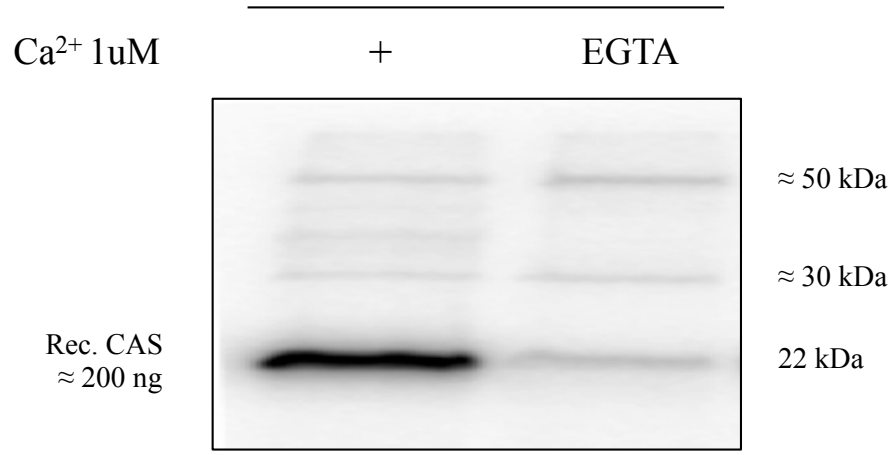

Figure 18: Ca^{2+}-dependent phosphorylation of CAS by stromal protein extracts

7.3 Characterization of photoacclimation responses in the *cas* mutant

7.3.1 Analysis of chlorophyll fluorescence emission spectra at 77K

After having established that CAS is a target of phosphorylation by the two light-responsive thylakoid-localized kinases STN7 and STN8 it was decided to investigate its potential involvement in photoacclimation responses. While STN7 acts as the main regulator of the phenomenon of state transitions, STN8 is a crucial component of the protective mechanisms against photoinactivation and photodamage, To this end, the performance of the *cas* mutant was assessed by means of spectrometric analysis following different light treatments and compared with wild type and the *stn7* mutant plants. In particular, the emission spectra of chlorophyll fluorescence at 77K from isolated thylakoids were analyzed to assess potential defects in the ability to perform dynamic adjustments in response to specific light conditions. With this technique it is in fact possible to estimate how the energy excitation is redistributed between the two photosystems via the transient modification of their relative cross-section, a process that is dynamically regulated by a phosphorylation-dependent reversible mechanism of association and dissociation of a mobile fraction of LHCII proteins.

The analysis of chlorophyll fluorescence emission curves were performed on isolated thylakoid membranes (Chlorophyll concentration 1 mg/ml) following specific light treatments and included the three following genotypes: wild type, *cas* and *stn7*. The latter served as the internal negative control due to its inability to perform the state 1 to state 2 transition.

As visible in figure 19, the acclimation from darkness (red trace, reproducing state 1) to 2 hours of GL (black trace, reproducing state 2) produced in the wild type a characteristic increase (Tikkanen et al., 2006) of the PSI specific peak at 733 nm, indicating the occurrence of state transition and phosphorylation-mediated migration of the mobile fraction of LHCII proteins from PSII towards PSI.

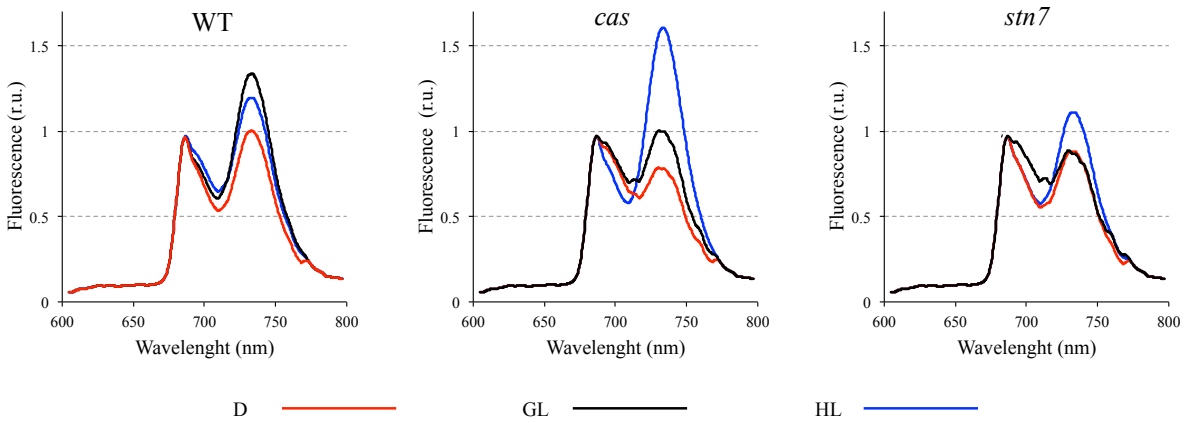

Figure 19: The *cas* mutant maintains strong excitation of PSI under high light.

The chlorophyll emission spectra between 600 and 800 nm were recorded at 77K from isolated thylakoids of the wild type, *cas* and *stn7* mutant lines after different light treatments. After two hours of high light (HL) treatment the *cas* mutant showed a sustained excitation of the PSI specific peak at 733 nm.

In agreement with previous studies (Mekala et al., 2015), a high light treatment of 2 hours was sufficient to cause a significant decrease of the PSI peak (blue trace) in the wild type, a process that relies on the dephosphorylation of LHCII by the TAP38 phosphatase.

The *cas* mutant, instead, maintained a strong excitation of PSI under high light, as shown by a significantly higher PSI peak compared to PSII (blue trace). This situation strikingly resembles the phenotype previously described for the *tap38* and *pgr5* mutants.

In this analysis, the *stn7* mutant behaved as expected, showing no change in the PSI height upon dark-growth light shift (Tikkanen et al., 2006) and only a slight increase of the PSI peak under high light, albeit significantly lower than in the *cas* mutant.

7.3.2 Immunodetection of phosphorylated thylakoid proteins

The phosphorylation status of thylakoid phosphoproteins upon acclimation to different light treatments was assessed with a α-pThr antibody to confirm the abovementioned results.
This analysis was performed on isolated thylakoid membranes following the same light treatments that were employed in the spectrometric analysis. Thylakoid proteins were separated on SDS PAGE gel and subsequently immunoprobed with the α-pThr.
This revealed specific phosphorylation patterns of individual thylakoid proteins that varied according to the applied light treatments and showed differences between genotypes.
As seen in figure 20, the phosphorylation profiles of the protein D1 (component of the PSII core) and of LHCII in the wild type were consistent with previous observations. Accordingly, LHCII phosphorylation was nearly absent in dark (D), it increased under growth light (GL) and was partially reversed by high light (HL). In contrast, the D1 protein showed a constitutive phosphorylation in both D and GL but a marked increase under HL. The *stn7* mutant showed no LHCII phosphorylation under all conditions and a strong constitutive phosphorylation of D1 in all light conditions.

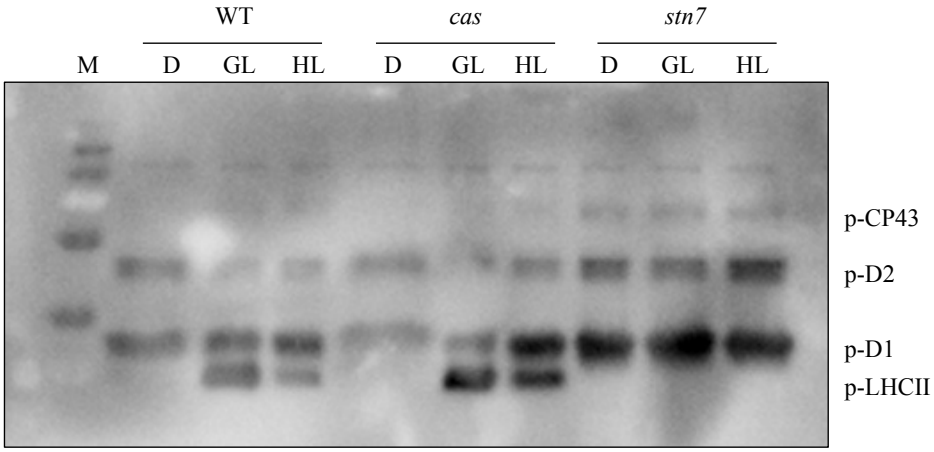

Figure 20: The *cas* mutant has highly phosphorylated LHCII and PSII under high light.

The phosphorylation profile of the thylakoid proteins was investigated via immunoblotting with an anti-phosphorylated threonine antibody. This revealed a high light-associated phosphorylation pattern of the *cas* mutant that is consistent with the spectrometric data, consisting in a concomitant sustained phosphorylation of LHCII and PSII core (D1 and D2 proteins).

Interestingly, the *cas* mutant showed the characteristic increase of D1 phosphorylation under HL but also a concomitant strong phosphorylation of LHCII under this condition.
Overall, these findings corroborated the observations that emerged from the spectrometric analysis and suggested a defect in the dephosphorylation of LHCII under high irradiance in the absence of CAS, further indicating a potential role for this protein in mediating phosphorylation-mediated acclimation mechanisms to high light.

7.3.3 BN-PAGE analysis of thylakoid megacomplexes

A final experimental approach was employed to study the reversible formation of the PSI-LHCII state transitions megacomplexes (PSI-LCHIImc) in the *cas* mutant.
As visible in figure 21, the formation of the PSI-LCHIImc upon GL acclimation is clear in the wild type and is not impaired in the *cas* mutant. As expected, no complex is formed in the *stn7* mutant. The ST megacomplex is partially reversed after a 2 hours light exposure in both the wild type and the *cas* mutant.

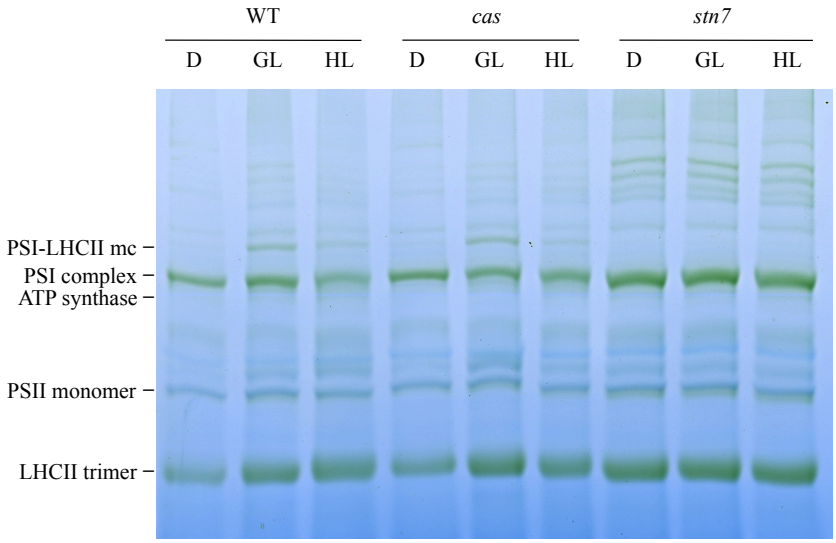

Figure 21: BN-PAGE analysis of ST complex dynamics.

The dynamics of the state transition (ST) complex formation were investigated in the wild type, *cas* and *stn7* following different light treatments. In wild type and the *cas* mutant a ST complex consisting of PSI-LHCII megacomplexes is formed upon shift from darkness to growth light conditions. Upon a 2 hours high light treatment the ST complex is partially reversed in both genotypes.

This last observation is partially in contrast with the spectrometric and immunoblotting data from the *cas* mutant, which suggested an impaired ability to reverse the PSI-LHCII association under high light. Nevertheless, this experiment was only performed once and no definitive conclusions could be made from it.

7.4 Analysis of the transcriptional regulation of CAS

The next series of experiments analyzed the transcriptional regulation behind the expression of the CAS gene. To this end, an online search was conducted to retrieve any available information concerning potential binding sites for transcription factors (TFs) within the promoter region of CAS. In the AGRIS database (Arabidopsis Gene Regulatory Information Server) (Yilmaz et al., 2011) a predicted potential binding site for the circadian Myb-related TF CCA1 (Circadian-Clock Associated 1) was found. In particular, the sequence -aaaaatct- matched a so-called evening element (EE), which is highly represented in CCA1-regulated genes (Nagel et al., 2015). CCA1 is a morning-phased clock gene and one of the main transcriptional regulators of the plant circadian clock network and its expression peaks at dawn whereby it activates daytime-expressed genes (Hsu and Harmer, 2014).
In the following section it will be described the experimental approaches that were used to analyze the transcriptional regulation of CAS and to verify its predicted diurnal behavior.

7.4.1 RT-qPCR analysis of CAS transcript levels

7.4.1.1 Transcript abundance analysis from total mRNA sampled over 48 hours

A RT-qPCR-based analysis was employed to analyze the levels of the CAS mRNA over a total period of 48 hours in 3-4 weeks old plants grown under long day diel (LD) conditions (16 hours of light and 8 hours of darkness). Total mRNA samples were collected at 13 time points at 6 or 3 hours intervals. As visible in figure 22, the abundance of the CAS transcript (normalized to the levels of the reference gene PDF2) oscillates with 12 hours time intervals in wild type *A. thaliana* plants.

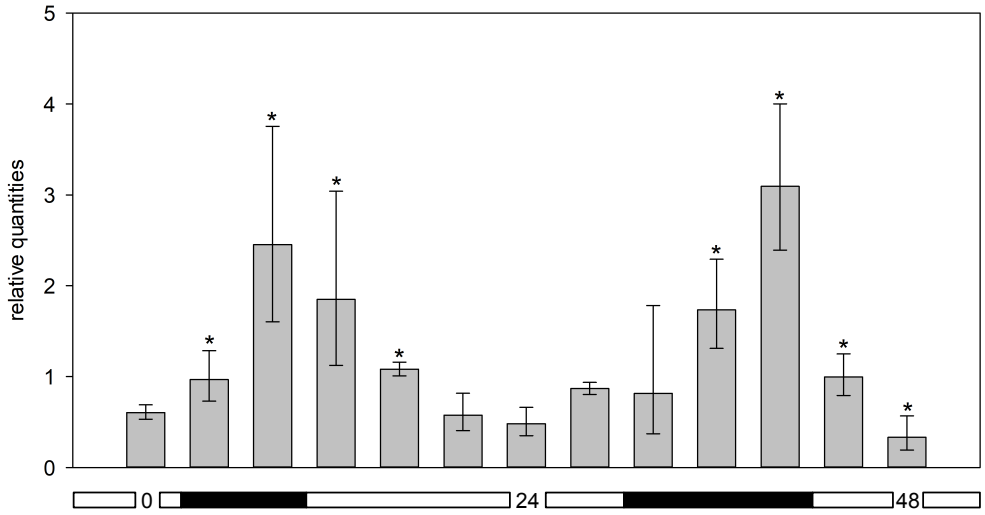

Figure 22: RT-qPCR analysis of CAS mRNA levels over 48 hours.

The relative abundance of the CAS transcript was measured over 48 hours including 13 time points in Col-0 background. Horizontal bottom bar indicates light (empty) and dark (filled) sampling times. Time point 0 refers to 5 pm of the day. Each value represents the mean of 3 independent biological and 2 technical replicates. Error bars represent 95% confidence intervals. Asterisks above the bars denote statistically significant differences compared with time 0 sample (one-way ANOVA, $P < 0.05$).

In particular, the peak of CAS mRNA accumulation coincided with the end of night (5 a.m., EON), 2 hours before the switching on of the lights in the growth cabinet, while minimum levels corresponded to the late day (5 p.m., EOD). Up to 6-fold difference of transcript levels was observed between EON and EOD. The reproducibility of the results over two consecutive days indicated the existence of a physiological diurnal transcriptional regulation of the CAS gene. The reliability of the above-mentioned results was further assessed by testing the behavior of the known circadian, evening-phased, TF gene TOC1 (TIMING OF CAB EXPRESSION), whose mRNA levels peak at the EOD, being its activity required to repress the expression of day-phased genes (Hsu and Harmer, 2014). As seen in Figure 23, the expected rhythmic pattern could be observed for the TOC1 transcript levels peaking at the EOD. These latter results support the choice of PDF2 as a stable reference gene for the normalization process in the analysis of circadian cycling genes.

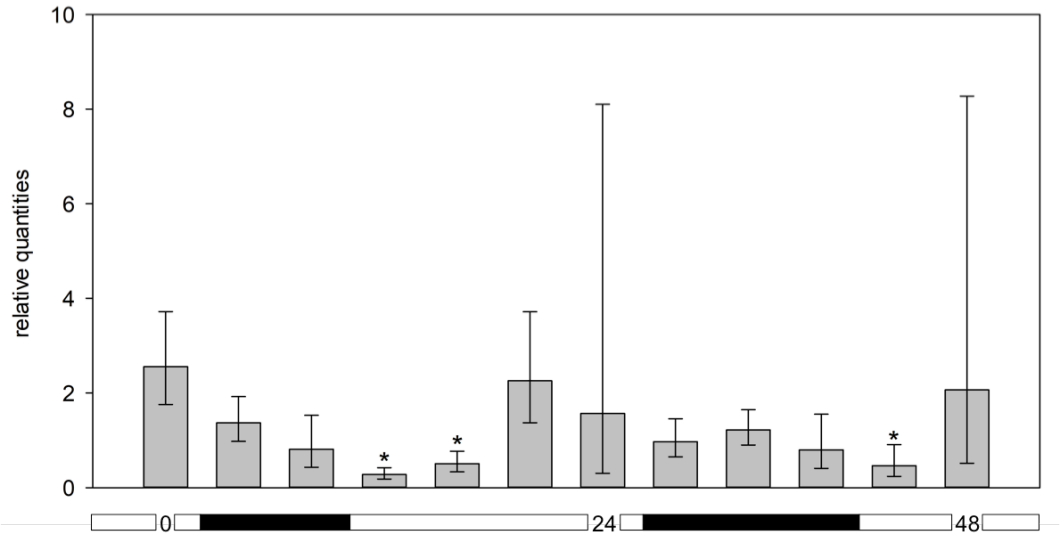

Figure 23: RT-qPCR analysis of TOC1 mRNA levels over 48 hours.

The relative abundance of the TOC1 transcript was measured over 48 hours at 12 time points in the Col-0 background. Horizontal bottom bars indicate light (empty) and dark (filled) sampling times. Time point 0 refers to 5 pm of the day. Each value represents the calculated mean of 3 independent biological and 2 technical replicates. Error bars represent 95% confidence intervals. Asterisks above the bars denote statistically significant differences compared with time 0 sample (one-way ANOVA, $P < 0.05$).

7.4.1.2 Analysis of CAS transcriptional regulation in the cca1 mutant

The role of the transcription factor CCA1 in the diurnal transcriptional regulation of CAS was subsequently tested in the *cca1 A. thaliana* mutant. In this case the number of samples was reduced to the 5, corresponding to the time points where the highest and lowest CAS mRNA levels were found in the previous experiment: i.e. 5 a.m. and 5 p.m., respectively.
By doing so, a consistent transcriptional pattern emerged (Figure 24), where the highest CAS mRNA levels peaked and reached their lowest levels at the same time points as in the wild type.

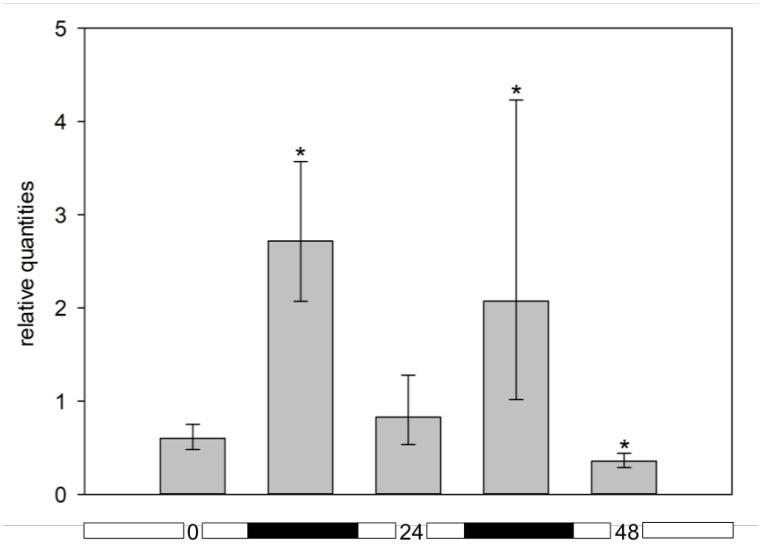

Figure 24: RT-qPCR analysis of CAS mRNA levels over 48 hours in the *cca1* mutant.

The relative abundance of the CAS transcript was measured over 48 hours at 5 time points in *cca1* background. Horizontal bottom bars indicate light (empty) and dark (filled) sampling times. Time point 0 refers to 5 pm of the day. Each value represents the calculated mean of 3 independent and 2 technical replicates. Error bars represent 95% confidence intervals. Asterisks above the bars denote statistically significant differences compared with time 0 sample (one-way ANOVA, $P < 0.05$).

These results indicate the existence of a more complex transcriptional regulation behind the observed cycling behavior of the CAS gene, possibly involving a network of transcription factors. CCA1 might still nevertheless be involved in this regulatory mechanism, but does not appear to be the dominating component.

7.4.1.3 Role of light entrainment in the establishment of cycling activity of the CAS mRNA

To further confirm the diurnal regulation behind the transcriptional activity of the CAS mRNA and to test the role of light entrainment in this process, the relative abundance of the CAS transcript was assessed under normal growing conditions and in plants germinated and grown under constant light (LL). As observed in figure 25, a complete loss of the cycling behavior of the CAS transcript was observed when plants did not experience the alternation of day and night.

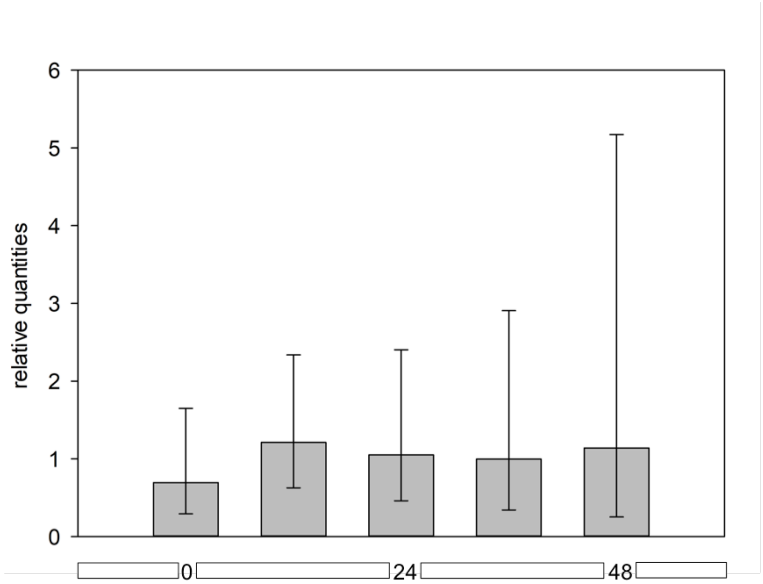

Figure 25: RT-qPCR analysis of CAS mRNA levels over 48 hours under constant light.

The relative abundance of the CAS transcript was measured over 48 hours at 5 time points in the Col-0 background. Horizontal bottom bars indicate sampling times. Time point 0 refers to 5 pm of the day. Each value represents the calculated mean of 3 independent biological and 2 technical replicates. Error bars represent 95% confidence intervals. Asterisks above the bars denote statistically significant differences compared with time 0 sample (one-way ANOVA, $P < 0.05$).

This last observation corroborated the relevance of a diurnal activity behind the transcriptional regulation of CAS and highlighted the relevance of the light-dependent entrainment of specific circadian gene networks in order to establish the oscillating behavior of the CAS mRNA.

7.4.2 Analysis of diurnal oscillations of the CAS protein

7.4.2.1 Immunoblot analysis of the CAS protein levels at different day times

The observed cycling behavior of the CAS transcript raised the legitimate question as to whether this pattern was also reflected at the protein level. To investigate this, the abundance of the CAS protein was assessed across the same 13 time points via immunoblot analysis in total leaf protein samples using the α-CT-CAS antibody.

Interestingly, this analysis also revealed a seemingly diurnal regulation of the CAS protein accumulation but with an opposite trend compared to the transcript (Figure 26). Highest protein levels were detected at EOD, while lowest at EON. This counter-intuitive observation indicates an anticipation of the transcript accumulation before the protein reaches its highest levels.

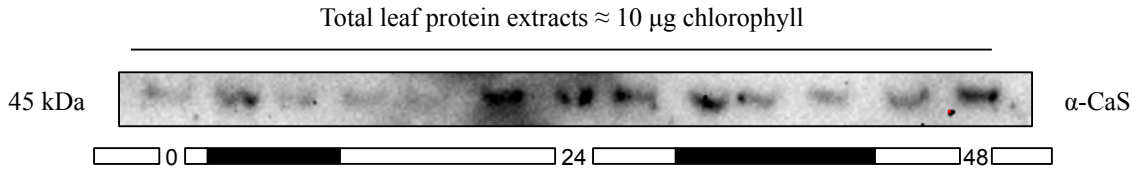

Figure 26: Immunodetection of *in vivo* CAS protein levels over 48 hours.

Circadian oscillations of the CAS protein abundance were measured at 13 time points over 48 hours via immunoblot on total leaf protein extracts. Highest protein levels are detected at time points corresponding to EOD and lowest at EON.

7.4.2.2 In silico search for candidate proteases active on CAS

In order to identify candidate proteases active on CAS, an *in silico* search was performed by submitting the immature CAS sequence (AA 1-387) to the Protease Specificity Prediction Server (PROSPER) (Song et al., 2012). This online tool enables the prediction of client protease and of the cleavage sites in the query substrate sequence. In this case, two cleavage sites were predicted within the CAS sequence, one mapping to position 154 in the NTD and one at position 247 in the CTD (figure 27). A thylakoid processing peptidase annotated as S26.088 in the MEROPS Pepdidase Database (Rawlings et al., 2018) was indicated as the enzyme responsible for these proteolytic events. This protein corresponds to the *A. thaliana* locus AT2G30440 and is also referred to as Plastidic Type I Signal peptidase 2B (Plsp2B) (Hsu et al., 2011).

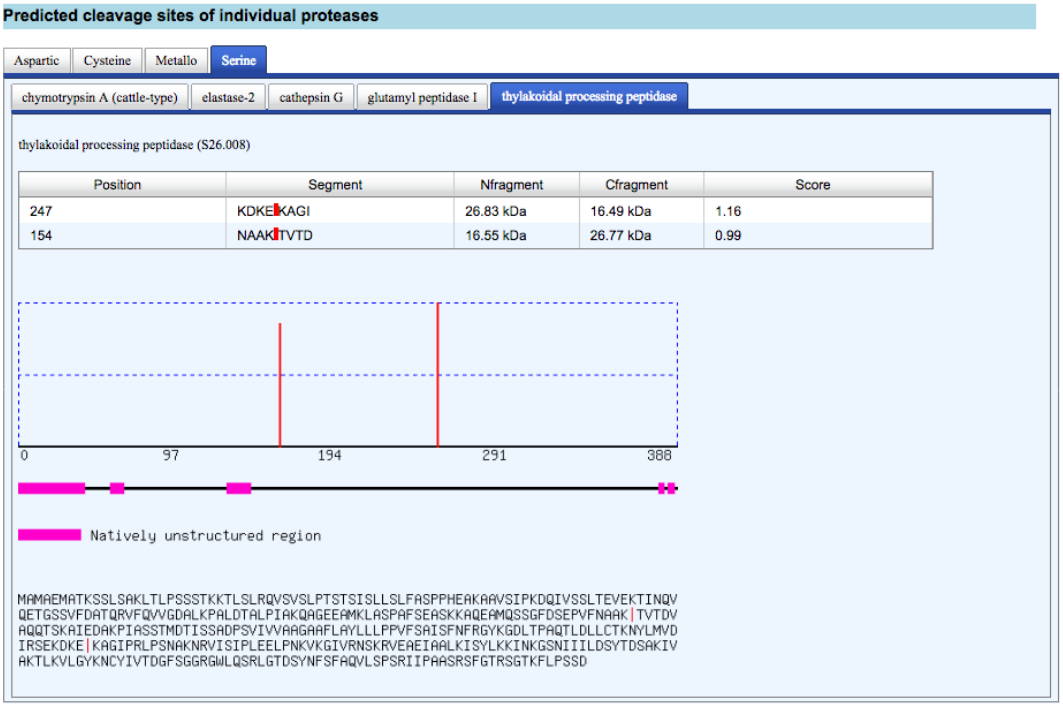

Figure 27: Predicted cleavage sites of CAS by the thylakoid processing peptidase Plsp2B

7.5 Analysis of growth and photosynthetic performance under drought stress

A high-throughput screening analysis of the growth and photosynthetic performance was conducted in order to phenotypically characterize in detail the *A. thaliana cas* mutant along with the *stn7* and *stn8* mutants. A drought treatment was also applied in order to maximize any potential growth or photosynthetic phenotype. Such kind of stress was chosen due to the previously suggested involvement of CAS in the regulation of stomatal physiology and water use efficiency (Han et al., 2003, Nomura et al., 2008, Weinl et al., 2008, Vainonen et al., 2008, Zhao et al., 2015, Wang et al., 2016, Wang et al., 2014). As visible in figure 28, the application of the drought stress resulted in a marked phenotype characterized by strongly reduced growth.

Figure 28: Drought stress application during the high-throughput screening.

Representative RGB picture showing the randomization of the four genotypes (wild type, *cas*, *stn7* and *stn8*) and of the watering protocol on measuring trays. A clear difference in the growth phenotype between control plants (maintained at 60% of the soil water-holding capacity) and water-stressed (13 days after water withholding) is clearly recognizable.

As shown in figure 29, the growth performance of the two watering groups diverged already 2 days after the split between treatments. The four genotypes showed a clear separation in their growth performance according to their watering regime.

In contrast with previous reports (Vainonen et al., 2008), no striking growth phenotype could be observed for the *cas* mutant even under harsh water stress.

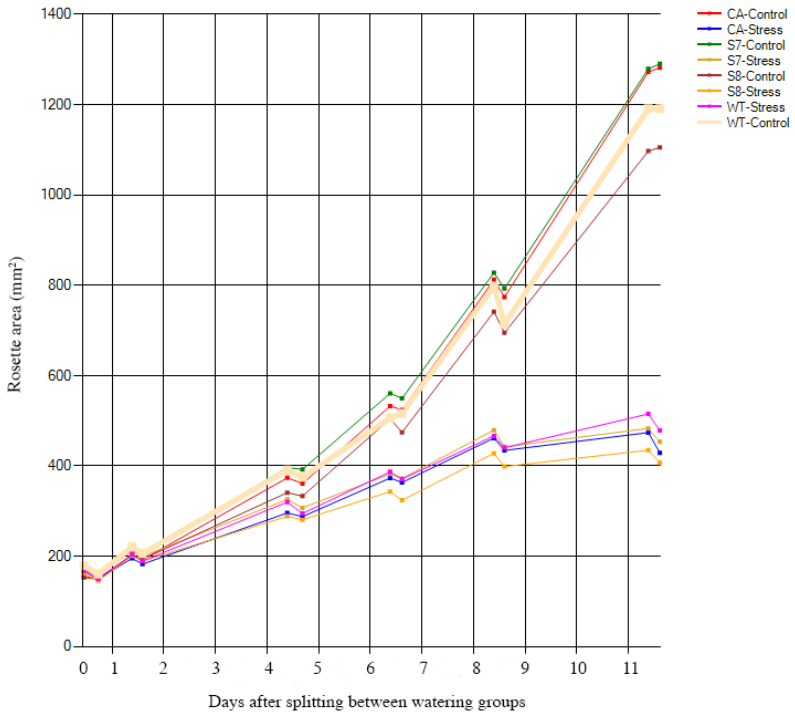

Figure 29: Growth performance under drought stress.

Projected rosette area over time of wild type (WT), *cas* (CA), *stn7* (S7) and *stn8* (S8) plants from the day of splitting between watering groups (day 18, labeled day 0) until the reaching of wilting (day 30, labeled day 12). Values represent the averages of 10 replicates per genotype and treatment. The transient reduction in the apparent rosette area observed at several points reflects the physiological movements of the leaves during the day due to the measurements being occasionally performed at different daytimes.

Accordingly, no striking difference emerged in the photosynthetic performance between the four genotypes. Very similar kinetics of the photosynthetic parameters QY (operating efficiency of the primary photochemistry in PSII) and NPQ (fast, reversible, Energy-dependent component of Non-Photochemical Quenching, qE) were detected in the four

genotypes under both conditions, but with very pronounced and consistent differences observed between the start (day 18) and the end (day 30) of the drought stress application (Figures 30, 31, 32 and 33).

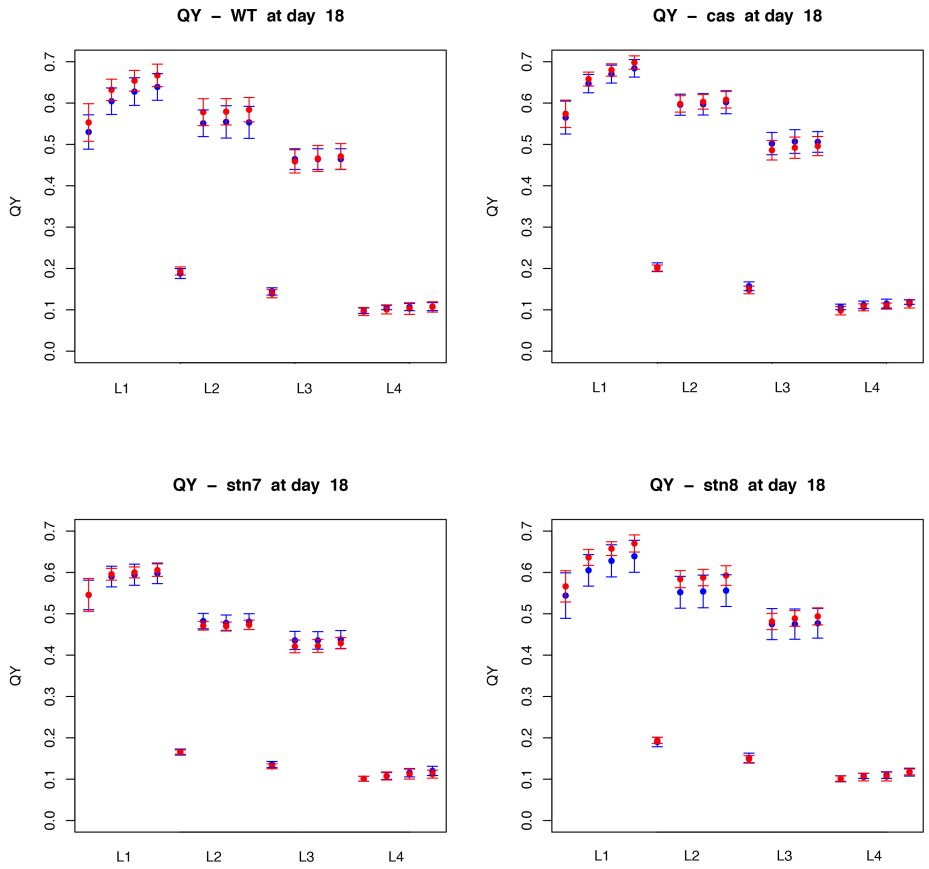

Figure 30: QY in control and drought stress at the beginning of the drought treatment. Calculated QY values (operating efficiency of the primary photochemistry in PSII) of the four genotypes measured at different time points during the light curve PAM protocol of increasing actinic light steps of 5 minutes (35, 125, 250, and 1194 µmol m^{-2} s^{-1}, corresponding to L1, L2, L3, and L4) at the beginning of the drought stress treatment, when all plants are found at similar watering status. Red and blue refer to water-stressed and control conditions, respectively. Values refer to the average of 10 biological replicates while bars represent standard deviation.

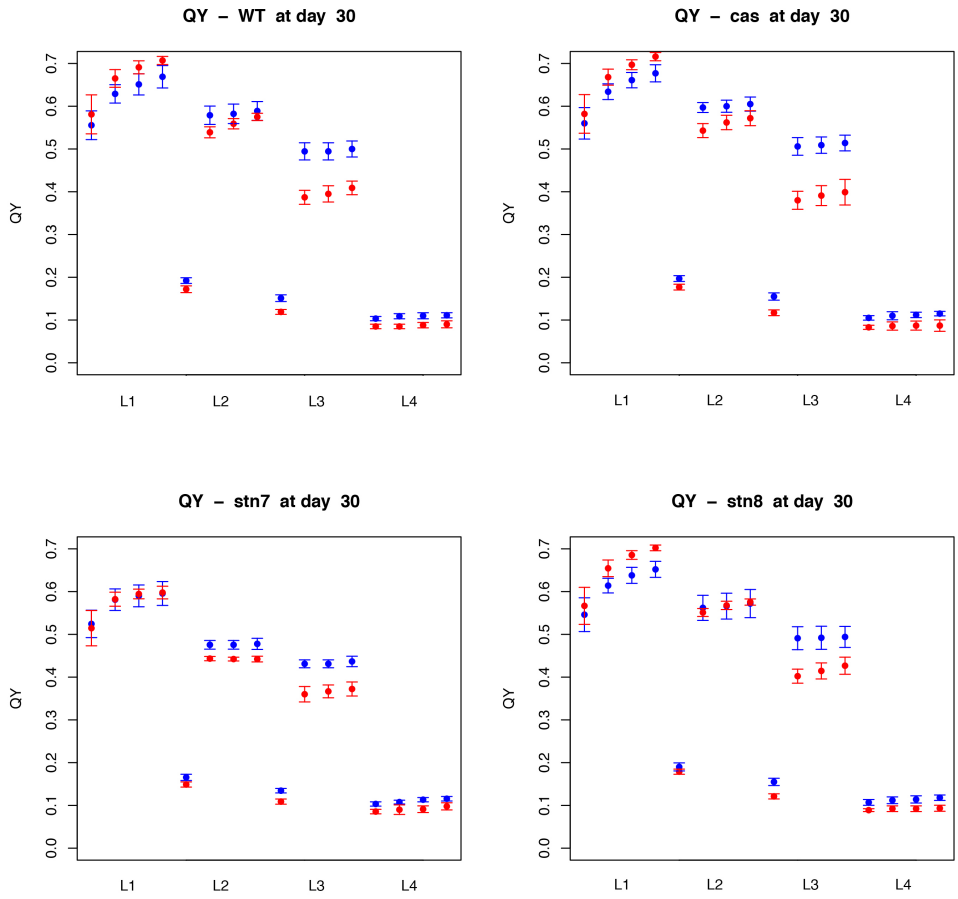

Figure 31: QY in control and drought stress at the end of the drought treatment.

Calculated QY values (operating efficiency of the primary photochemistry in PSII) of the four genotypes measured at different time points during the light curve PAM protocol of increasing actinic light steps of 5 minutes (35, 125, 250, and 1194 µmol m^{-2} s^{-1}, corresponding to L1, L2, L3, and L4) at the end of the drought stress treatment, when water-stressed plants reached wilting point. Red and blue refer to water-stressed and control conditions, respectively. Values refer to the average of 10 biological replicates while bars represent standard deviation.

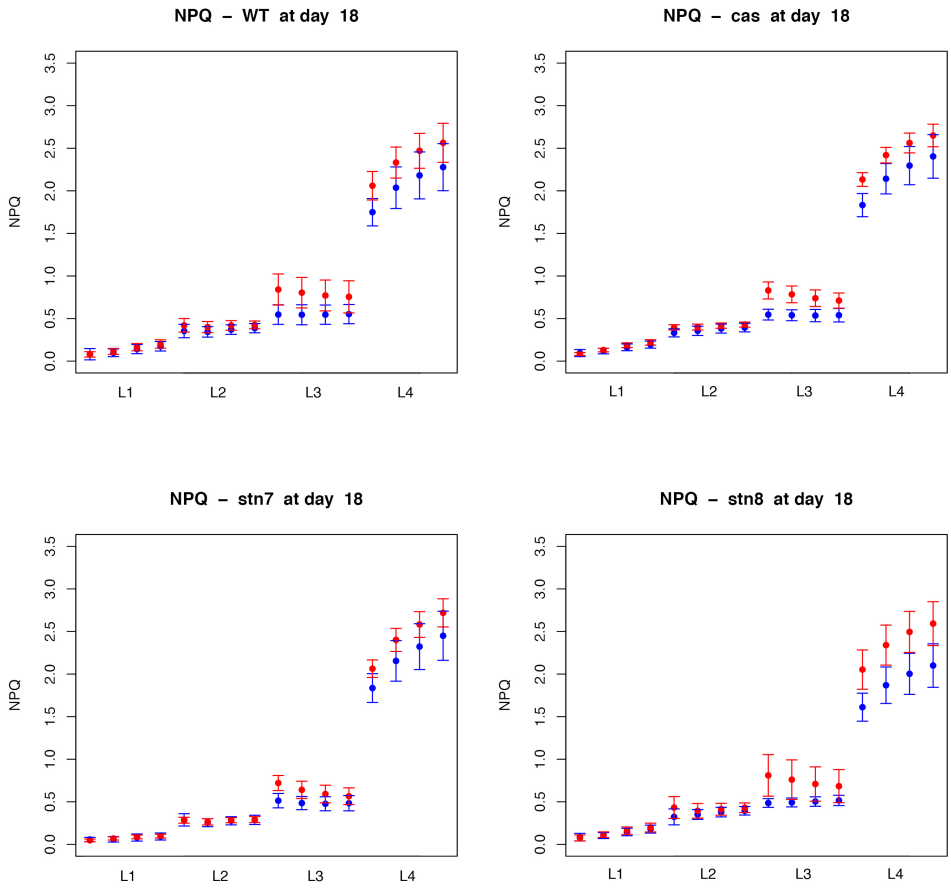

Figure 32: NPQ in control and drought stress at the beginning of the drought treatment.

Calculated NPQ values (qE) of the four genotypes measured at different time points during the light curve PAM protocol of increasing actinic light steps of 5 minutes (35, 125, 250, and 1194 µmol m^{-2} s^{-1}, corresponding to L1, L2, L3, and L4) at the beginning of the drought stress treatment, when all plants are found at similar watering status. Red and blue refer to water-stressed and control conditions, respectively. Values refer to the average of 10 biological replicates while bars represent standard deviation.

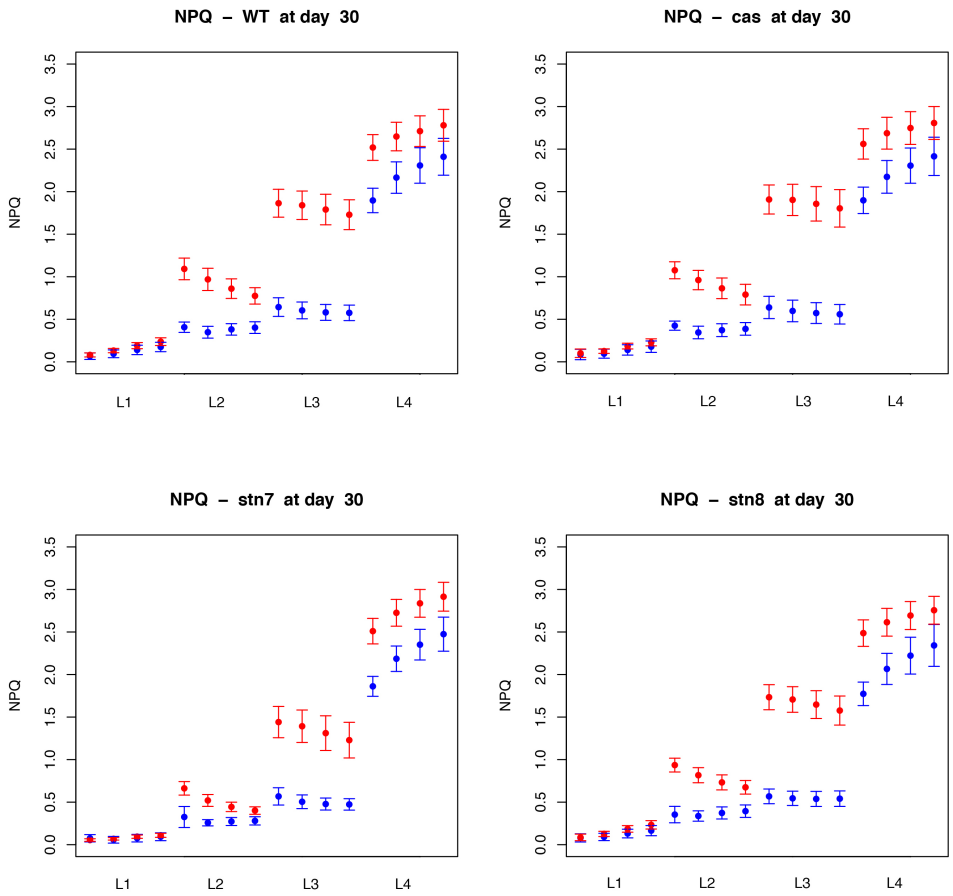

Figure 33: NPQ in control and drought stress at the end of the drought treatment.

Calculated NPQ values (qE) of the four genotypes measured at different time points during the light curve PAM protocol of increasing actinic light steps of 5 minutes (35, 125, 250, and 1194 µmol m^{-2} s^{-1}, corresponding to L1, L2, L3, and L4) at the end of the drought stress treatment, when water-stressed plants reached wilting point. Red and blue refer to water-stressed and control conditions, respectively. Values refer to the average of 10 biological replicates while bars represent standard deviation.

8 Discussion

Reversible protein phosphorylation is recognized as an important molecular mechanisms used in cellular systems to regulate function, localization, stability and interactions of proteins. Phosphorylation of target residues within specific types of proteins also represents a crucial step in the activation of signal transduction pathways, ultimately leading to the fine-tuning of a myriad of regulatory physiological processes.

In plants, just as in all other biological systems, protein phosphorylation regulates many biological processes ranging from cellular proliferation and differentiation to metabolism and gene expression (Stone and Walker, 1995). Due to their sessile nature plants have evolved complex networks of signaling pathways that enable them to perceive potentially stressing conditions and to quickly counteract by adapting their physiology on several levels (Zhu, 2016). Indeed, one crucial task that many plant specific protein kinases and phosphatases do is to mediate rapid physiological responses to the fluctuations of the environment, most notably the changes in light conditions (Rochaix et al., 2012).

A number of rearrangements of the supramolecular composition of photosynthetic complexes occur in response to both limiting and stressing light conditions and in several cases these are mediated by the antagonistic activity of protein kinases and phosphatases targeting photosynthetic, thylakloid-localized proteins. These events are often required to prevent the occurrence of imbalances in the redox state of components that could potentially lead to poor photosynthetic performance and, under persisting stressing conditions, eventually to the damage of the core components of the photosynthetic apparatus.

The understanding and functional characterization of the role(s) of protein phosphorylation in the chloroplast has significantly progressed during the last years but still many open questions persist regarding the biological significance of many of the described phosphorylation events, their regulation and the identity of the protein kinase(s) involved.

8.1 CAS is part of a phosphorylation network involving several protein kinases

In the present work the phosphorylation profile of the CAS was investigated in detail and it was shown that CAS is phosphorylated by multiple protein kinases on several residues.

It appears that a number of independent phosphorylation events occur on this protein in response to different activating stimuli leading to potentially different physiological outcomes.

In the initial work that described CAS as a phosphoprotein (Vainonen et al., 2008) the authors proposed that CAS is a target of the STN8 kinase and that its modification occurs at the level of the Thr-380 residue in response to increasing light intensities. Nevertheless, this conclusion was based on the use of a α-pThr antibody-based strategy that could not distinguish between individually phosphorylated residues and also could not provide any information regarding potentially phosphorylated serine residues. In addition, the single phosphopeptide detected in this work via MS/MS only started at position Ser-378 and was unable to provide information regarding any phosphorylated residues outside this peptide.

The present work, instead, used a combined approach based on *in vitro* kinase assays and phosphoproteomics in order to characterize the phosphorylation profile of CAS by dissecting the relevance of selected phosphorylation sites and the involvement of candidate protein kinases. By doing so, it was possible to confirm at least 4 of the previously experimentally described phoshorylation sites of CAS in *A. thaliana* (Thr-350, Thr-376, Ser-378 and Thr-380). The positions Thr-376, Ser-378 and Thr-380 were found phosphorylated in the present phosphoproteomics study, while positions Thr-376 and Thr-380 emerged as the most critical ones from the *in vitro* approach. The substitution of Thr-376 with the non-phosphorylatable amino acid valine caused the strongest reduction in the intensity of phosphorylation, suggesting that this position is the main target of phosphorylation of CAS, at least in the model organism *A. thaliana*.

This last observation was also corroborated by the phylogenetic analysis of the conservation status of the experimentally described *A. thaliana* pS/Ts in several evolutionary lineages. Indeed, positions Thr-376 and Thr-350, and to a lesser extent Thr-380, show the highest conservation from green algae to angiosperms. Intriguingly, in the phosphoproteomics databases of several organisms the positions corresponding to the residues Thr-376 and Thr-380 of their CAS orthologs were also found phosphorylated.

From this work it also emerged that STN8 is likely not the only kinase targeting CAS since the phosphoproteomics analysis detected the same phosphopeptides in the wild type as in the *stn8* mutant, albeit with lower abundances. This indicates that residual phosphorylation of CAS can occur in the absence of STN8 by additional protein kinase(s), including STN7 and potentially others. The *in vitro* assays revealed indeed that CAS could be equally phosphorylated when STN7 and STN8 are lacking, suggesting that both kinases are involved.

8.2 Light and Ca^{2+} signals regulate the phosphorylation of CAS

In this work, a strong reduction in the phosphorylation of CAS could be observed in the absence of both STNs, leaving a residual signal that could be further reduced to negligible levels by the removal of Ca^{2+} ions from the assay conditions with EGTA. This observation supports the previously described Ca^{2+}-dependency of CAS phosphorylation (Stael et al., 2012a). Although the identity of this kinase is not known, at least the involvement of the two STNs can be excluded.

The role of light-dependent activation behind the phosphorylation of CAS was also investigated and it could be shown that, at least under growth light conditions, the STN7 kinase appears to be the main player. This observation does not negate the results of Vainonen et al. but rather suggests that the activity of the two STN kinases on CAS might be differentially regulated by the prevailing light conditions, with STN7 mainly active under low/growth light while STN8 being predominantly involved under high irradiance.

Overall, it emerged that CAS is part of a chloroplast phosphorylation network that involves the STN7 and STN8 kinases and, at least, another Ca^{2+}-dependent kinase.

According to the topological arrangement of CAS, as shown in this work, any other kinase targeting CAS must be localized within the stroma or, at least, have its catalytic domain exposed to the stromal compartment. The “phosphorylation hot spot” at the C-terminal end could potentially serve as a hub for integrating multiple signals required to promote protein interactions or other subtle regulatory processes of the photosynthetic reactions.

Concerning the described topology of CAS along the thylakoid membrane, it is not clear yet how this arrangement could be achieved if one considers the presence of a single TMD.

It is in fact possible to envisage the existence of a second TMD that is not defined by *in silico* tools.

Alternatively, the predicted TMD is actually an anchoring or docking domain that only enters a single leaflet of the membrane. Unfortunately, this issue could not be solved within the time frame of this work.

8.3 The physiological role of CAS phosphorylation remains elusive

The functional significance of the phosphorylation of CAS is yet not clear and it was not investigated directly in this work either. Furthermore, since the exact molecular function of CAS is not known, it is somewhat difficult to speculate on the biological role of its transient modifications. Vainonen et al. proposed that the phosphorylation of Thr-380 could serve to promote the interaction of CAS with other proteins. They speculated that the amino acid region surrounding this residue has protein-protein interaction ability (PPI) by referring to an *in silico* prediction that loosely likened this sequence to a consensus interaction motif with 14-3-3 proteins (Denison et al., 2011) and a Fork Head Associated Domain (FHAD).

Of note, no 14-3-3 module containing protein has been experimentally described in the chloroplast so far, although some are involved in the process of protein import from outside the organelle (May and Soll, 2000). Only one FHAD containing protein (At2g21530) is predicted for the chloroplast and it would be interesting to validate its physical interaction with CAS.

In summary, in according with previous work and data presented in this work, it appears that CAS is mostly found in a phosphorylated status during the day promoted by the activity of the two STN kinases. It can be envisaged that different residues are targeted by one or the other STNs kinases according to the prevailing light conditions and that the outcomes of these modifications depends on the specific residue(s) involved, but also on the overall phosphorylation status. It is in fact conceivable that the phosphorylation profile of CAS changes regularly during the day and also in response to sudden changes in the light conditions. Under low light irradiation, corresponding to the early and late times of the day, phosphorylation of CAS might be under the control of the STN7 kinase. This modification could represent a steady state condition required to promote balanced excitation of the two photosystems and to favoring specific interactions between components of the photosynthetic apparatus leading to optimal electron fluxes within the thylakoid membrane.

On the other hand, under higher irradiance usually found at midday, STN8-dependent phosphorylation might become predominant on CAS and could be required to promote photoprotective mechanisms or photoacclimation strategies. The occurrence of subtle changes of the *in vivo* phosphorylation status of CAS in response to different light conditions cannot easily be monitored but represents an interesting question that should be addressed in the future via carefully designed proteomics-based experiments.

Based on the evidence emerged from this work, a speculative working model summarizing the dynamics of phosphorylation of CAS and its potential physiological consequences is presented in figure 34.

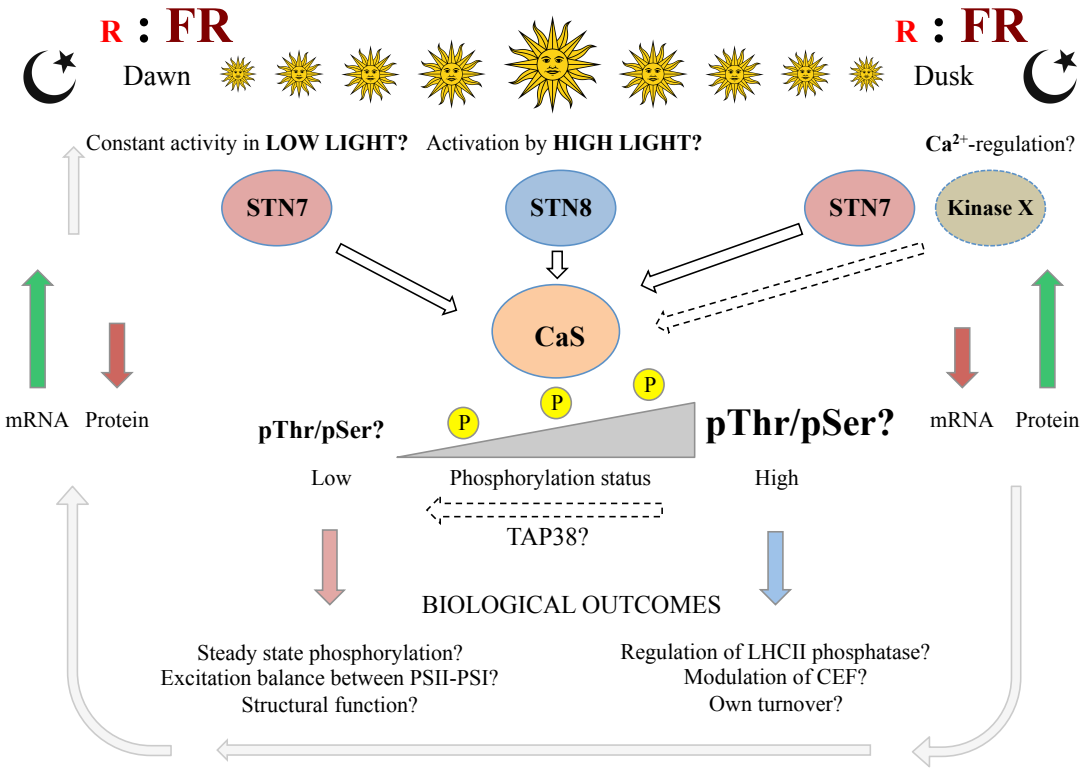

Figure 34: Proposed working model for CAS phosphorylation and biological outcomes.

The phosphorylation profile of CAS could vary during the day in response to the prevailing light conditions under the activity of the STN7 and STN8 kinases. A third, so far uncharacterized, Ca^{2+}-dependent phosphorylation event could follow the increase in the stromal calcium levels upon the transition from light to dark. The opposite observed diurnal patterns of the CAS mRNA and protein accumulation are integrated in this model and the potential outcomes of its differential phosphorylation events are presented.

8.4 A role for CAS in photoacclimation responses to high light?

In this work, it was possible to show the existence of a photosynthetic phenotype of the *cas* mutant, which suggested the involvement of this protein in the photoacclimation responses to high light. The analysis of the chlorophyll fluorescence curves from isolated thylakoids at 77K revealed a strong excitation of PSI under highlight in the *cas* mutant, suggesting a defective reversal of PSI-LHCII complexes under this stressing conditions. Accordingly, when the phosphorylation status of thylakoid proteins was monitored using an α-pThr antibody, the absence of CAS resulted in a concomitant high phosphorylation level of both LHCII and the PSII core protein D1 and D2. These observations indicate that the high light-induced process of dephosphorylation of LHCII by the phosphatase TAP38 might be impaired in the *cas* mutant. It can be speculated that CAS, possibly in an STN8-driven phosphorylated form could directly affect the function of TAP38. This suggestion might be supported by the 77K spectra of the *cas* mutant recorded after a high light treatment that strongly resembled the previously described phenotype of the *tap38,* however, similar changes in the spectrum are also described for the cyclic electron transport mutant *pgr5* (Mekala et al., 2015).

8.5 The role of Ca^{2+} in the phosphorylation of CAS is not fully understood

Concerning the role of Ca^{2+} in the phosphorylation of CAS it is difficult to provide any biological explanation and context, such as in the case of all other so far described chloroplast targets of Ca^{2+}-dependent phosphorylation (Stael et al., 2012a, Rocha et al., 2014). Many Ca^{2+}-dependent (CDPK) and CDPK-related (CRK) protein kinase are known to exist in plants (Harper et al., 2004, Harmon, 2003, Schulz et al., 2013, Valmonte et al., 2014) but none of these has been experimentally proven to localize in the chloroplast (Simeunovic et al., 2016, Schliebner et al., 2008, Bayer et al., 2012). Still, a substantial body of experimental evidence has accumulated and points towards a crucial role for Ca^{2+} signals the chloroplast (Nomura and Shiina, 2014, Rocha and Vothknecht, 2012, Stael et al., 2012b) and new components of the so-called chloroplast *"calcium signaling toolkit"* are being continuously described.

Oscillations in levels of free Ca^{2+} ions in the chloroplast stroma are known to be caused by stimuli of biotic and abiotic origin and are involved in the regulation of different plant physiological processes including guard cells responses (Wang et al., 2016, Wang et al., 2012, Wang and Zheng, 2012, Kim et al., 2010), expression of immunity-related genes and synthesis of hormones (Nomura et al., 2012). Moreover, regular circadian oscillations of the chloroplast Ca^{2+} concentration occur upon the transition from light to dark (Johnson et al., 1995, Sai and Johnson, 2002, Sello et al., 2018). It is conceivable that such transient increases in the local concentration of Ca^{2+}, especially if taking place within microdomains adjacent to thylakoid membranes, are sufficient to modulate the activity of Ca^{2+} sensor proteins, including protein kinases. In this scenario, CAS could be a target of such events, although the identity of the involved kinase, the involved residue(s) and the biological outcome of this event(s) still remain largely unknown.

8.6 CAS is a potential novel component of the chloroplast circadian network

The Q-PCR analysis performed in this work indicated the existence of a circadian regulation behind the transcription of the CAS gene and this might also be reflected in the accumulation of the protein. Although the protein data are not sufficiently robust yet, these observations provide new evidence towards the understanding of the function of CAS. In fact, while the abundance of the CAS transcript reaches its highest levels at the EON, its protein levels appear to increase during the day, reaching its highest levels at the EOD.

This seemingly opposite behavior between transcription and translation of CAS are characterized by a 12 hours shift, suggesting the presence of high mRNA levels available in the early day that are then slowly translated into the corresponding protein product.

It can be speculated that such pattern of transcription/translation would provide a mechanism for anticipating predictable and regularly stressing condition potentially occurring during the day. For example, this mechanism could serve as potential reservoir for readily available mRNA that could be used to produce more protein in the case of a sudden or extreme stress. It can also be imagined that the phosphorylation status of CAS varies in a regular fashion during the day and that its modifications could serve as signals to regulate protein content via controlled protein degradation.

Circadian regulation of photosynthesis is a well established concept (Dodd et al., 2014) and a number of plastid and nuclear genes (PhANGs) - above all the Light Harvesting Complex (LHC) genes CHLOROPHYLL A/B BINDING PROTEIN2 (CAB2) (Millar et al., 1992) - are under circadian or diurnal transcriptional regulation (Schaffer et al., 2001). Accordingly, several photosynthesis-related processes, including oxygen evolution, electron transport and the accumulation of chloroplast ATP, indeed display diurnal patterns, implying the existence of a concerted network of chloroplast components following circadian-regulated activities. The data here presented suggest that CAS is a newly identified component of the chloroplast circadian network, although no conclusion can be made at this point about its biological role in this scenario. Nevertheless, considering the original description of CAS as a low affinity, high capacity Ca^{2+}-binding protein (Han et al., 2003) and the herein described diurnal changes in the its protein levels, it is tempting to speculate on a potential involvement of CAS in shaping the afore-mentioned diurnal circadian oscillations of free Ca^{2+} ions in the chloroplast stroma. It should be nevertheless noted that the *in vitro* Ca^{2+} binding ability of CAS determined by Han et al. would need much higher concentrations (5 mM) than the maximal physiological levels found within the stroma (5 - 10 μM). Also, the CAS protein does not possess any canonical Ca^{2+} binding domain, such as the EF hand (Day et al., 2002) and its potential ability to bind Ca^{2+} is attributed to a stretch of negatively charged amino acids within its NTD.

Based on the topological description presented in this work, the N-terminus of CAS is facing the stromal environment and is thus compatible with a potential Ca^{2+}-buffering activity in this compartment. One of the activities of CAS could consist in Ca^{2+}-binding and to sequester Ca^{2+} ions in the vicinity of the thylakoid membranes, thereby contributing to create local Ca^{2+} microdomains. At the same time, the degradation of the CAS protein towards the EOD would determine a release of Ca^{2+} in the chloroplast stroma contributing to the described increase of free Ca^{2+} towards the EOD.

Although these are pure speculations, it is known that most of the free Ca^{2+} within chloroplast is associated with thylakoid membrane proteins and that high free stromal Ca^{2+} levels lead to the inhibition of several enzymes of the CBB cycle (Hochmal et al., 2015). In light of these evidences, it is reasonable to speculate that CAS is a component of the chloroplast "*calcium toolkit*" and could act as a Ca^{2+}-storing element.

While there is no experimental evidence for a controlled degradation of CAS, the *in silico* identified target sites for the thylakoid processing protease (TPP) could have a biological relevance with respect to the physiological role of CAS. The TPP protein is part of a protease family including two other thylakoid processing peptidases (Hsu et al., 2011) for which no native substrates are known. The Pslp2B protein is the best characterized protease of this family and a truncated version including its catalytic domain was previously expressed recombinantly and shown to *in vitro* cleave the 23kD extrinsic protein of photosystem II (Chaal et al., 1998). Interestingly a number of chloroplast proteases, including members of the Deg family, have been shown to be pH- or redox- regulated, pointing to a light dependent processing activity promoted by high light conditions (Stroher and Dietz, 2008, Kley et al., 2011, Haussuhl et al., 2001).

8.7 Outlook and future directions

In conclusion, this work has established the chloroplast Calcium Sensing Protein CAS as a potential component of the photoacclimation responses to high light in *A. thaliana* and has significantly progressed the understanding of its multiple phosphorylation events. Nevertheless, a number of questions concerning both the function of CAS and the significance of its phosphorylation still remain.

In the future it would be of great interest to establish direct kinase-residue relationships and to deeply investigate under which conditions specific residues are targeted by their client kinase(s). This would require the design of phosphoproteomics-based experiments using mutant lines of individual kinases, the application of specific light treatments and semiquantitative analysis of the relative abundance of individual phosphorylated residues.

It would be interesting to explore whether the phosphorylation pattern of CAS varies regularly during the day and whether this correlates with diurnal variations of the protein levels.

The interaction of CAS with other proteins, and the role of phosphorylation in this respect, was suggested but never experimentally proven. For this reason, the follow-up work on this project should include the search for potential interacting partners of CAS and their characterization via complementary approaches. Strong candidates for this line of research are the phosphatase TAP38, PGR5 and At2g21530.

Also, it would be of great interest to test whether a recombinant version of TPP (or PlsP2B) is able to cleave recombinant CAS fragments or the native protein from isolated thylakoids.

Finally, a detailed photosynthetic characterisation of the *cas* mutant should be performed.

In this work no discernible growth phenotype could be observed in the *cas* mutant even when grown under harsh water stress. Accordingly, the PAM analysis did not reveal any specific defect in the main photosynthetic parameters *in vivo* under these conditions. Nevertheless, considering the potential role of CAS in the fine-tuning of photosynthesis it would be advisable to perform different phenotyping protocols. As an example, a so-called called fluctuating light regime, consisting of regular intervals of low and high light periods, could potentially reveal a defect in the growth and photosynthetic performance of this mutant.

This condition is more similar to the growing conditions experienced by plants in their natural environment and requires dynamic and rapidly reversible acclimation mechanisms, mostly mediated by protein phosphorylation. It is possible that such conditions would reveal new phenotypes that are caused by a defective adjustment of the activity of photosynthetic apparatus in response to sudden redox imbalances and altered electron fluxes caused by changes in the light quality and intensity.

9 References

ALTSCHUL, S. F., GISH, W., MILLER, W., MYERS, E. W. & LIPMAN, D. J. 1990. Basic local alignment search tool. *J Mol Biol,* 215**,** 403-10.

ANDERSON, J. M., HORTON, P., KIM, E. H. & CHOW, W. S. 2012. Towards elucidation of dynamic structural changes of plant thylakoid architecture. *Philos Trans R Soc Lond B Biol Sci,* 367**,** 3515-24.

ARSOVA, B. & SCHULZE, W. X. 2012. Current status of the plant phosphorylation site database PhosPhAt and its use as a resource for molecular plant physiology. *Front Plant Sci,* 3**,** 132.

ATKINS, K. A. & DODD, A. N. 2014. Circadian regulation of chloroplasts. *Curr Opin Plant Biol,* 21**,** 43-50.

AUSTIN, J. R., 2ND & STAEHELIN, L. A. 2011. Three-dimensional architecture of grana and stroma thylakoids of higher plants as determined by electron tomography. *Plant Physiol,* 155**,** 1601-11.

AWLIA, M., NIGRO, A., FAJKUS, J., SCHMOECKEL, S. M., NEGRAO, S., SANTELIA, D., TRTILEK, M., TESTER, M., JULKOWSKA, M. M. & PANZAROVA, K. 2016. High-Throughput Non-destructive Phenotyping of Traits that Contribute to Salinity Tolerance in Arabidopsis thaliana. *Front Plant Sci,* 7**,** 1414.

BAENA-GONZALEZ, E., BARBATO, R. & ARO, E. 1998. Role of Phosphorylation in the Repair Cycle and Oligomeric Structure of Photosystem II. *In Planta,* 208**,** 196 - 204.

BAGINSKY, S. 2016. Protein phosphorylation in chloroplasts - a survey of phosphorylation targets. *J Exp Bot*.

BAGINSKY, S. & GRUISSEM, W. 2009. The chloroplast kinase network: new insights from large-scale phosphoproteome profiling. *Mol Plant,* 2**,** 1141-53.

BAKER, N. R. 2008. Chlorophyll fluorescence: a probe of photosynthesis in vivo. *Annu Rev Plant Biol,* 59**,** 89-113.

BAYER, R. G., STAEL, S., ROCHA, A. G., MAIR, A., VOTHKNECHT, U. C. & TEIGE, M. 2012. Chloroplast-localized protein kinases: a step forward towards a complete inventory. *J Exp Bot,* 63**,** 1713-23.

BELLAFIORE, S., BARNECHE, F., PELTIER, G. & ROCHAIX, J. D. 2005. State transitions and light adaptation require chloroplast thylakoid protein kinase STN7. *Nature,* 433**,** 892-5.

BENNETT, J. 1977. Phosphorylation of chloroplast membrane polypeptides. *Nature,* 269**,** 344.

BHASKARA, G. B., WEN, T. N., NGUYEN, T. T. & VERSLUES, P. E. 2017. Protein Phosphatase 2Cs and Microtubule-Associated Stress Protein 1 Control Microtubule Stability, Plant Growth, and Drought Response. *Plant Cell,* 29**,** 169-191.

BODENMILLER, B., MUELLER, L. N., MUELLER, M., DOMON, B. & AEBERSOLD, R. 2007. Reproducible isolation of distinct, overlapping segments of the phosphoproteome. *Nature Methods,* 4**,** 231-237.

BOLOURI MOGHADDAM, M. R. & VAN DEN ENDE, W. 2013. Sweet immunity in the plant circadian regulatory network. *J Exp Bot,* 64**,** 1439-49.

BONARDI, V., PESARESI, P., BECKER, T., SCHLEIFF, E., WAGNER, R., PFANNSCHMIDT, T., JAHNS, P. & LEISTER, D. 2005. Photosystem II core phosphorylation and photosynthetic acclimation require two different protein kinases. *Nature,* 437**,** 1179-82.

BONENTE, G., BALLOTTARI, M., TRUONG, T. B., MOROSINOTTO, T., AHN, T. K., FLEMING, G. R., NIYOGI, K. K. & BASSI, R. 2011. Analysis of LhcSR3, a protein essential for feedback de-excitation in the green alga Chlamydomonas reinhardtii. *PLoS Biol,* 9**,** e1000577.

BONHOMME, L., VALOT, B., TARDIEU, F. & ZIVY, M. 2012. Phosphoproteome Dynamics Upon Changes in Plant Water Status Reveal Early Events Associated With Rapid Growth Adjustment in Maize Leaves. *Molecular & Cellular Proteomics : MCP,* 11**,** 957-972.

BRUCE, B. D. 2000. Chloroplast transit peptides: structure, function and evolution. *Trends Cell Biol,* 10**,** 440-7.

BUSCH, A. & HIPPLER, M. 2011. The structure and function of eukaryotic photosystem I. *Biochim Biophys Acta,* 1807**,** 864-77.

CABANTOUS, S., TERWILLIGER, T. C. & WALDO, G. S. 2005. Protein tagging and detection with engineered self-assembling fragments of green fluorescent protein. *Nat Biotechnol,* 23**,** 102-7.

CHAAL, B. K., MOULD, R. M., BARBROOK, A. C., GRAY, J. C. & HOWE, C. J. 1998. Characterization of a cDNA encoding the thylakoidal processing peptidase from Arabidopsis thaliana. Implications for the origin and catalytic mechanism of the enzyme. *J Biol Chem,* 273**,** 689-92.

CHAN, K. X., PHUA, S. Y., CRISP, P., MCQUINN, R. & POGSON, B. J. 2016. Learning the Languages of the Chloroplast: Retrograde Signaling and Beyond. *Annu Rev Plant Biol,* 67**,** 25-53.

CHEN, Y., HOEHENWARTER, W. & WECKWERTH, W. 2010. Comparative analysis of phytohormone-responsive phosphoproteins in Arabidopsis thaliana using TiO2-phosphopeptide enrichment and mass accuracy precursor alignment. *Plant J,* 63**,** 1-17.

CLAUSEN, C. H., BROOKS, M. D., LI, T. D., GROB, P., KEMALYAN, G., NOGALES, E., NIYOGI, K. K. & FLETCHER, D. A. 2014. Dynamic mechanical responses of Arabidopsis thylakoid membranes during PSII-specific illumination. *Biophys J,* 106**,** 1864-70.

COHEN, P. 2000. The regulation of protein function by multisite phosphorylation--a 25 year update. *Trends Biochem Sci,* 25**,** 596-601.

COLLINGRIDGE, P. W. & KELLY, S. 2012. MergeAlign: improving multiple sequence alignment performance by dynamic reconstruction of consensus multiple sequence alignments. *BMC Bioinformatics,* 13**,** 117.

COX, J. & MANN, M. 2008. MaxQuant enables high peptide identification rates, individualized p.p.b.-range mass accuracies and proteome-wide protein quantification. *Nature Biotechnology,* 26**,** 1367-1372.

COX, J., NEUHAUSER, N., MICHALSKI, A., SCHELTEMA, R. A., OLSEN, J. V. & MANN, M. 2011. Andromeda: A Peptide Search Engine Integrated into the MaxQuant Environment. *Journal of Proteome Research,* 10**,** 1794-1805.

CROOKS, G. E., HON, G., CHANDONIA, J. M. & BRENNER, S. E. 2004. WebLogo: a sequence logo generator. *Genome Res,* 14**,** 1188-90.

CZECHOWSKI, T., STITT, M., ALTMANN, T., UDVARDI, M. K. & SCHEIBLE, W. R. 2005. Genome-wide identification and testing of superior reference genes for transcript normalization in Arabidopsis. *Plant Physiol,* 139**,** 5-17.
DATLA, R. S., HAMMERLINDL, J. K., PANCHUK, B., PELCHER, L. E. & KELLER, W. 1992. Modified binary plant transformation vectors with the wild-type gene encoding NPTII. *Gene,* 122**,** 383-4.
DAY, I. S., REDDY, V. S., SHAD ALI, G. & REDDY, A. S. N. 2002. Analysis of EF-hand-containing proteins in Arabidopsis. *Genome Biology,* 3**,** research0056.1-research0056.24.
DENISON, F. C., PAUL, A. L., ZUPANSKA, A. K. & FERL, R. J. 2011. 14-3-3 proteins in plant physiology. *Semin Cell Dev Biol,* 22**,** 720-7.
DODD, A. N., BELBIN, F. E., FRANK, A. & WEBB, A. A. 2015. Interactions between circadian clocks and photosynthesis for the temporal and spatial coordination of metabolism. *Front Plant Sci,* 6**,** 245.
DODD, A. N., KUSAKINA, J., HALL, A., GOULD, P. D. & HANAOKA, M. 2014. The circadian regulation of photosynthesis. *Photosynth Res,* 119**,** 181-90.
FAN, S., MENG, Y., SONG, M., PANG, C., WEI, H., LIU, J., ZHAN, X., LAN, J., FENG, C., ZHANG, S. & YU, S. 2014. Quantitative Phosphoproteomics Analysis of Nitric Oxide–Responsive Phosphoproteins in Cotton Leaf. *PLoS ONE,* 9**,** e94261.
FRISTEDT, R., WASILEWSKA, W., ROMANOWSKA, E. & VENER, A. V. 2012. Differential phosphorylation of thylakoid proteins in mesophyll and bundle sheath chloroplasts from maize plants grown under low or high light. *Proteomics,* 12**,** 2852-61.
FRISTEDT, R., WILLIG, A., GRANATH, P., CREVECOEUR, M., ROCHAIX, J. D. & VENER, A. V. 2009. Phosphorylation of photosystem II controls functional macroscopic folding of photosynthetic membranes in Arabidopsis. *Plant Cell,* 21**,** 3950-64.
GIAROLA, V., CHALLABATHULA, D. & BARTELS, D. 2015. Quantification of expression of dehydrin isoforms in the desiccation tolerant plant Craterostigma plantagineum using specifically designed reference genes. *Plant Sci,* 236**,** 103-15.
GOLLAN, P. J., TIKKANEN, M. & ARO, E. M. 2015. Photosynthetic light reactions: integral to chloroplast retrograde signalling. *Curr Opin Plant Biol,* 27**,** 180-91.
GOSS, R. & LEPETIT, B. 2015. Biodiversity of NPQ. *J Plant Physiol,* 172**,** 13-32.
GUO, H., FENG, P., CHI, W., SUN, X., XU, X., LI, Y., REN, D., LU, C., DAVID ROCHAIX, J., LEISTER, D. & ZHANG, L. 2016. Plastid-nucleus communication involves calcium-modulated MAPK signalling. *Nat Commun,* 7**,** 12173.
HAN, S., TANG, R., ANDERSON, L. K., WOERNER, T. E. & PEI, Z. M. 2003. A cell surface receptor mediates extracellular Ca(2+) sensing in guard cells. *Nature,* 425**,** 196-200.
HARMON, A. C. 2003. Calcium-regulated protein kinases of plants. *Gravit Space Biol Bull,* 16**,** 83-90.
HARPER, J. F., BRETON, G. & HARMON, A. 2004. Decoding Ca(2+) signals through plant protein kinases. *Annu Rev Plant Biol,* 55**,** 263-88.
HAUSSUHL, K., ANDERSSON, B. & ADAMSKA, I. 2001. A chloroplast DegP2 protease performs the primary cleavage of the photodamaged D1 protein in plant photosystem II. *Embo j,* 20**,** 713-22.
HEAZLEWOOD, J. L., DUREK, P., HUMMEL, J., SELBIG, J., WECKWERTH, W., WALTHER, D. & SCHULZE, W. X. 2008. PhosPhAt: a database of phosphorylation sites in

Arabidopsis thaliana and a plant-specific phosphorylation site predictor. *Nucleic Acids Res,* 36**,** D1015-21.
HENLEY, W. J. 1993. MEASUREMENT AND INTERPRETATION OF PHOTOSYNTHETIC LIGHT-RESPONSE CURVES IN ALGAE IN THE CONTEXT OF PHOTOINHIBITION AND DIEL CHANGES. *Journal of Phycology,* 29**,** 729-739.
HOCHMAL, A. K., SCHULZE, S., TROMPELT, K. & HIPPLER, M. 2015. Calcium-dependent regulation of photosynthesis. *Biochim Biophys Acta,* 1847**,** 993-1003.
HOEHENWARTER, W., THOMAS, M., NUKARINEN, E., EGELHOFER, V., ROHRIG, H., WECKWERTH, W., CONRATH, U. & BECKERS, G. J. 2013. Identification of novel in vivo MAP kinase substrates in Arabidopsis thaliana through use of tandem metal oxide affinity chromatography. *Mol Cell Proteomics,* 12**,** 369-80.
HSU, P. Y. & HARMER, S. L. 2014. Wheels within wheels: the plant circadian system. *Trends Plant Sci,* 19**,** 240-9.
HSU, S. C., ENDOW, J. K., RUPPEL, N. J., ROSTON, R. L., BALDWIN, A. J. & INOUE, K. 2011. Functional diversification of thylakoidal processing peptidases in Arabidopsis thaliana. *PLoS One,* 6**,** e27258.
HUANG, M., FRISO, G., NISHIMURA, K., QU, X., OLINARES, P. D., MAJERAN, W., SUN, Q. & VAN WIJK, K. J. 2013. Construction of plastid reference proteomes for maize and Arabidopsis and evaluation of their orthologous relationships; the concept of orthoproteomics. *J Proteome Res,* 12**,** 491-504.
JARVI, S., SUORSA, M., PAAKKARINEN, V. & ARO, E. M. 2011. Optimized native gel systems for separation of thylakoid protein complexes: novel super- and mega-complexes. *Biochem J,* 439**,** 207-14.
JOHNSON, C. H., KNIGHT, M. R., KONDO, T., MASSON, P., SEDBROOK, J., HALEY, A. & TREWAVAS, A. 1995. Circadian oscillations of cytosolic and chloroplastic free calcium in plants. *Science,* 269**,** 1863-5.
KAISER, E., MORALES, A. & HARBINSON, J. 2018. Fluctuating Light Takes Crop Photosynthesis on a Rollercoaster Ride. *Plant Physiol,* 176**,** 977-989.
KEELING, P. J. 2010. The endosymbiotic origin, diversification and fate of plastids. *Philos Trans R Soc Lond B Biol Sci,* 365**,** 729-48.
KIM, T. H., BOHMER, M., HU, H., NISHIMURA, N. & SCHROEDER, J. I. 2010. Guard cell signal transduction network: advances in understanding abscisic acid, CO2, and Ca2+ signaling. *Annu Rev Plant Biol,* 61**,** 561-91.
KIRCHHOFF, H. 2013. Architectural switches in plant thylakoid membranes. *Photosynth Res,* 116**,** 481-7.
KLEY, J., SCHMIDT, B., BOYANOV, B., STOLT-BERGNER, P. C., KIRK, R., EHRMANN, M., KNOPF, R. R., NAVEH, L., ADAM, Z. & CLAUSEN, T. 2011. Structural adaptation of the plant protease Deg1 to repair photosystem II during light exposure. *Nat Struct Mol Biol,* 18**,** 728-31.
KOOP, H. U., STEINMULLER, K., WAGNER, H., ROSSLER, C., EIBL, C. & SACHER, L. 1996. Integration of foreign sequences into the tobacco plastome via polyethylene glycol-mediated protoplast transformation. *Planta,* 199**,** 193-201.
KORESSAAR, T. & REMM, M. 2007. Enhancements and modifications of primer design program Primer3. *Bioinformatics,* 23**,** 1289-91.
KRUSE, O. 2001. Light-induced short-term adaptation mechanisms under redox control in the PS II-LHCII supercomplex: LHC II state transitions and PS II repair cycle. *Naturwissenschaften,* 88**,** 284-92.

LAEMMLI, U. K. 1970. Cleavage of structural proteins during the assembly of the head of bacteriophage T4. *Nature,* 227**,** 680-5.
LEISTER, D. 2012. Retrograde signaling in plants: from simple to complex scenarios. *Front Plant Sci,* 3**,** 135.
LIN, L. L., HSU, C. L., HU, C. W., KO, S. Y., HSIEH, H. L., HUANG, H. C. & JUAN, H. F. 2015. Integrating Phosphoproteomics and Bioinformatics to Study Brassinosteroid-Regulated Phosphorylation Dynamics in Arabidopsis. *BMC Genomics,* 16**,** 533.
LV, D. W., GE, P., ZHANG, M., CHENG, Z. W., LI, X. H. & YAN, Y. M. 2014a. Integrative network analysis of the signaling cascades in seedling leaves of bread wheat by large-scale phosphoproteomic profiling. *J Proteome Res,* 13**,** 2381-95.
LV, D. W., LI, X., ZHANG, M., GU, A. Q., ZHEN, S. M., WANG, C., LI, X. H. & YAN, Y. M. 2014b. Large-scale phosphoproteome analysis in seedling leaves of Brachypodium distachyon L. *BMC Genomics,* 15**,** 375.
LV, D. W., SUBBURAJ, S., CAO, M., YAN, X., LI, X., APPELS, R., SUN, D. F., MA, W. & YAN, Y. M. 2014c. Proteome and phosphoproteome characterization reveals new response and defense mechanisms of Brachypodium distachyon leaves under salt stress. *Mol Cell Proteomics,* 13**,** 632-52.
MARTINEZ-GARCIA, J. F., MONTE, E. & QUAIL, P. H. 1999. A simple, rapid and quantitative method for preparing Arabidopsis protein extracts for immunoblot analysis. *Plant J,* 20**,** 251-7.
MAY, T. & SOLL, J. 2000. 14-3-3 proteins form a guidance complex with chloroplast precursor proteins in plants. *Plant Cell,* 12**,** 53-64.
MEKALA, N. R., SUORSA, M., RANTALA, M., ARO, E. M. & TIKKANEN, M. 2015. Plants Actively Avoid State Transitions upon Changes in Light Intensity: Role of Light-Harvesting Complex II Protein Dephosphorylation in High Light. *Plant Physiol,* 168**,** 721-34.
MILLAR, A. J., SHORT, S. R., CHUA, N. H. & KAY, S. A. 1992. A novel circadian phenotype based on firefly luciferase expression in transgenic plants. *Plant Cell,* 4**,** 1075-87.
MINAGAWA, J. 2011. State transitions--the molecular remodeling of photosynthetic supercomplexes that controls energy flow in the chloroplast. *Biochim Biophys Acta,* 1807**,** 897-905.
MULLER, P., LI, X. P. & NIYOGI, K. K. 2001. Non-photochemical quenching. A response to excess light energy. *Plant Physiol,* 125**,** 1558-66.
NAGEL, D. H., DOHERTY, C. J., PRUNEDA-PAZ, J. L., SCHMITZ, R. J., ECKER, J. R. & KAY, S. A. 2015. Genome-wide identification of CCA1 targets uncovers an expanded clock network in Arabidopsis. *Proc Natl Acad Sci U S A,* 112**,** E4802-10.
NOMURA, H., KOMORI, T., KOBORI, M., NAKAHIRA, Y. & SHIINA, T. 2008. Evidence for chloroplast control of external Ca2+-induced cytosolic Ca2+ transients and stomatal closure. *Plant J,* 53**,** 988-98.
NOMURA, H., KOMORI, T., UEMURA, S., KANDA, Y., SHIMOTANI, K., NAKAI, K., FURUICHI, T., TAKEBAYASHI, K., SUGIMOTO, T., SANO, S., SUWASTIKA, I. N., FUKUSAKI, E., YOSHIOKA, H., NAKAHIRA, Y. & SHIINA, T. 2012. Chloroplast-mediated activation of plant immune signalling in Arabidopsis. *Nat Commun,* 3**,** 926.
NOMURA, H. & SHIINA, T. 2014. Calcium signaling in plant endosymbiotic organelles: mechanism and role in physiology. *Mol Plant,* 7**,** 1094-104.
OLSEN, J. V., BLAGOEV, B., GNAD, F., MACEK, B., KUMAR, C., MORTENSEN, P. & MANN, M. 2006. Global, in vivo, and site-specific phosphorylation dynamics in signaling networks. *Cell,* 127**,** 635-48.

PETROUTSOS, D., BUSCH, A., JANSSEN, I., TROMPELT, K., BERGNER, S. V., WEINL, S., HOLTKAMP, M., KARST, U., KUDLA, J. & HIPPLER, M. 2011. The chloroplast calcium sensor CAS is required for photoacclimation in Chlamydomonas reinhardtii. *Plant Cell,* 23**,** 2950-63.

PINNOLA, A. & BASSI, R. 2018. Molecular mechanisms involved in plant photoprotection. *Biochem Soc Trans,* 46**,** 467-482.

PORRA, R. J., THOMPSON, W. A. & KRIEDEMANN, P. E. 1989. Determination of accurate extinction coefficients and simultaneous equations for assaying chlorophylls a and b extracted with four different solvents: verification of the concentration of chlorophyll standards by atomic absorption spectroscopy. *Biochimica et Biophysica Acta (BBA) - Bioenergetics,* 975**,** 384-394.

PRIBIL, M., LABS, M. & LEISTER, D. 2014. Structure and dynamics of thylakoids in land plants. *J Exp Bot,* 65**,** 1955-72.

PRIBIL, M., PESARESI, P., HERTLE, A., BARBATO, R. & LEISTER, D. 2010. Role of plastid protein phosphatase TAP38 in LHCII dephosphorylation and thylakoid electron flow. *PLoS Biol,* 8**,** e1000288.

RAWLINGS, N. D., BARRETT, A. J., THOMAS, P. D., HUANG, X., BATEMAN, A. & FINN, R. D. 2018. The MEROPS database of proteolytic enzymes, their substrates and inhibitors in 2017 and a comparison with peptidases in the PANTHER database. *Nucleic Acids Res,* 46**,** D624-d632.

REILAND, S., FINAZZI, G., ENDLER, A., WILLIG, A., BAERENFALLER, K., GROSSMANN, J., GERRITS, B., RUTISHAUSER, D., GRUISSEM, W., ROCHAIX, J. D. & BAGINSKY, S. 2011. Comparative phosphoproteome profiling reveals a function of the STN8 kinase in fine-tuning of cyclic electron flow (CEF). *Proc Natl Acad Sci U S A,* 108**,** 12955-60.

REILAND, S., MESSERLI, G., BAERENFALLER, K., GERRITS, B., ENDLER, A., GROSSMANN, J., GRUISSEM, W. & BAGINSKY, S. 2009. Large-scale Arabidopsis phosphoproteome profiling reveals novel chloroplast kinase substrates and phosphorylation networks. *Plant Physiol,* 150**,** 889-903.

ROACH, T. & KRIEGER-LISZKAY, A. 2012. The role of the PsbS protein in the protection of photosystems I and II against high light in Arabidopsis thaliana. *Biochim Biophys Acta,* 1817**,** 2158-65.

ROCHA, A. G., MEHLMER, N., STAEL, S., MAIR, A., PARVIN, N., CHIGRI, F., TEIGE, M. & VOTHKNECHT, U. C. 2014. Phosphorylation of Arabidopsis transketolase at Ser428 provides a potential paradigm for the metabolic control of chloroplast carbon metabolism. *Biochem J,* 458**,** 313-22.

ROCHA, A. G. & VOTHKNECHT, U. C. 2012. The role of calcium in chloroplasts--an intriguing and unresolved puzzle. *Protoplasma,* 249**,** 957-66.

ROCHAIX, J. D. 2014. Regulation and dynamics of the light-harvesting system. *Annu Rev Plant Biol,* 65**,** 287-309.

ROCHAIX, J. D., LEMEILLE, S., SHAPIGUZOV, A., SAMOL, I., FUCILE, G., WILLIG, A. & GOLDSCHMIDT-CLERMONT, M. 2012. Protein kinases and phosphatases involved in the acclimation of the photosynthetic apparatus to a changing light environment. *Philos Trans R Soc Lond B Biol Sci,* 367**,** 3466-74.

ROITINGER, E., HOFER, M., KOCHER, T., PICHLER, P., NOVATCHKOVA, M., YANG, J., SCHLOGELHOFER, P. & MECHTLER, K. 2015. Quantitative phosphoproteomics of the ataxia telangiectasia-mutated (ATM) and ataxia telangiectasia-mutated and

rad3-related (ATR) dependent DNA damage response in Arabidopsis thaliana. *Mol Cell Proteomics,* 14**,** 556-71.
ROKKA, A., ARO, E. M. & VENER, A. V. 2011. Thylakoid phosphoproteins: identification of phosphorylation sites. *Methods Mol Biol,* 684**,** 171-86.
ROSE, C. M., VENKATESHWARAN, M., VOLKENING, J. D., GRIMSRUD, P. A., MAEDA, J., BAILEY, D. J., PARK, K., HOWES-PODOLL, M., DEN OS, D., YEUN, L. H., WESTPHALL, M. S., SUSSMAN, M. R., ANE, J. M. & COON, J. J. 2012. Rapid phosphoproteomic and transcriptomic changes in the rhizobia-legume symbiosis. *Mol Cell Proteomics,* 11**,** 724-44.
RUNGRAT, T., AWLIA, M., BROWN, T., CHENG, R., SIRAULT, X., FAJKUS, J., TRTILEK, M., FURBANK, B., BADGER, M., TESTER, M., POGSON, B. J., BOREVITZ, J. O. & WILSON, P. 2016. Using Phenomic Analysis of Photosynthetic Function for Abiotic Stress Response Gene Discovery. *Arabidopsis Book,* 14**,** e0185.
SAGAN, L. 1967. On the origin of mitosing cells. *J Theor Biol,* 14**,** 255-74.
SAI, J. & JOHNSON, C. H. 2002. Dark-stimulated calcium ion fluxes in the chloroplast stroma and cytosol. *Plant Cell,* 14**,** 1279-91.
SCHAFFER, R., LANDGRAF, J., ACCERBI, M., SIMON, V., LARSON, M. & WISMAN, E. 2001. Microarray Analysis of Diurnal and Circadian-Regulated Genes in Arabidopsis. *The Plant Cell,* 13**,** 113-124.
SCHIMPER, A. F. W. 1883. Uber die entwicklung der chlorophyllkoerner und farbkoerper. *Bot Zeitung,* 41**,** 105–146.
SCHLIEBNER, I., PRIBIL, M., ZUHLKE, J., DIETZMANN, A. & LEISTER, D. 2008. A Survey of Chloroplast Protein Kinases and Phosphatases in Arabidopsis thaliana. *Curr Genomics,* 9**,** 184-90.
SCHONBERG, A. & BAGINSKY, S. 2012. Signal integration by chloroplast phosphorylation networks: an update. *Front Plant Sci,* 3**,** 256.
SCHONBERG, A., RODIGER, A., MEHWALD, W., GALONSKA, J., CHRIST, G., HELM, S., THIEME, D., MAJOVSKY, P., HOEHENWARTER, W. & BAGINSKY, S. 2017. Identification of STN7/STN8 kinase targets reveals connections between electron transport, metabolism and gene expression. *Plant J,* 90**,** 1176-1186.
SCHULZ, P., HERDE, M. & ROMEIS, T. 2013. Calcium-dependent protein kinases: hubs in plant stress signaling and development. *Plant Physiol,* 163**,** 523-30.
SEIGNEURIN-BERNY, D., SALVI, D., DORNE, A. J., JOYARD, J. & ROLLAND, N. 2008. Percoll-purified and photosynthetically active chloroplasts from Arabidopsis thaliana leaves. *Plant Physiol Biochem,* 46**,** 951-5.
SELLO, S., MOSCATIELLO, R., MEHLMER, N., LEONARDELLI, M., CARRARETTO, L., CORTESE, E., ZANELLA, F. G., BALDAN, B., SZABO, I., VOTHKNECHT, U. C. & NAVAZIO, L. 2018. Chloroplast Ca(2+) Fluxes into and across Thylakoids Revealed by Thylakoid-Targeted Aequorin Probes. *Plant Physiol,* 177**,** 38-51.
SIMEUNOVIC, A., MAIR, A., WURZINGER, B. & TEIGE, M. 2016. Know where your clients are: subcellular localization and targets of calcium-dependent protein kinases. *J Exp Bot,* 67**,** 3855-72.
SMITH, H. 1982. Light Quality, Photoperception, and Plant Strategy. *Annual Review of Plant Physiology,* 33**,** 481-518.
SONG, J., TAN, H., PERRY, A. J., AKUTSU, T., WEBB, G. I., WHISSTOCK, J. C. & PIKE, R. N. 2012. PROSPER: an integrated feature-based tool for predicting protease substrate cleavage sites. *PLoS One,* 7**,** e50300.

STAEL, S., ROCHA, A. G., WIMBERGER, T., ANRATHER, D., VOTHKNECHT, U. C. & TEIGE, M. 2012a. Cross-talk between calcium signalling and protein phosphorylation at the thylakoid. *J Exp Bot,* 63**,** 1725-33.
STAEL, S., WURZINGER, B., MAIR, A., MEHLMER, N., VOTHKNECHT, U. C. & TEIGE, M. 2012b. Plant organellar calcium signalling: an emerging field. *J Exp Bot,* 63**,** 1525-42.
STONE, J. M. & WALKER, J. C. 1995. Plant protein kinase families and signal transduction. *Plant Physiology,* 108**,** 451-457.
STRITTMATTER, P., SOLL, J. & BOLTER, B. 2010. The chloroplast protein import machinery: a review. *Methods Mol Biol,* 619**,** 307-21.
STROHER, E. & DIETZ, K. J. 2008. The dynamic thiol-disulphide redox proteome of the Arabidopsis thaliana chloroplast as revealed by differential electrophoretic mobility. *Physiol Plant,* 133**,** 566-83.
SUGIURA, M. 1995. The chloroplast genome. *Essays Biochem,* 30**,** 49-57.
TERASHIMA, M., PETROUTSOS, D., HUDIG, M., TOLSTYGINA, I., TROMPELT, K., GABELEIN, P., FUFEZAN, C., KUDLA, J., WEINL, S., FINAZZI, G. & HIPPLER, M. 2012. Calcium-dependent regulation of cyclic photosynthetic electron transfer by a CAS, ANR1, and PGRL1 complex. *Proc Natl Acad Sci U S A,* 109**,** 17717-22.
THEIS, J. & SCHRODA, M. 2016. Revisiting the photosystem II repair cycle. *Plant Signal Behav,* 11**,** e1218587.
THOMPSON, J. D., GIBSON, T. J., PLEWNIAK, F., JEANMOUGIN, F. & HIGGINS, D. G. 1997. The CLUSTAL_X windows interface: flexible strategies for multiple sequence alignment aided by quality analysis tools. *Nucleic Acids Research,* 25**,** 4876-4882.
TIKKANEN, M. & ARO, E. M. 2014. Integrative regulatory network of plant thylakoid energy transduction. *Trends Plant Sci,* 19**,** 10-7.
TIKKANEN, M., GOLLAN, P. J., SUORSA, M., KANGASJARVI, S. & ARO, E. M. 2012a. STN7 Operates in Retrograde Signaling through Controlling Redox Balance in the Electron Transfer Chain. *Front Plant Sci,* 3**,** 277.
TIKKANEN, M., GRIECO, M., NURMI, M., RANTALA, M., SUORSA, M. & ARO, E. M. 2012b. Regulation of the photosynthetic apparatus under fluctuating growth light. *Philos Trans R Soc Lond B Biol Sci,* 367**,** 3486-93.
TIKKANEN, M., PIIPPO, M., SUORSA, M., SIRPIO, S., MULO, P., VAINONEN, J., VENER, A. V., ALLAHVERDIYEVA, Y. & ARO, E. M. 2006. State transitions revisited-a buffering system for dynamic low light acclimation of Arabidopsis. *Plant Mol Biol,* 62**,** 779-93.
TORABI, S., PLÖCHINGER, M. & MEURER, J. 2014. Localization and Topology of Thylakoid Membrane Proteins in Land Plants. *Bio-protocol,* 4.
TYANOVA, S., TEMU, T., SINITCYN, P., CARLSON, A., HEIN, M. Y., GEIGER, T., MANN, M. & COX, J. 2016. The Perseus computational platform for comprehensive analysis of (prote)omics data. *Nature Methods,* 13**,** 731-740.
UNTERGASSER, A., CUTCUTACHE, I., KORESSAAR, T., YE, J., FAIRCLOTH, B. C., REMM, M. & ROZEN, S. G. 2012. Primer3--new capabilities and interfaces. *Nucleic Acids Res,* 40**,** e115.
VAINONEN, J. P., HANSSON, M. & VENER, A. V. 2005. STN8 protein kinase in Arabidopsis thaliana is specific in phosphorylation of photosystem II core proteins. *J Biol Chem,* 280**,** 33679-86.
VAINONEN, J. P., SAKURAGI, Y., STAEL, S., TIKKANEN, M., ALLAHVERDIYEVA, Y., PAAKKARINEN, V., ARO, E., SUORSA, M., SCHELLER, H. V., VENER, A. V. & ARO, E.

M. 2008. Light regulation of CaS, a novel phosphoprotein in the thylakoid membrane of Arabidopsis thaliana. *FEBS J,* 275**,** 1767-77.
VALMONTE, G. R., ARTHUR, K., HIGGINS, C. M. & MACDIARMID, R. M. 2014. Calcium-dependent protein kinases in plants: evolution, expression and function. *Plant Cell Physiol,* 55**,** 551-69.
VOINNET, O., RIVAS, S., MESTRE, P. & BAULCOMBE, D. 2003. An enhanced transient expression system in plants based on suppression of gene silencing by the p19 protein of tomato bushy stunt virus. *Plant J,* 33**,** 949-56.
WANG, W. H., CHEN, J., LIU, T. W., CHEN, J., HAN, A. D., SIMON, M., DONG, X. J., HE, J. X. & ZHENG, H. L. 2014. Regulation of the calcium-sensing receptor in both stomatal movement and photosynthetic electron transport is crucial for water use efficiency and drought tolerance in Arabidopsis. *J Exp Bot,* 65**,** 223-34.
WANG, W. H., HE, E. M., CHEN, J., GUO, Y., CHEN, J., LIU, X. & ZHENG, H. L. 2016. The reduced state of the plastoquinone pool is required for chloroplast-mediated stomatal closure in response to calcium stimulation. *Plant J,* 86**,** 132-44.
WANG, W. H., YI, X. Q., HAN, A. D., LIU, T. W., CHEN, J., WU, F. H., DONG, X. J., HE, J. X., PEI, Z. M. & ZHENG, H. L. 2012. Calcium-sensing receptor regulates stomatal closure through hydrogen peroxide and nitric oxide in response to extracellular calcium in Arabidopsis. *J Exp Bot,* 63**,** 177-90.
WANG, W. H. & ZHENG, H. L. 2012. Mechanisms for calcium sensing receptor-regulated stomatal closure in response to the extracellular calcium signal. *Plant Signal Behav,* 7**,** 289-91.
WANG, X., BIAN, Y., CHENG, K., GU, L. F., YE, M., ZOU, H., SUN, S. S. & HE, J. X. 2013. A large-scale protein phosphorylation analysis reveals novel phosphorylation motifs and phosphoregulatory networks in Arabidopsis. *J Proteomics,* 78**,** 486-98.
WEINL, S., HELD, K., SCHLUCKING, K., STEINHORST, L., KUHLGERT, S., HIPPLER, M. & KUDLA, J. 2008. A plastid protein crucial for Ca2+-regulated stomatal responses. *New Phytol,* 179**,** 675-86.
WENDEN, B., KOZMA-BOGNAR, L., EDWARDS, K. D., HALL, A. J., LOCKE, J. C. & MILLAR, A. J. 2011. Light inputs shape the Arabidopsis circadian system. *Plant J,* 66**,** 480-91.
WHITEMAN, S. A., NUHSE, T. S., ASHFORD, D. A., SANDERS, D. & MAATHUIS, F. J. 2008. A proteomic and phosphoproteomic analysis of Oryza sativa plasma membrane and vacuolar membrane. *Plant J,* 56**,** 146-56.
WITMARSH, J. & GOVINDJEE 2002. Photosystem II. *ENCYCLOPEDIA OF LIFE SCIENCES*.
WUNDER, T., XU, W., LIU, Q., WANNER, G., LEISTER, D. & PRIBIL, M. 2013. The major thylakoid protein kinases STN7 and STN8 revisited: effects of altered STN8 levels and regulatory specificities of the STN kinases. *Front Plant Sci,* 4**,** 417.
YAMORI, W. & SHIKANAI, T. 2016. Physiological Functions of Cyclic Electron Transport Around Photosystem I in Sustaining Photosynthesis and Plant Growth. *Annu Rev Plant Biol,* 67**,** 81-106.
YANG, Z., GUO, G., ZHANG, M., LIU, C. Y., HU, Q., LAM, H., CHENG, H., XUE, Y., LI, J. & LI, N. 2013. Stable isotope metabolic labeling-based quantitative phosphoproteomic analysis of Arabidopsis mutants reveals ethylene-regulated time-dependent phosphoproteins and putative substrates of constitutive triple response 1 kinase. *Mol Cell Proteomics,* 12**,** 3559-82.

YILMAZ, A., MEJIA-GUERRA, M. K., KURZ, K., LIANG, X., WELCH, L. & GROTEWOLD, E. 2011. AGRIS: the Arabidopsis Gene Regulatory Information Server, an update. *Nucleic Acids Res,* 39**,** D1118-22.
ZHAO, X., XU, M., WEI, R. & LIU, Y. 2015. Expression of OsCAS (Calcium-Sensing Receptor) in an Arabidopsis Mutant Increases Drought Tolerance. *PLoS One,* 10**,** e0131272.
ZHENG, L., BAUMANN, U. & REYMOND, J. L. 2004. An efficient one-step site-directed and site-saturation mutagenesis protocol. *Nucleic Acids Res,* 32**,** e115.
ZHU, J.-K. 2016. Abiotic stress signaling and responses in plants. *Cell,* 167**,** 313-324.
ZIMORSKI, V., KU, C., MARTIN, W. F. & GOULD, S. B. 2014. Endosymbiotic theory for organelle origins. *Curr Opin Microbiol,* 22**,** 38-48.
ZUKER, M. 2003. Mfold web server for nucleic acid folding and hybridization prediction. *Nucleic Acids Res,* 31**,** 3406-15.

10 Acknowledgments

I would like to express my deepest gratitude to Prof. Dr. Ute Vothknecht for allowing me to achieve this ambitious personal goal in her laboratory, first in Munich and then in Bonn.
Her constant and scrupulous supervision was instrumental in the development of this work and provided me with the motivation and encouragement to pursue my scientific interests.
I also want to express my sincere appreciation to Prof. Dr. Markus Teige (University of Vienna) for being an excellent coordinator of the Marie Curie CALIPSO Network and for providing very useful support and guidance during my PhD.
I am indebted to the following collaborators and friends from other institutions for fruitful discussions and for providing a friendly hosting environment and practical help during the execution of experiments: Dr. Michele Grieco (IPK Gatersleben), Dr. Valentino Giarola (IMBIO, University of Bonn), Dr. Veronique Larosa (Université de Liege) and Valentin Roustan (MoSys, University of Vienna).
I want to also extend my thankfulness to old and present members of the Vothknecht lab for being wonderful colleagues and providing help and assistance in the lab, especially at the beginning of my PhD in Munich: thank you Fatima, Henning, Nargis and Julia!!
A special thank goes also to Silvjia Fleischmann for making her home my home in Munich.
Finally, I would like to thank my family, Marta and Ricardo for always providing precious support and believing in me.
I especially thank you, Laura, for always being on my side during the good and the difficult times. This work would not have been possible without you next to me.

11 Supplementary Information

11.1 Immunoblot analyses

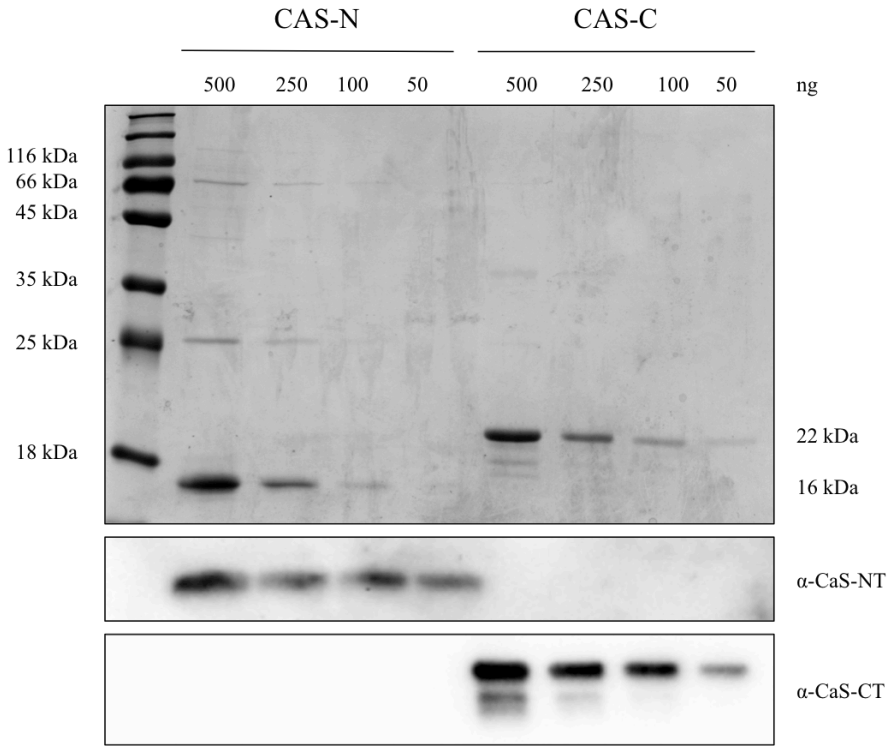

Sup. Figure 1: Non cross-reactivity of α-CaS-NT and α-CaS-CT antibodies.

The non-cross reactivity of the two α-CaS-NT and α-CaS-CT antibodies was tested via immunodetection of the recombinantly expressed CAS-N and CAS-C fragments. The upper panel shows the coomassie stained gel indicating the amounts of loaded protein. Lower panels show the specific reactions for the two CAS antibodies.

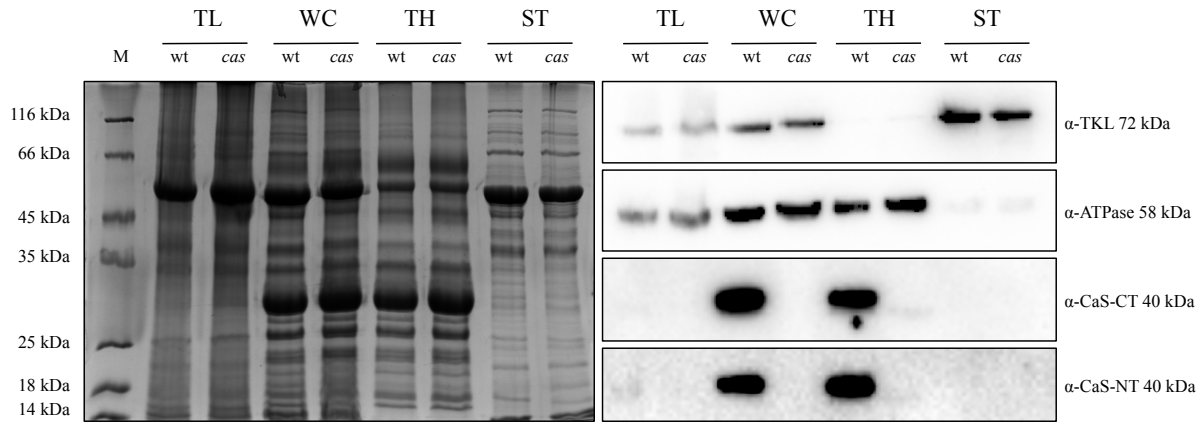

Sup. Figure 2: Immunodetection of native CAS in chloroplast protein fractions.

The coomassie stained gel picture on the left shows equal loading of all the samples from different fractions: total leaf protein extracts (TL), whole chloroplast (WC), thylakoids (TH) and stroma (ST) (≈ 10 µg chlorophyll). The specificity of the α-CaS-CT and α-CaS-NT was tested *in vivo* on wild type and *cas* mutant plants (reactions on TL samples was repeated with higher protein amounts, shown below). Boxes on the right show the specific reactions for the CAS antibodies and two control antibodies (α-TKL and α-ATPase) to show the purity of the different fractions.

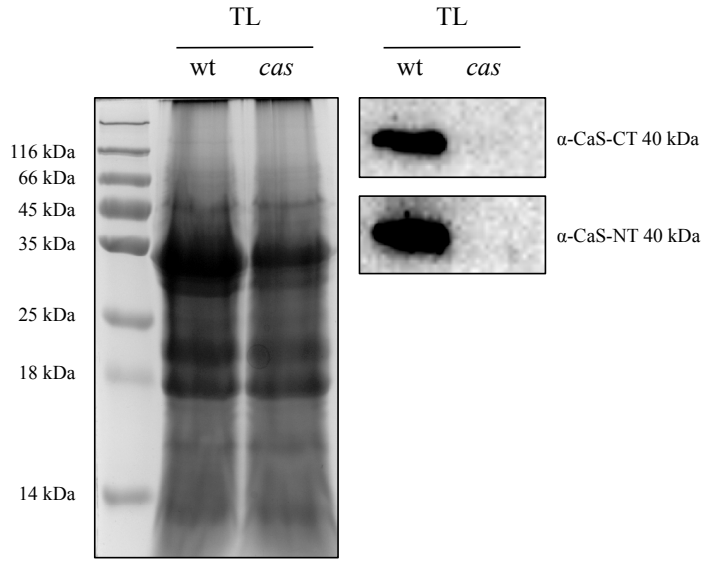

Sup. Figure 3: Immunodetection of native CAS from total leaf protein extracts

11.2 RT-qPCR analysis

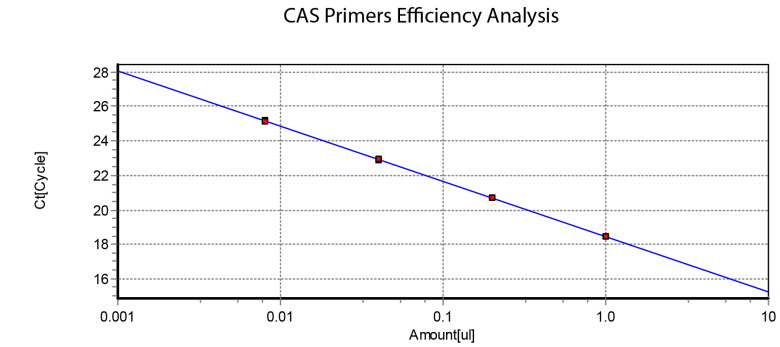

Slope: -3.195
Y-Intercept: 18.46
Efficiency: 1.06
R^2: 1.000

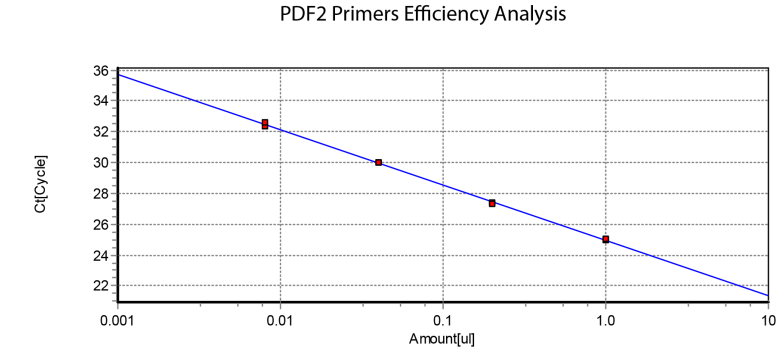

Slope: -3.587
Y-Intercept: 24.95
Efficiency: 0.90
R^2: 0.999

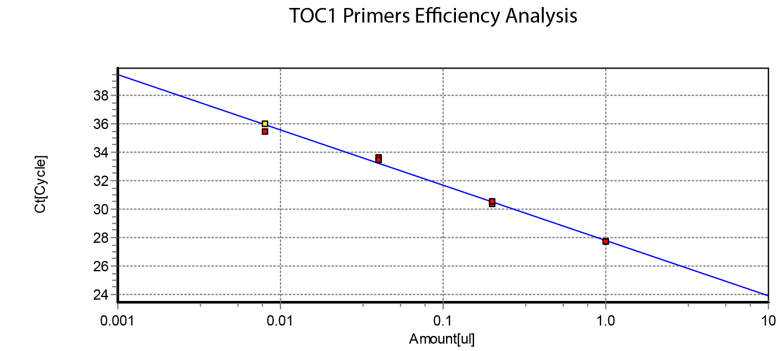

Slope: -3.880
Y-Intercept: 27.83
Efficiency: 0.81
R^2: 0.993

Sup. Figure 4: PCR amplification efficiencies for CAS, PDF2 and TOC1.

The amplification efficiency of the CAS, PDF2 and TOC1 cDNA was tested using standard curves with cDNA dilutions spanning four sequential dilutions (1:5).

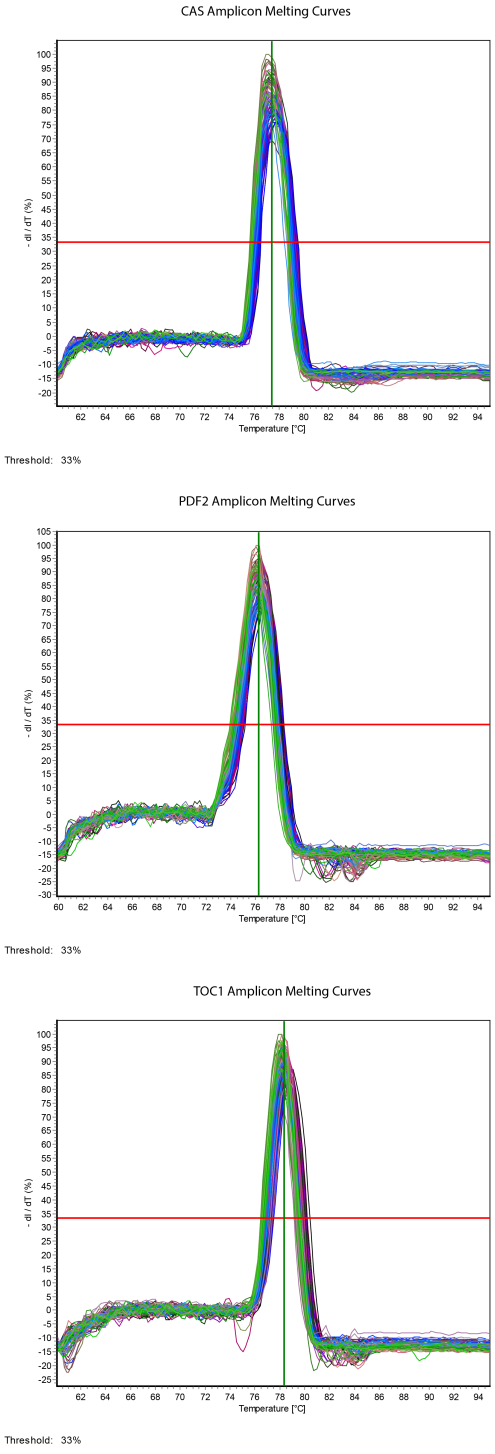

Sup. Figure 5: Primer specificities for the CAS, TOC1 and PDF2 cDNAs.

The specificity of the designed primers was confirmed by the analysis of the profile of the melting curve after the amplification of the subsequent RT-qPCR analysis showing a single detected species.

11.3 Phosphoproteomics analysis

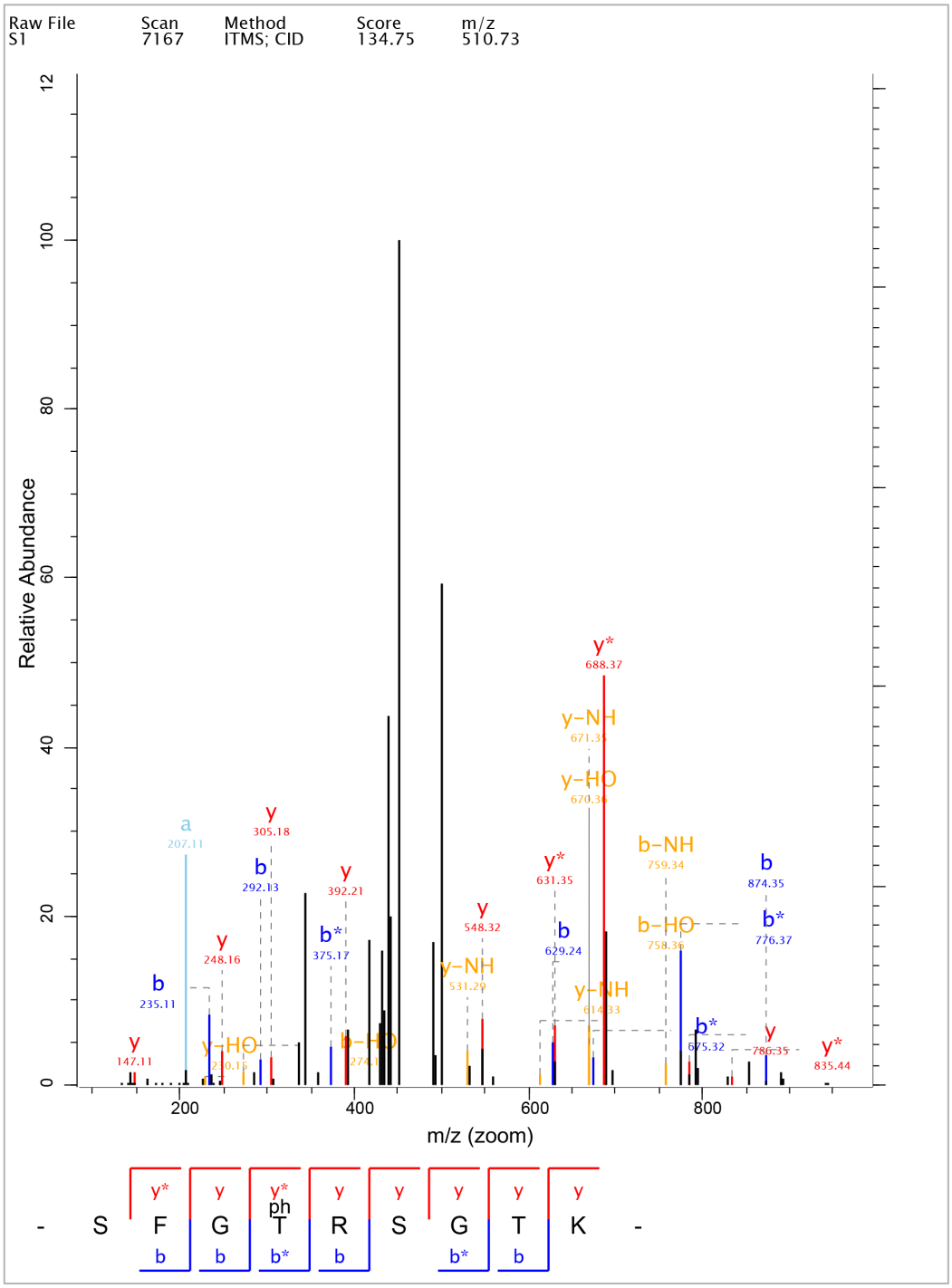

Sup. Figure 6: MS/MS spectra of CAS phosphopeptide carrying pThr-376

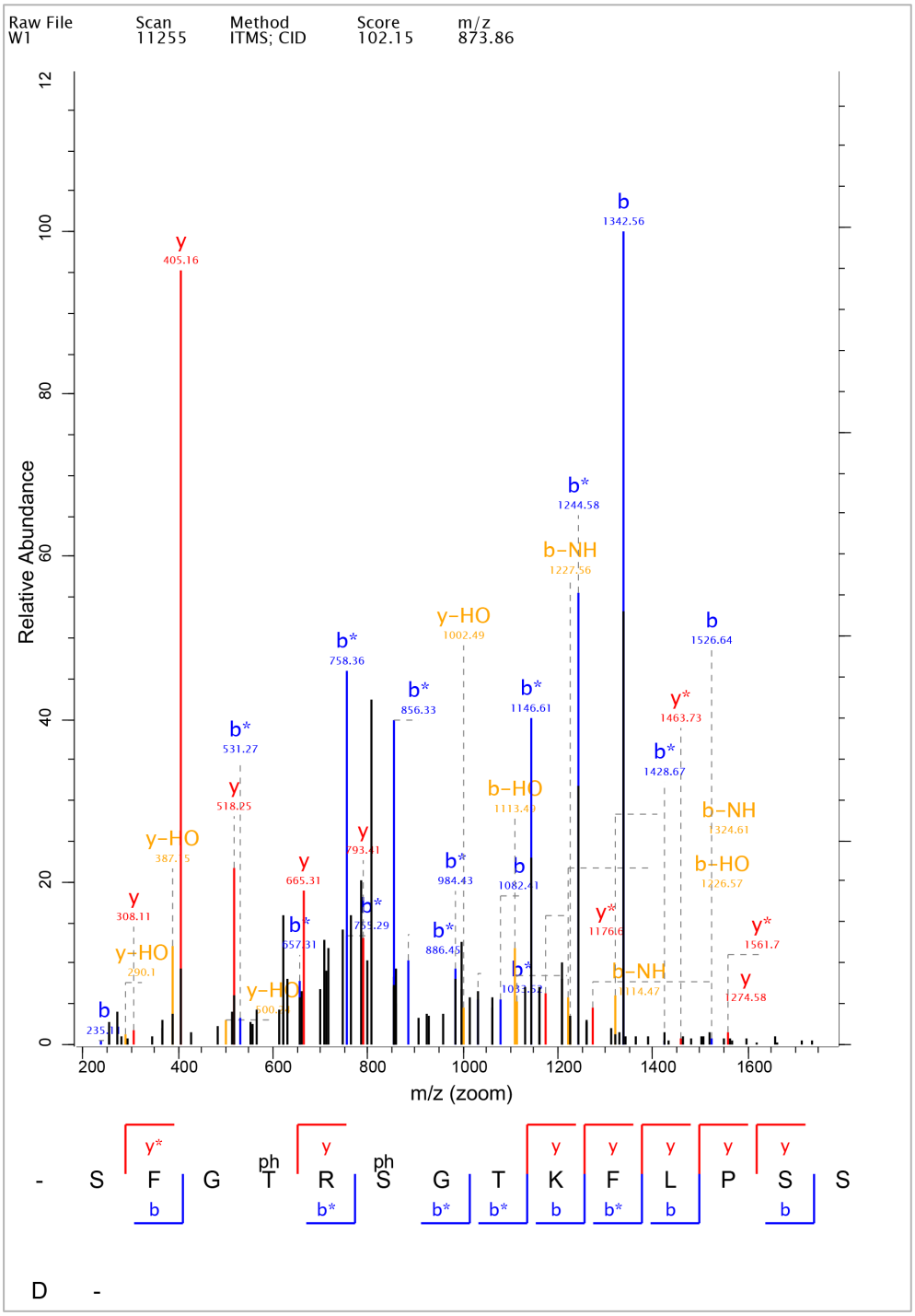

Sup. Figure 7: MS/MS spectra of CAS phosphopeptide carrying pSer-378 and pThr-376

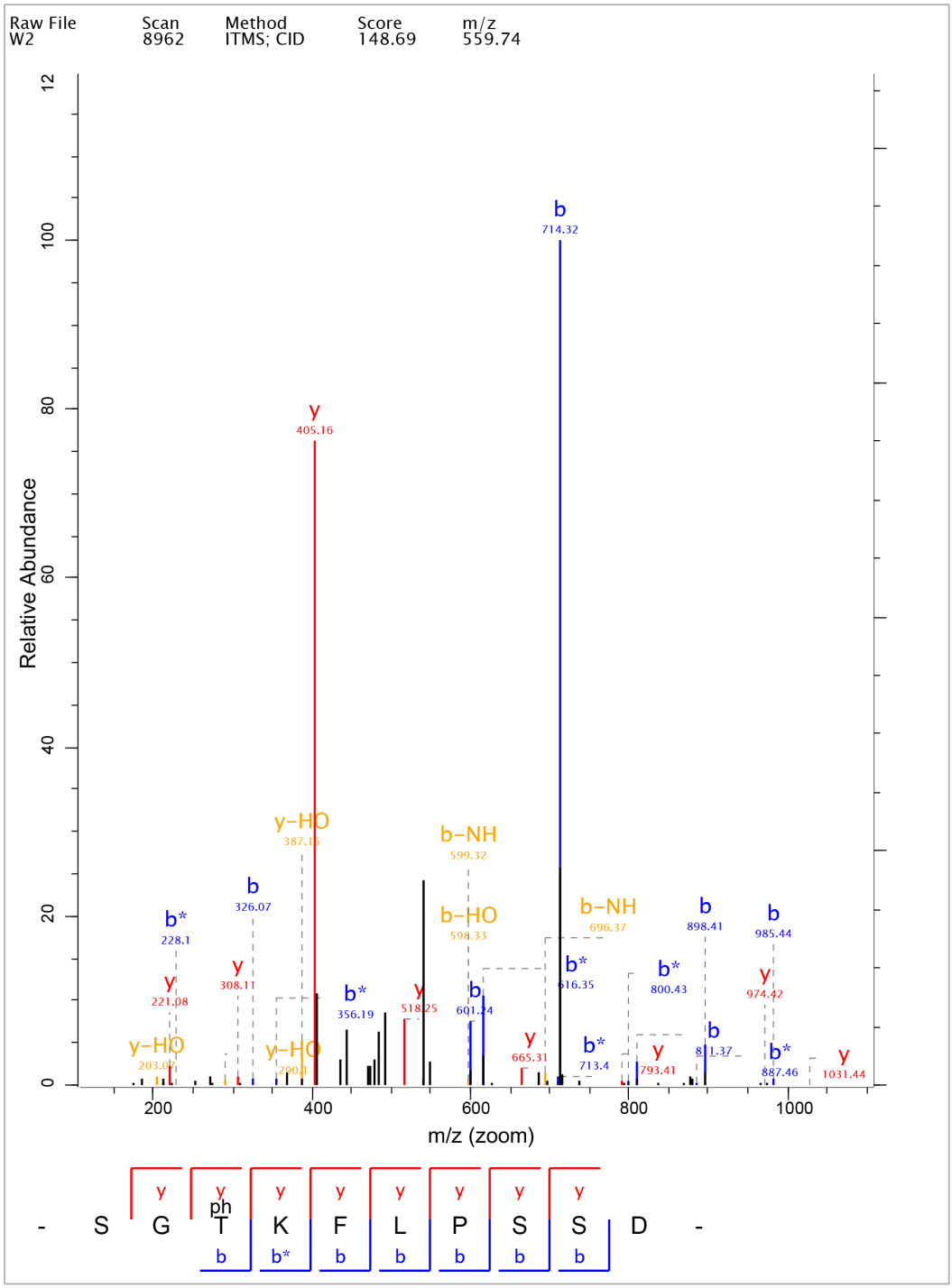

Sup. Figure 8: MS/MS spectra of CAS phosphopeptide carrying pThr-380

11.4 In vitro phosphorylation assays

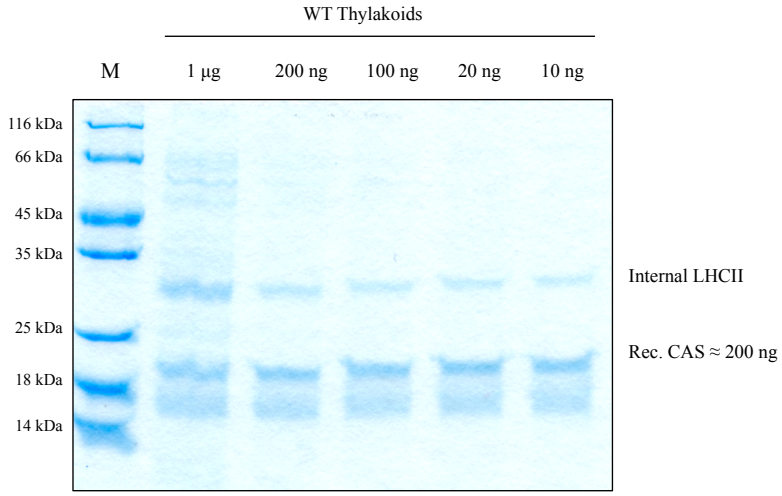

Sup. Figure 9: *In vitro* phosphorylation of recombinant CAS by a thylakoid gradient.

Coomassie stain of the gel of the assays performed using a gradient of thylakoid proteins used to phosphorylate in vitro the recombinant CAS-C fragment. Amounts of chlorophyll equivalent are shown on top.

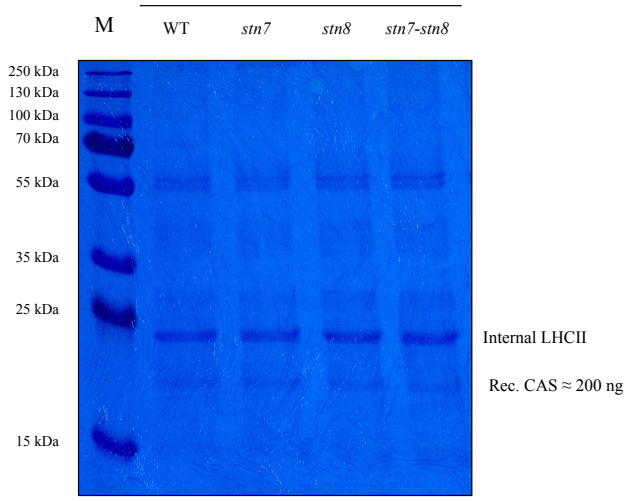

Sup. Figure 10: *In vitro* phosphorylation of recombinant CAS by mutant thylakoids

Coomassie stain of the gel showing equal loading of isolated thylakoid protein fractions from different genotypes and of the recombinant CAS-C substrate.

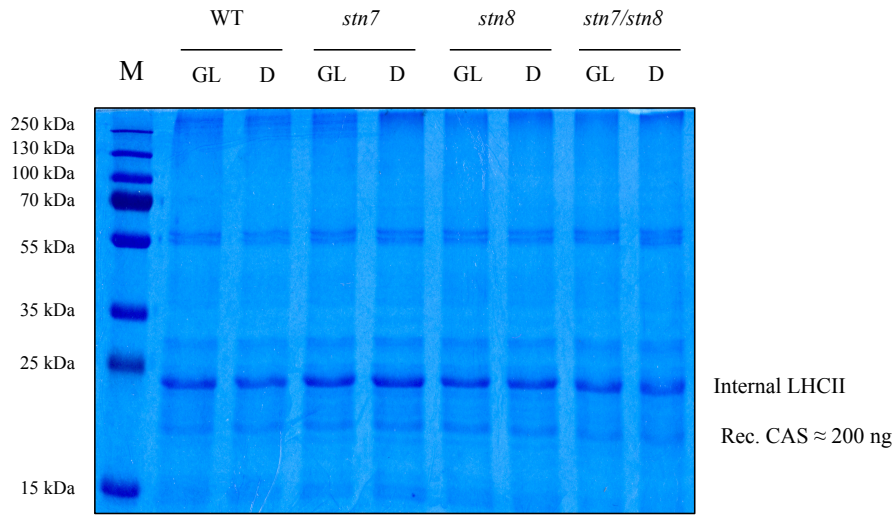

Sup. Figure 11: *In vitro* phosphorylation of recombinant CAS by mutant thylakoids isolated under light or dark conditions. Coomassie stain of the gel showing equal loading of isolated thylakoid protein fractions from different genotypes and harvesting conditions and of the recombinant CAS-C substrate.

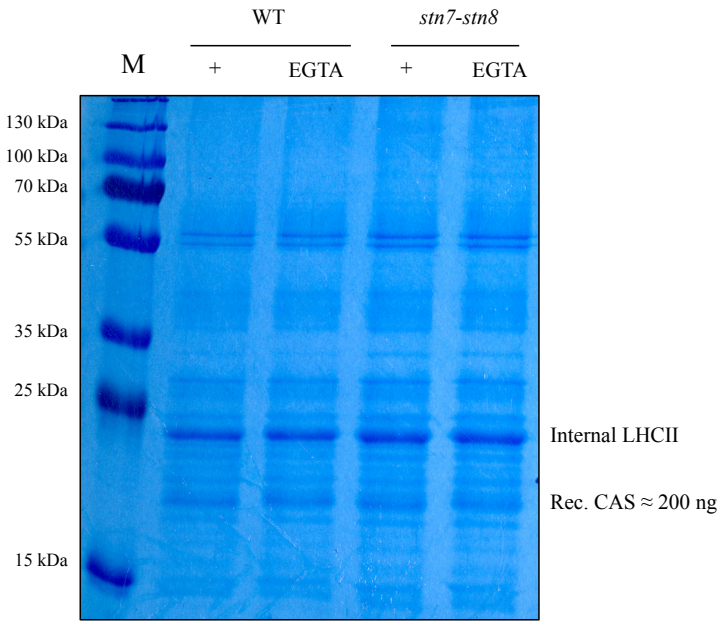

Sup. Figure 12: *In vitro* phosphorylation of recombinant CAS by mutant thylakoids isolated in the presence or absence of Ca^{2+}. Coomassie stain of the gel showing equal loading of isolated thylakoid protein fractions from different genotypes conditions and of the recombinant CAS-C substrate.

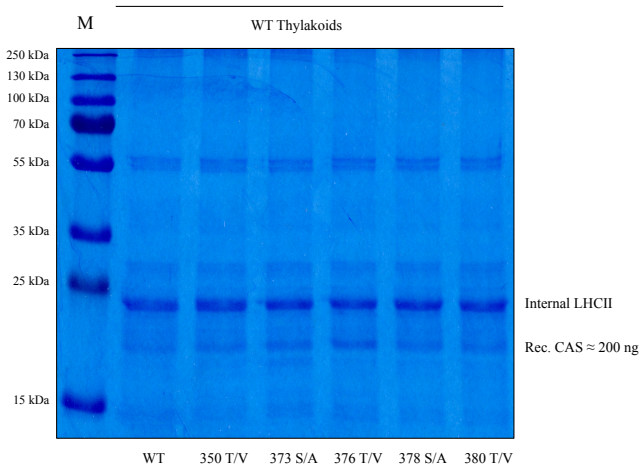

Sup. Figure 13: *In vitro* phosphorylation of recombinant phosphomutant CAS fragments by wild type thylakoids proteins. Coomassie stain of the gel showing equal loading of isolated thylakoid protein fractions of the six recombinant phosphomutant CAS-C fragments.

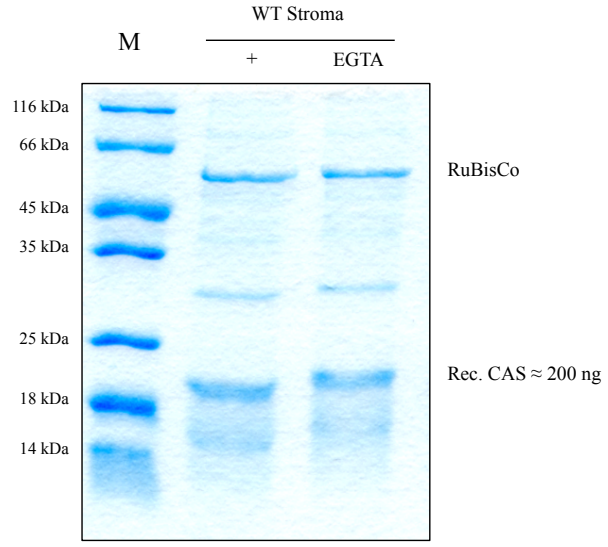

Sup. Figure 14: *In vitro* phosphorylation of recombinant CAS by wild type stromal proteins in the presence and absence of Ca^{2+}. Coomassie stain of the gel showing equal loading of the isolated stromal protein fraction and of the recombinant CAS-C substrate.

11.5 Bioinformatics analyses

Table 1: List of CAS orthologs included in the phylogenetic analysis

ACCESSION NUMBER	SPECIES	ORDER	DIVISION/CLADE	GROUP
XP_011078735.1	*Sesamum indicum*	*Lamiales*	Angiosperms	Dicots
XP_012836576.1	*Erythranthe guttata*	*Lamiales*	Angiosperms	Dicots
CDO98499.1	*Coffea canephora*	*Gentianales*	Angiosperms	Dicots
XP_019167034.1	*Ipomoea nil*	*Solanales*	Angiosperms	Dicots
XP_016458050.1	*Nicotiana tabacum*	*Solanales*	Angiosperms	Dicots
XP_009607865.1	*Nicotiana tomentosiformis*	*Solanales*	Angiosperms	Dicots
XP_009762078.1	*Nicotiana sylvestris*	*Solanales*	Angiosperms	Dicots
XP_019247644.1	*Nicotiana attenuata*	*Solanales*	Angiosperms	Dicots
BAM66423.1	*Nicotiana benthamiana*	*Solanales*	Angiosperms	Dicots
XP_015070026.1	*Solanum pennellii*	*Solanales*	Angiosperms	Dicots
XP_004236097.1	*Solanum lycopersicum*	*Solanales*	Angiosperms	Dicots
XP_006345067.1	*Solanum tuberosum*	*Solanales*	Angiosperms	Dicots
XP_016556216.1	*Capsicum annuum*	*Solanales*	Angiosperms	Dicots
OTF90663.1	*Helianthus annuus*	*Asterales*	Angiosperms	Dicots
KVI06483.1	*Cynara cardunculus var. scolymus*	*Asterales*	Angiosperms	Dicots
XP_017245888.1	*Daucus carota subsp. sativus*	*Apiales*	Angiosperms	Dicots
FA51419.1	*Schima superba*	*Ericales*	Angiosperms	Dicots
Q9FN48	*Arabidopsis thaliana*	*Brassicales*	Angiosperms	Dicots
XP_002874110	*Arabidopsis lyrata subsp. Lyrata*	*Brassicales*	Angiosperms	Dicots
XP_010497107.1	*Camelina sativa*	*Brassicales*	Angiosperms	Dicots
XP_006287921.1	*Capsella rubella*	*Brassicales*	Angiosperms	Dicots
XP_009136394.1	*Brassica rapa*	*Brassicales*	Angiosperms	Dicots
XP_013736900.1	*Brassica napus*	*Brassicales*	Angiosperms	Dicots
XP_013599226.1	*Brassica oleracea var. oleracea*	*Brassicales*	Angiosperms	Dicots
XP_018478757.1	*Raphanus sativus*	*Brassicales*	Angiosperms	Dicots
XP_006394572.1	*Eutrema salsugineum*	*Brassicales*	Angiosperms	Dicots
JAU51671.1	*Noccaea caerulescens*	*Capparales*	Angiosperms	Dicots
XP_010695780.1	*Beta vulgaris subsp. vulgaris*	*Caryophyllales*	Angiosperms	Dicots
KNA14182.1	*Spinacia oleracea*	*Caryophyllales*	Angiosperms	Dicots
ACU11587.1	*Liquidambar formosana*	*Saxifragales*	Angiosperms	Dicots

XP_010663515.1	*Vitis vinifera*	*Vitales*	Angiosperms	Dicots
XP_006374339.1	*Populus trichocarpa*	*Malpighiales*	Angiosperms	Dicots
XP_011012408.1	*Populus euphratica*	*Malpighiales*	Angiosperms	Dicots
GAV63690.1	*Cephalotus follicularis*	*Oxalidales*	Angiosperms	Dicots
XP_008244069.1	*Prunus mume*	*Rosales*	Angiosperms	Dicots
XP_007209216.1	*Prunus persica*	*Rosales*	Angiosperms	Dicots
XP_009337628.1	*Pyrus x bretschneideri*	*Rosales*	Angiosperms	Dicots
XP_008360891.1	*Malus domestica*	*Rosales*	Angiosperms	Dicots
XP_004299254.1	*Fragaria vesca subsp. vesca*	*Rosales*	Angiosperms	Dicots
XP_015883197.1	*Ziziphus jujuba*	*Rosales*	Angiosperms	Dicots
AEP13979.1	*CAStanopsis chinensis*	*Fagales*	Angiosperms	Dicots
XP_018858081.1	*Juglans regia*	*Fagales*	Angiosperms	Dicots
OMO60951.1	*Corchorus capsularis*	*Malvales*	Angiosperms	Dicots
OMO63928.1	*Corchorus olitorius*	*Malvales*	Angiosperms	Dicots
XP_016712995.1	*Gossypium hirsutum*	*Malvales*	Angiosperms	Dicots
XP_017629010.1	*Gossypium arboreum*	*Malvales*	Angiosperms	Dicots
XP_012468788.1	*Gossypium raimondii*	*Malvales*	Angiosperms	Dicots
EOY22243.1	*Theobroma cacao*	*Malvales*	Angiosperms	Dicots
XP_006494243.1	*Citrus sinensis*	*Sapindales*	Angiosperms	Dicots
XP_012092927.1	*Jatropha curCAS*	*Malpighiales*	Angiosperms	Dicots
OAY59312.1	*Manihot esculenta*	*Malpighiales*	Angiosperms	Dicots
XP_002512005.1	*Ricinus communis*	*Malpighiales*	Angiosperms	Dicots
GAU19019.1	*Trifolium subterraneum*	*Fabales*	Angiosperms	Dicots
XP_003609151.2	*Medicago truncatula*	*Fabales*	Angiosperms	Dicots
XP_004508601.1	*Cicer arietinum*	*Fabales*	Angiosperms	Dicots
XP_019463659.1	*Lupinus angustifolius*	*Fabales*	Angiosperms	Dicots
NP_001239903.1	*Glycine max*	*Fabales*	Angiosperms	Dicots
KHN15173.1	*Glycine soja*	*Fabales*	Angiosperms	Dicots
XP_017423515.1	*Vigna angularis*	*Fabales*	Angiosperms	Dicots
XP_014505979.1	*Vigna radiata var. radiata*	*Fabales*	Angiosperms	Dicots
XP_007155178.1	*Phaseolus vulgaris*	*Fabales*	Angiosperms	Dicots
XP_020226796.1	*Cajanus cajan*	*Fabales*	Angiosperms	Dicots
XP_015944026.1	*Arachis duranensis*	*Fabales*	Angiosperms	Dicots
XP_016193993.1	*Arachis ipaensis*	*Fabales*	Angiosperms	Dicots
XP_008455203.1	*Cucumis melo*	*Cucurbitales*	Angiosperms	Dicots
XP_004137457.1	*Cucumis sativus*	*Cucurbitales*	Angiosperms	Dicots
XP_010262208.1	*Nelumbo nucifera*	*Proteales*	Angiosperms	Dicots
XP_010913586.1	*Elaeis guineensis*	*Arecales*	Angiosperms	Dicots

XP_008782048.1	*Phoenix dactylifera*	*Arecales*	Angiosperms	Dicots
XP_020090059.1	*Ananas comosus*	*Poales*	Angiosperms	Dicots
KZV16003.1	*Boea hygrometrica*	*Lamiales*	Angiosperms	Dicots
XP_020274983.1	*Asparagus officinalis*	*Asparagales*	Angiosperms	Monocots
XP_020685732.1	*Dendrobium catenatum*	*Asparagales*	Angiosperms	Monocots
XP_020580506.1	*Phalaenopsis equestris*	*Asparagales*	Angiosperms	Monocots
XP_015622662.1	*Oryza sativa Japonica Group*	*Poales*	Angiosperms	Monocots
XP_015688987	*Oryza brachyantha*	*Poales*	Angiosperms	Monocots
XP_003570449	*Brachypodium distachyon*	*Poales*	Angiosperms	Monocots
BAJ86075	*Hordeum vulgare subsp. vulgare*	*Poales*	Angiosperms	Monocots
XP_020155630	*Aegilops tauschii subsp. tauschii*	*Poales*	Angiosperms	Monocots
XP_004953792	*Setaria italica*	*Poales*	Angiosperms	Monocots
OEL36345	*Dichanthelium oligosanthes*	*Poales*	Angiosperms	Monocots
NP_001150975.1	*Zea mays*	*Poales*	Angiosperms	Monocots
XP_002452613.1	*Sorghum bicolor*	*Poales*	Angiosperms	Monocots
lcl|SI042933	*Syringodium isoetifolium*	*Alismatales*	Angiosperms	Monocots
lcl|PO069894	*Posidonia oceanica*	*Alismatales*	Angiosperms	Monocots
lcl|CS015345	*Cymodocea serrulata*	*Alismatales*	Angiosperms	Monocots
lcl|HO077784	*Halophila ovalis*	*Alismatales*	Angiosperms	Monocots
lcl|LM102276	*Lemna minor*	*Alismatales*	Angiosperms	Monocots
ABK25223	*Picea sitchensis*	*Pinales*	Gymnosperms	
BT109530	*Picea glauca*	*Pinales*	Gymnosperms	
AFA51418	*Pinus massoniana*	*Pinales*	Gymnosperms	
AEQ59234	*Taxus wallichiana var. chinensis*	*Pinales*	Gymnosperms	
KXZ43342.1	*Gonium pectorale*	*Chlamydomonales*	Chlorophyta	
XP_002947936.1	*Volvox carteri f. nagariensis*	*Chlamydomonales*	Chlorophyta	
GAX74748.1	*Chlamydomonas eustigma*	*Chlamydomonales*	Chlorophyta	
XP_001702364.1	*Chlamydomonas reinhardtii*	*Chlamydomonales*	Chlorophyta	
PNH01519.1	*Tetrabaena socialis*	*Chlamydomonales*	Chlorophyta	
XP_013903874.1	*Monoraphidium neglectum*	*Sphaeropleales*	Chlorophyta	
XP_001782854	*Physcomitrella patens*	*Funariales*	Bryophyta	
OAE30096	*Marchantia polymorpha subsp. ruderalis*	*Marchantiales*	Marchatiophyta	
XP_002972782.1	*Selaginella moellendorffii*	*Selaginellales*	Lycopodiophyta	
ABD64881.1	*Pteris vittata*	*Polypodiales*	Pteridophyta	

Table 2: Phosphopeptides from CAS orthologs from phosphoproteomics studies

Species/Locus identifier	**phospho-site position**	**Corresponding residue position in *A. thaliana***	**Phosphopeptide sequence**	**Reference**
A. thaliana At5G23060	Thr-350; Ser-352; Ser-362; Ser-364		LGTDSYNFSFAQVLSPSR	a, b
	Ser-371		IIPAA**pS**R**pS**FGTR IIPAA**pS**R**pS**FG**pT**R	f, g
	Ser-373		IIPAA**pS**R**pS**FGTR IIPAA**pS**R**pS**FG**pT**R IIPAASR**pS**FG**pT**R **pS**FGTRSGTKFLPSSD **pS**FGTR**pS**GTKFLPSSD **pS**FGTRSG**pT**KFLPSSD	a-c; e-g
	Thr-376		IIPAASR**pS**FG**pT**R IIPAA**pS**R**pS**FG**pT**R SFG**pT**RSGTKFLPSSD SFG**pT**RSG**pT**KLPSSD	b, e, g this work
	Ser-378		SFGTR**pS**G**pT**K **pS**GTKFLPSSD **pS**FGTR**pS**GTKFLPSSD	a-e; g; Nguyen et al., 2012 this work
	Thr-380		SFGTRSG**pT**KFLPSSD **pS**FGTRSG**pT**KFLPSSD SFG**pT**RSG**pT**KLPSSD SG**pT**KFLPSSD SFGTR**pS**G**pT**K	c, e, g, h; Nguyen this work
	Ser-385; Ser-386		SGTKFLPSSD	b
M. truncatula MTR_4g112530	**Thr-378**	**Thr-376**	GGFG**pT**TSR	i
G. hirsutum gene_10022751	**Thr-390**	**Thr-376**	FG**pT**TSTK	j
B. distachyon XP_003570449	**Thr-369**	**Thr-376**	FV**pT**ASS**pT**pSTTSGTNR FV**pT**ASSTS**pT**TSG**pT**NR	l, m
	Thr-373	**Thr-380**	FV**pT**ASS**pT**p**S**TTSGTNR	l
	Ser-374	-/-	FV**pT**ASS**pT**p**S**TTSGTNR	l
	Thr-375	-/-	FV**pT**ASSTS**pT**TSG**pT**NR	m
	Thr-379	-/-	FV**pT**ASSTS**pT**TSG**pT**NR	m
	Ser-387	**Ser-386**	KLLPG**pS**VDG	l, m
T. aestivum F775_31728	**Thr-368**	**Thr-376**	FV**pT**VSSTSTPSR**pT**SR	k
	Ser-373	**-/-**	FV**pT**VSST**pS**TPSRTTR	k
	Thr-378	**-/-**	FV**pT**VSSTSTPSR**pT**SR	k
O. sativa	**Ser-384**	**Ser-386**	KLLPG**pS**VDG	n

XP_015622662.1	**Thr-366**	**Thr-376**	LV**pT**ASSSASR	n
Z. mays NP_001150975.1	**Thr-377**	-/-	IG**pT**ASSASR	o, p
a) (Reiland et al., 2009); b)(Reiland et al., 2011); c)(Hoehenwarter et al., 2013); d) (Wang et al., 2013); e) (Yang et al., 2013); f) (Lin et al., 2015); g) (Roitinger et al., 2015); h) (Bhaskara et al., 2017); i) (Rose et al., 2012); j) (Fan et al., 2014); k) (Lv et al., 2014a); l) (Lv et al., 2014b); m) (Lv et al., 2014c); n) (Whiteman et al., 2008); o) (Bonhomme et al., 2012); p) (Fristedt et al., 2012)				

11.6 Specific materials used in this work

Table 3: List of DNA oligomers used in this work

PRIMER NAME	**SEQUENCE**	**PURPOSE**
CAS_cDNA_fw	ATGGCTATGGCGGAAATGGC	Amplification of full length CAS CDNA
CAS_cDNA_rv	TCAGTCGGAGCTAGGAAGG	Amplification of full length CAS CDNA
CAS_fl+tp_ApaI_F	CCTGGGCCCATGGCTATGGCGGAAATGGC	Cloning of CAS-YFP fusion construct in pBIN (also for saGFP)
CAS_fl+tp_NotI_R	CTTGCGGCCGCCGTCGGAGCTAGGAAG	Cloning of CAS-YFP fusion construct in pBIN (also for saGFP)
CAS_fl-tp_ApaI_F	CCTGGGCCCGTTTCACTTCCAACATCAACTTC	Cloning of CAS-YFP fusion construct in pBIN
RBCS-1A_Fw	GATGGGCCCATGGCTTCCTCTATGCTCTCTTCCG	Cloning of RBCS-1A in pBIN-saGFP
RBCS-1A_Rev	TACGCGGCCGCCACCGGTGAAGCTTGG	Cloning of RBCS-1A in pBIN-saGFP
pGFP2FW	TATATAAGGAAGTTCATTTC	Sequencing of assembled constructs
CamVTRV	CTGGGAACTACTCACACATT	Sequencing of assembled constructs
ntCAS_SapI_fw	GGTGGTTGCTCTTCCAACGTTTCACTTCCAACATC	Cloning of CAS-NT in pTWIN1
ntCAS_PstI_rv	GGTGGTCTGCAGTTACGTATCCATGGTCGATG	Cloning of CAS-NT in pTWIN1
CAS_T350V_F	GTTTAGGCGTTGATTCTTACAACTTCTCGTTTG	Site directed mutagenesis
CAS_T350V_R	GTAAGAATCAACGCCTAAACGGCTCTGCAACC	Site directed mutagenesis
CAS_T376V_F	GCTTTGGCGTTAGGTCCGGAACCAAGTTCC	Site directed mutagenesis

CAS_T376V_R	CGGACCTAACGCCAAAGCTTCTCGAAGCTG	Site directed mutagenesis
CAS_S373A_F	GCAGCTTCGAGAGCCTTTGGCACTAGG	Site directed mutagenesis
CAS_S373A_R	CCTAGTGCCAAAGGCTCTCGAAGCTGC	Site directed mutagenesis
CAS_S378A_F	GGCACTAGGGCCGGAACCAAGTTCCTTC	Site directed mutagenesis
CAS_S378A_R	GAAGGAACTTGGTTCCGGCCCTAGTGCC	Site directed mutagenesis
CAS_T380V_F	GGCACTAGGTCCGGAGTCAAGTTCCTTC	Site directed mutagenesis
CAS_T380V_R	GAAGGAACTTGACTCCGGACCTAGTGCC	Site directed mutagenesis
pTWIN_seq_fW	ACTGGGACTCCATCGTTTCT	Sequencing of assembled constructs
T7_terminator_rv	TATGCTAGTTATTGCTCAG	Sequencing of assembled constructs
CAS_cDNA_3UTR_FW	TCAACTTTGAGAGATCTTTTGAT	RT-pPCR target gene (self desiged)
CAS_cDNA_3UTR_RV	TTCAGTTTGATGTAATCTTTTCC	RT-pPCR target gene (self desiged)
TOC1_FW	ATCTTCGCAGAGTCCCTGTGATA	RT-pPCR target gene (Wenden et al., 2011)
TOC1_RV	GCACCTAGCTTCAAGCACTTTACA	RT-pPCR target gene (Wenden et al., 2011)
*PDF*2_cDNA_FW	TAACGTGGCCAAAATGATGC	RT-pPCR reference gene (Czechowski et al., 2005)
*PDF*2_cDNA_RV	GTTCTCCACAACCGCTTGGT	RT-pPCR reference gene (Czechowski et al., 2005)
LP CAS Salk1	ATGTGTGTTTGCTCGTCTTCC	Genotyping
RP CAS Salk1	TGGTTGATTGTTTTCTCCACC	Genotyping
stn7-1_Salk_LP	GAGCTTGTGGGAATAGCTGTG	Genotyping
stn7-1_Salk_RP	TAGTTGAACATGCGTGAGTCG	Genotyping
Stn8-1_Salk_LP	TCTCCTTGAGCTTCTCTGCAG	Genotyping
Stn8-1_Salk_RP	GAATTCTTGGGGAGTAGGACG	Genotyping
Lba1	TGGTTCACGTAGTGGGCCATCG	Genotyping

Table 4: List of constructs generated in this work

Construct	Agi code	Vector	Purpose	Author
CAS-C	AT5G23060 (aa 216–387)	pTWIN1	Protein expression	Stael et al. 2011
CAS-C_{T350V}	AT5G23060 (aa 216–387)	pTWIN1	Protein expression	Self made
CAS-C_{S373A}	AT5G23060 (aa 216–387)	pTWIN1	Protein expression	Self made
CAS-C_{T376V}	AT5G23060 (aa 216–387)	pTWIN1	Protein expression	Self made
CAS-C_{S378A}	AT5G23060 (aa 216–387)	pTWIN1	Protein expression	Self made
CAS-C_{T380V}	AT5G23060 (aa 216–387)	pTWIN1	Protein expression	Self made
CAS-N	AT5G23060 (aa 34–147)	pTWIN1	Protein expression	Self made
CAS-YFP	AT5G23060 (aa 1–387)	pBIN-YFP	Localization analysis	Self made
ΔTP-CAS-YFP	AT5G23060 (aa 34–387)	pBIN-YFP	Localization analysis	Self made
saCAS-GFP1-10	AT5G23060 (aa 1–387)	pBIN-saGFP1-10C	Topology analysis	Self made
saCAS-GFP11	AT5G23060 (aa 1 – 387)	pBIN- saGFP11C	Topology analysis	Self made
saRUBISCO-GFP1-10	AT1G67090 (aa 1 – 181)	pBIN-saGFP1-10C	Topology analysis	Self made
saRUBISCO-GFP_{11}	AT1G67090 (aa 1 – 181)	pBIN- saGFP11C	Topology analysis	Self made

Table 5 List of bacterial strains used in this work

Organism	Strain	Purpose	Company/reference
E. coli	DH5α	Amplification of DNA plasmid /cloning	Stratagene, USA
E. coli	ER2566	Protein expression	NEB, Germany
A. tumefaciens	GV3101	Stable *A. thaliana* transformation via floral dipping method	Van Larebeke et al., 1974
A. tumefaciens	LBA1334	Transient transformation of tobacco	Diaz et al., 1989

Table 6 List of *A. thaliana* germplasms used in this work

Protein/Gene	**Locus**	**Line name**	**Background**	**Source**	**Mutant type**
Calcium Sensing receptor - CAS	AT5G23060	SALK_070416/CAS-1	Col-0	Salk	T-DNA insertion
State Transition Kinase 7 – STN7	AT1G68830	SALK_073254/stn7-1	Col-0	Salk	T-DNA insertion
State Transition Kinase 8 – STN8	AT5G01920	SALK_060869/stn8-1	Col-0	Salk	T-DNA insertion
STN7/STN8	AT1G68830 AT5G01920	*stn7stn8*	Col-0	Prof. Eva Mari Aro, University of Turku	T-DNA insertion
Circadian Clock Associated 1 – CCA1	AT2G46830	*cca1*	Col-0	Prof. George Coupland, Max Planck Institute for Plant Breeding Research, Cologne	T-DNA insertion